

**Functionalization of Multi-walled Carbon
Nanotubes and Localization of Functionalized
Multi-walled Carbon Nanotubes in an SAN/PPE
Blend**

**Dissertation with the aim of achieving a doctoral degree
at the Faculty of Mathematics, Informatics and Natural Sciences**

**Department of Chemistry
of Universität Hamburg**

submitted by Bing Du

2013 in Hamburg

--- corrected version ---

Date of oral defense: 22.11.2013

The following evaluators recommend the admission of the dissertation:

1. Gutachter Prof. Dr. Volker Abetz
2. Gutachter Prof. Dr. Patrick Theato

Declaration

The present study was processed from September 2009 to July 2013 at the Institute of Polymer Research, Helmholtz-Centre in Geesthacht in the department of Material Characterization and Processing with the direction of Prof. Dr. Volker Abetz. I hereby declare that the submitted dissertation has been independently prepared by my own and I have not used any tools or sources other than the cited. This dissertation has never been submitted to any University or examining agency for evaluation.

Table of Content

<i>Chapter 1 Introduction</i>	- 1 -
References.....	- 6 -
<i>Chapter 2 Theoretical Background</i>	- 7 -
2.1 Carbon nanotubes.....	- 7 -
2.1.1 Structure of carbon nanotubes.....	- 8 -
2.1.2 Fabrication methods of carbon nanotubes.....	- 10 -
2.1.3 Dispersion of carbon nanotubes.....	- 12 -
2.1.3.1 Nature of dispersion problem for carbon nanotubes	- 13 -
2.1.3.2 Techniques of dispersing carbon nanotubes	- 14 -
2.1.4 Functionalization of carbon nanotubes	- 16 -
2.1.4.1 Covalent functionalization	- 16 -
2.1.4.2 Non-covalent functionalization.....	- 20 -
2.2 Atom transfer radical polymerization	- 22 -
2.3 Immiscible polymer blends.....	- 25 -
2.3.1 Thermodynamics.....	- 25 -
2.3.2 Flory-Huggins Theory	- 27 -
2.3.3 Compatibilization of immiscible blends	- 29 -
2.3.3.1 Non-reactive compatibilization.....	- 29 -
2.3.3.2 Reactive compatibilization.....	- 31 -
2.3.4 Rheological properties of phase separated blends	- 32 -
2.4 Polymer nano-composites with carbon nanotubes.....	- 33 -
2.4.1 Fabrication of polymer composites with carbon nanotubes.....	- 33 -
2.4.2 Properties of polymeric composites with carbon nanotubes.....	- 36 -
2.4.2.1 Rheological properties	- 36 -
2.4.2.2 Electrical conductivity	- 38 -
References.....	- 40 -
<i>Chapter 3 Experimental Part</i>	- 44 -
3.1 Materials	- 44 -
3.2 Functionalization of MWCNT by “grafting-from” method via ATRP.....	- 46 -
3.2.1 Anchoring initiator on the surface of MWCNT	- 46 -
3.2.2 Functionalization of MWCNT with homopolymers via ATRP	- 47 -
3.2.3 Functionalization of MWCNT with P(MMA- <i>co</i> -S) random copolymers via ATRP.....	- 49 -
3.3 Functionalization of MWCNT by “grafting-to” method via Diels-Alder reaction.....	- 50 -
3.3.1 Synthesis of furfuryl-2-bromoisobutyrate.....	- 50 -
3.3.2 Synthesis of furfuryl-capped polymers via ATRP	- 51 -
3.3.3 Functionalization of MWCNT via Diels-Alder reaction	- 52 -
3.4 Preparation of SAN/PPE composites containing functionalized MWCNT with polystyrene	- 53 -

3.5 Preparation of SAN/PPE composites containing functionalized MWCNT with random copolymers	- 54 -
3.6 Characterization	- 55 -
3.6.1 Differential scanning calorimetry	- 55 -
3.6.2 Nuclear magnetic resonance spectroscopy.....	- 55 -
3.6.3 Gel permeation chromatography.....	- 56 -
3.6.4 Thermal gravimetric analysis.....	- 56 -
3.6.5 Fourier transform infrared spectroscopy	- 56 -
3.6.6 Transmission and scanning electron microscopy.....	- 57 -
3.6.7 Rheological measurement	- 57 -
3.6.8 Dielectric spectroscopy	- 58 -
References.....	- 58 -
<i>Chapter 4 Functionalization of carbon nanotubes</i>	- 60 -
4.1 Introduction.....	- 60 -
4.2 Results and discussion	- 61 -
4.2.1 Anchoring Initiator onto the surface of MWCNT.....	- 61 -
4.2.2 Functionalization of MWCNT with polystyrene	- 65 -
4.2.3 Functionalization of MWCNT with PMMA.....	- 68 -
4.2.4 Functionalization of MWCNT with P(MMA- <i>co</i> -S) copolymers.....	- 69 -
4.2.5 Functionalization of MWCNT via Diels-Alder reaction	- 74 -
4.3 Conclusions.....	- 80 -
References.....	- 81 -
<i>Chapter 5 SAN/PPE 40/60 blend filled with functionalized MWCNT with polystyrene: Influence of molecular weight of grafted polystyrene on localization of MWCNT and the properties of its composites</i>	- 83 -
5.1 Introduction.....	- 83 -
5.2 Results and discussion	- 85 -
5.2.1 Characteristics of the used MWCNT fillers in SAN/PPE 40/60 blend.....	- 85 -
5.2.2 Morphological properties of composites with MWCNT fillers	- 86 -
5.2.2.1 Morphology of SAN/MWCNT composites	- 86 -
5.2.2.2 Morphology of SAN/PPE 40/60 blend filled with MWCNT	- 88 -
5.2.3 Rheological properties of composites with MWCNT fillers	- 91 -
5.2.3.1 Thermal stability of neat SAN and PPE.....	- 91 -
5.2.3.2 Linear viscoelastic properties of neat SAN and pre-mixed SAN composites with MWCNT	- 92 -
5.2.3.3 Linear viscoelastic properties of SAN/PPE 40/60 composites with various MWCNT	- 95 -
References.....	- 99 -
<i>Chapter 6 SAN/PPE 40/60 blend filled with functionalized MWCNT with P(MMA-<i>co</i>-S) random copolymers: Influence of molecular weight of grafted polymer on localization of MWCNT and the properties of its composites</i>	- 100 -
6.1 Introduction.....	- 100 -
6. 2 Results and discussion	- 102 -

6.2.1 Morphology of SAN/PPE 40/60 blend filled with MWCNT.....	- 102 -
6.2.1.1 Theoretical prediction of the localization of pristine MWCNT in the SAN/PPE blends. -	102 -
6.2.1.2 Theoretical prediction of microstructure of SAN/PPE/P(MMA- <i>co</i> -S) ternary blends	- 106 -
6.2.1.3 Influence of molecular weight of grafted copolymers on the location of MWCNT fillers in immiscible SAN/PPE 40/60 blend.....	- 109 -
6.2.1.4 The influence of molecular weight of grafted copolymers on the morphologies of SAN/PPE blends	- 112 -
6.2.2 Rheological properties of SAN/PPE 40/60 blend filled with MWCNT fillers	- 114 -
6.2.3 Dielectric properties of SAN/PPE 40/60 blend filled with MWCNT fillers.....	- 117 -
6.3 Conclusions.....	- 119 -
References.....	- 121 -
<i>Chapter 7 Summary and Outlook</i>	- 123 -
7.1 Summary and Outlook	- 123 -
7.2 Zusammenfassung und Ausblick	- 126 -
<i>Acknowledgement</i>	- 130 -
<i>Appendix</i>	- 132 -
<i>List of Publications</i>	- 134 -

List of Figures

Chapter 2

Fig. 2.1 Models of multi-walled CNT and single-walled CNT	- 8 -
Fig. 2.2 Schematic diagram showing how a hexagonal sheet of graphite is “rolled” to form a carbon nanotube.....	- 9 -
Fig. 2.3 Structures of CNT: (a) armchair nanotubes, (b) zig-zag nanotubes and (c) chiral nanotubes ..	- 10 -
Fig. 2.4 Scheme of arc discharge method for preparing CNT	- 11 -
Fig. 2.5 Scheme of a chemical vapor deposition step of preparing CNT	- 12 -
Fig. 2.6 Distribution of different fillers of the same loading in a reference volume of 1 mm ³	- 13 -
Fig. 2.7 Calendering machine used for particle dispersion into a polymer matrix (A) and corresponding schematic of processing (B)	- 15 -
Fig. 2.8 Grafting of alkoxyamine end-capped copolymers onto MWCNT	- 18 -
Fig. 2.9 Scheme of functionalizing MWCNT with PMMA via ATRP	- 20 -
Fig. 2.10 Scheme of general mechanism of ATRP	- 23 -
Fig. 2.11 Scheme of the dependence of the conversion as function of time on linear and semilogarithmic scale.....	- 24 -
Fig. 2.12 Upper (UCST) and lower critical solution temperatures (LCST). UCST-type and LCST-type phase diagrams are depicted as solid curves with a one phase region between. The phase diagram where UCST and LCST overlap is shown as a dashed set of curves.....	- 27 -
Fig. 2.13 Storage modulus G' of CNT filled polycarbonate at 260°C	- 37 -
Fig. 2.14 Percolation threshold of CNT/Polymer nanocompositess based on different polymer matrices	- 39 -
Fig. 2.15 Optical micrographs of compression molded CNT/PE composite film with CNT (a) and the electrical conductivity as a function of the CNTs content for CNT/PE composite (b)	- 40 -

Chapter 3

Fig. 3.1 Scheme of anchoring initiator on the surface of MWCNT-NH ₂	- 46 -
Fig. 3.2 Scheme of anchoring initiator on the surface of MWCNT-OH.....	- 47 -
Fig. 3.3 Scheme of functionalizing MWCNT with homopolymers via ATRP.....	- 47 -
Fig. 3.4 Scheme of synthesis of furfuryl-2-bromoisoctyrate	- 50 -
Fig. 3.5 Scheme of synthesis furfuryl-capped polymer via ATRP	- 51 -
Fig. 3.6 Scheme of functionalization of MWCNT via Diels-Alder reaction	- 52 -
Fig. 3.7 Scheme of preparation of SAN/PPE blend filled with MWCNT-PS	- 53 -
Fig. 3.8 Scheme of preparation of SAN/PPE blend filled with MWCNT-CO	- 55 -

Chapter 4

Fig. 4.1 TGA results of anchoring initiator onto MWCNT-OH (a) and MWCNT-NH ₂ (b).....	- 63 -
Fig. 4.2 TGA and DTG results of functionalization of MWCNT-NH ₂ via ATRP	- 66 -
Fig. 4.3 FT-IR spectra of pristine MWCNT and different functionalized MWCNT	- 67 -
Fig. 4.4 TGA results of functionalized MWCNT with PMMA	- 68 -
Fig. 4.5 FT-IR spectra of functionalized MWCNT.....	- 70 -

Fig. 4.6 TGA curves of MWCNT-NH ₂ , MWCNT-Br and functionalized MWCNT with P(MMA- <i>co</i> -S) copolymers prepared with different reaction times (a) and the content of grafted P(MMA- <i>co</i> -S) copolymers as a function of the total monomer conversion (b).....	- 71 -
Fig. 4.7 Number-average molecular weight of P(MMA- <i>co</i> -S) copolymers (M_n) and polydispersity index (PDI) as a function of total monomer conversion	- 72 -
Fig. 4.8 ¹ H-NMR spectra of functionalized MWCNT prepared at different reaction times in CDCl ₃ at 25°C	- 74 -
Fig. 4.9 ¹ H-NMR spectrum of furfuryl alcohol (a) and furfuryl-2-bromoisobutyrate (b).....	- 76 -
Fig. 4.10 ¹ H-NMR spectra of furfuryl-capped PS (a) and furfuryl-capped PMMA (b).....	- 77 -
Fig. 4.11 FT-IR spectra of furfuryl-capped PS, furfuryl-capped PMMA, functionalized MWCNT with both PMMA and PS as well as pristine MWCNT	- 80 -

Chapter 5

Fig. 5.1 TEM micrographs of SAN composites with various MWCNT fillers: SAN composites with pristine MWCNT-2.5 wt% (a); SAN composites with MWCNT – PS₂₈²¹ -2.5 wt% (b); SAN composites with MWCNT – PS₇₆⁷³ -2.5 wt% (c).	- 86 -
Fig. 5.2 SEM micrograph of SAN/PS ₇₃ 92/8 blend. The arrows indicate the PS drops in the SAN matrix ..-	88 -
Fig. 5.3 TEM micrographs of SAN/PPE 40/60 blend filled with various MWCNT having different surface functionalization: SAN/PPE-MWCNT-1 wt% (a-b); SAN/PPE- MWCNT – PS₂₈²¹ -1 wt% (c-d); SAN/PPE- MWCNT – PS₇₆⁷³ -1 wt% (e-f).....	- 89 -
Fig. 5.4 Storage modulus G' (a), loss modulus G'' (b) of SAN and PPE as a function of time at 260 °C.	- 91 -
Fig. 5.5 Storage modulus G' (a), loss modulus G'' (b) and complex viscosity $ \eta^* $ (c) of SAN and its pre-mixed SAN/MWCNT composite as a function of angular frequency at 260°C.	- 93 -
Fig. 5.6 Storage modulus G' (a), loss modulus G'' (b) and complex viscosity $ \eta^* $ (c) of SAN/PS blend as a function of angular frequency at 260°C.	- 94 -
Fig. 5.7 Storage modulus G' (a), loss modulus G'' (b) and complex viscosity $ \eta^* $ (c) of neat SAN, PPE and SAN/PPE 40/60 as a function of angular frequency at 260°C.	- 96 -
Fig. 5.8 Storage modulus G' (a), loss modulus G'' (b) and complex viscosity $ \eta^* $ (c) of SAN/PPE 40/60 and its composites with different MWCNT fillers as a function of angular frequency at 260 °C. -	97 -

Chapter 6

Fig. 6.1 TEM micrographs of SAN/PPE 40/60 blend filled with various MWCNT fillers: SAN/PPE-MWCNT (a), SAN/PPE-MWCNT-CO-L (b) and SAN/PPE-MWCNT-CO-H (c). The MWCNT locating at the interface are highlighted by the pairs of dashed lines and the arrows.	- 110 -
Fig. 6.2 Morphologies of SAN/PPE 40/60 blend and its composites with various MWCNT fillers: (a) SAN/PPE-MWCNT; (b) SAN/PPE-MWCNT-CO-L; (c) SAN/PPE-MWCNT-CO-H.....	- 112 -
Fig. 6.3 Storage modulus G' (a), loss modulus G'' (b) and complex viscosity $ \eta^* $ (c) of SAN/PPE 40/60 and its composites with MWCNT fillers as a function of angular frequency ω at 260 °C.	- 115 -
Fig. 6.4 Modified Cole-Cole plot of SAN/PPE 40/60 blend and its composites with MWCNT	- 116 -
Fig. 6.5 AC conductivity δ' (a) and real part of complex permittivity ϵ' (b) of SAN/PPE 40/60 and its composites with MWCNT fillers as a function of frequency at 20 °C.	- 117 -

Chapter 1

Introduction

Polymer is an important class of materials because of their several outstanding advantages over other material classes, such as lightweight, corrosion resistance, facile processing, low cost, etc. In order to achieve the strength as same as the traditional metallic materials which have relatively high prices and limited resources, investigations for improving the properties of polymers have never been stopped. Unfortunately, up to now, polymers still cannot substitute metals in many cases owing to their poor mechanical properties, electrical and thermal conductivity as well as thermal stability. One of the general solutions for strengthening polymers is to add a certain quantity of fillers, for example metal particles, glass fibers, silica and carbon materials, into polymer matrices. At the initial stage, micron sized fillers (microfillers) which have at least one dimension in the micrometer range were firstly studied and have been used in industrial production nowadays. Nevertheless, the main drawback of microfillers is that a high loading of fillers is necessary to achieve the desired properties, which can lead to an increase of weight and a poor surface appearance of the composites. In the recent two decades, more and more interest has been paid on the application of nanofillers in polymer composites. For nanofillers, at least one dimension is in the nanometer scale. Compared to microfillers,

significantly lower loading of nanofillers is sufficient to obtain composites with improved properties.

Among several kinds of nanofillers, carbon nanotubes (CNT) are considered as one kind of the most promising fillers for polymer composites, owing to their extremely high aspect ratio, unique mechanical properties as well as excellent electrical and thermal conductivity. Particularly, the effects of CNT are found to be more pronounced in the composites based on multi-phase blends than in homopolymer matrices. For instance, a lower percolation threshold for electrical conductivity can be achieved by filling CNT into binary blends as CNT selectively locate in one phase of the blends. This concept is well known as “double percolation” which describes the first percolation of the phase in blends where CNT disperse and the second percolation of formed CNT network in the percolated phase. Such “double percolation” phenomenon with remarkably enhanced electrical conductivity has been observed in several polymer blends and raised intensively discussions [1-6]. In rheological experiments, a similar “double percolation” phenomenon is also observed with the decrease of percolation threshold when CNT are filled [7]. Additionally, CNT present an effect on the morphological stability of binary blends [2, 8]. These advantages show a high potential of composites constituted by binary blends and CNT in material field.

However, it is noteworthy that the abovementioned improvements of blend composites with CNT are mostly on the basis of the localization of CNT in one specific phase of binary blends due to the extremely high aspect ratio of CNT [4]. For such kind of cylinder nanoparticle, it is improbable to get into equilibrium at the interface, only if CNT orient completely parallel to the interface where both components in blends have almost the same affinity with CNT. Thus, localization at the interface is an unstable state for CNT in practical situation. However, the

localization at the interface is believed to be an ideal situation to maximize the improving effects of CNT. An expected “triple percolation” might be realized if CNT could be confined at the interface of binary blends, which is beneficial to achieve the percolation threshold with lowest CNT loading. In this case, mechanical properties could be improved because of the load transfer through CNT at the interface. It is also possible to compatibilize immiscible blends using the functionalized CNT as compatibilizer at the interface. Thereby, in order to maximize the advantages of CNT, it is essential to study and develop the strategy of locating CNT at the interface of binary blends. One possible approach is to graft specific polymers on the surface of pristine CNT. The grafted polymers covering CNT can provide a driving force to adjust the localization of CNT, which originates from the specific thermodynamic relationship between grafted polymer and the components of blends [9, 10]. Moreover, functionalization of CNT is also helpful to improve the dispersibility and affinity of CNT in polymer matrices [11]. Generally, the approaches to functionalize CNT are classified into two groups: “*grafting-from*” and “*grafting-to*”. Higher content and density of grafted polymer chains can be attained by applying former approach. However, the procedure of “*grafting-from*” method usually involves several synthesis steps in the presence of CNT and makes the process harsh. On the other hand, the “*grafting-to*” method is one-step functionalization of CNT but with lower density of grafted polymer because of the limited reactivity between CNT and reactive group.

In this work, the influence of functionalization on the localization of multi-walled carbon nanotubes (MWCNT) in an immiscible blend of poly(styrene-*co*-acrylonitrile) and poly(2,6-dimethyl-1,4-phenylene ether) (SAN/PPE) attracts our interest. PPE is characterized by a high heat distortion temperature, outstanding toughness and flame-retardant behavior, which has promising potential in structural parts, electronics, household and automotive items. However,

the high melt viscosity of PPE leads to a poor processability even at high temperature, so that, the practical application of PPE is considerably hindered. Neat PPE is rarely used to practical production. Generally, people utilize blending PPE with other polymers to solve the processing issue. Since 1960s, polystyrene (PS) has been considered as one typical and effective polymer to blend with PPE for manufacturing commercial PPE products [12-14]. Recently, researchers attempt to use other polymers containing styrene units instead of pristine polystyrene, such as SAN. Compared to polystyrene, SAN has a higher chemical resistance if the acrylonitrile (AN) content ranges between 19% and 35%. Nevertheless, SAN is immiscible with PPE when AN content is higher than 12.4 wt%, so that, the two components form binary blends with a poor interfacial adhesion in the range from 19 wt% to 35 wt%. In order to overcome this shortcoming, copolymers containing methyl methacrylate (MMA) and styrene units were introduced as compatibilizer and successfully compatibilized the SAN/PPE blends with improved properties [15-19]. The localization of these block copolymers at the interface of SAN/PPE blends is determined by the thermodynamic equilibriums among components. PS has a driving force to permeate into the PPE phase ($\chi_{PPE/PS} = -0.1$) [19] and poly(methyl methacrylate) (PMMA) should enter in the SAN phase ($\chi_{SAN/PMMA} = -0.008$) [5, 20]. Based on this fact, the functionalization of MWCNT with grafted polymer containing styrene and/or MMA units is expected to provide a driving force to tune the localization of CNT at the interface of SAN/PPE blends. In present work, the influence of molecular weight of grafted polymer on the localization of MWCNT and the properties of the composites will be studied. The weight ratio between SAN and PPE in the studied blend is 40 to 60, since the optimum properties of SAN/PPE 40/60 blend were reported [16].

On the basis of the abovementioned motivation, the main objectives and contents of present study are to:

- 1) Functionalize MWCNT via both “*grafting-from*” and “*grafting-to*” methods through atom transfer radical polymerization (ATRP) reaction
- 2) Realize the up-scaling of the functionalization of MWCNT
- 3) Investigate the influence of molecular weight of grafted polymers on the properties of SAN/PPE composites filled with functionalized MWCNT

This thesis is organized in the following structure: The theoretical background is given in Chapter 2 with a brief discussion of the initial properties of CNT, the techniques to manufacture CNT, the approaches for improving the dispersibility of CNT including the functionalizing methods, the basic mechanism of ATRP reaction, the basic performance of immiscible blends and the properties of polymeric composites with CNT; Chapter 3 describes the experimental procedures of functionalizing MWCNT and preparing SAN/PPE composites with MWCNT as well as the characterization of samples. The discussion and analysis are divided into three chapters: Chapter 4 reports functionalization of MWCNT with different polymers; Chapter 5 discusses the influence of the molecular weights of grafted PS on the migration of MWCNT from the SAN phase to the PPE phase and the rheological properties of the composites. The localization of functionalized MWCNT with P(MMA-*co*-S) random copolymers in the SAN/PPE blend is presented in Chapter 6, which also includes the study of the performance of rheological and dielectric properties of the composites. Chapter 7 gives a short summary of this work.

References

1. Wu M and Shaw L. *Journal of Applied Polymer Science* 2006;99(2):477-488.
2. Wu D, Zhang Y, Zhang M, and Yu W. *Biomacromolecules* 2009;10(2):417-424.
3. Sun Y, Guo Z, and Yu J. *Macromolecular Materials and Engineering* 2010;295(3):263-268.
4. Göldel A, Kasaliwal G, and Pötschke P. *Macromolecular Rapid Communications* 2009;30(6):423 - 429.
5. Pötschke P, Pegel S, Claes M, and Bonduel D. *Macromolecular Rapid Communications* 2008;29(3):244-251.
6. Li Y and Shimizu H. *Macromolecules* 2008;41(14):5339-5344.
7. Hu G, Zhao C, Zhang S, Yang M, and Wang Z. *Polymer* 2006;47(1):480-488.
8. Zou H, Wang K, Zhang Q, and Fu Q. *Polymer* 2006;47(22):7821-7826.
9. Cohen E, Zonder L, Ophir A, Kenig S, McCarthy S, Barry C, and Mead J. *Macromolecules* 2013;46(5):1851-1859.
10. Chiu JJ, Kim BJ, Kramer EJ, and Pine DJ. *Journal of the American Chemical Society* 2005;127(14):5036-5037.
11. Albuerne J, Boschetti-de-Fierro A, Abetz C, Fierro D, and Abetz V. *Advanced Engineering Materials* 2011;13(8):803-810.
12. Stoelting J, Karasz FE, and Macknight WJ. *Polymer Engineering & Science* 1970;10(3):133 - 138.
13. Cavaille J, Etienne S, and Perez J. *Polymer* 1986;27(4):549 -562.
14. Utracki LA. *Polymer Engineering & Science* 1982;22(17):1166 -1175.
15. Lach R, Grellmann W, Weidisch R, Altstädt V, Kirschnick T, Ott H, Stadler R, and Mehler C. *Journal of Applied Polymer Science* 2000;78(11):2037-2045.
16. Ruckdäschel H, Sandler JKW, Altstädt V, Rettig C, Schmalz H, Abetz V, and Müller AHE. *Polymer* 2006;47(8):2772-2790.
17. Ruckdäschel H, Sandlera JKW, Altstädt V, Schmalz H, Abetz V, and Müller AHE. *Polymer* 2007;48(9):2700-2719.
18. Kirschnick T, Gottschalk A, Ott H, Abetz V, Puskas J, and Altstädt V. *Polymer* 2004;45(16):5653-5660.
29. Auschra C and Stadler R. *Macromolecules* 1993;26(24):6364 - 6377.
20. Pötschke P, Abdel-Goad M, Alig I, Dudkin S, and Lellinger D. *Polymer* 2004;45(26):8863-8870.

Chapter 2

Theoretical Background

2.1 Carbon nanotubes

Carbon nanotubes were first observed by Radushkevich and Lukyanovich in 1952 [1] and later caught a worldwide attention after Iijima discovered multi-walled carbon nanotubes when synthesizing fullerenes via arc-discharge in 1991 [2]. Thanks to their excellent combination of electrical, thermal and mechanical properties, the interest in CNT-based nanomaterials has rapidly grown [3-6]. Such composites containing CNT show great potential in various fields, such as electronic devices, computers, hydrogen storage, medical delivery, sensors, etc

In contrast to other carbon materials, CNT are one dimensional carbon materials, which can be defined as long cylinders of rolled-up graphene sheet with nano-scale diameters [7]. The ends of cylindrical tubes are capped by hemisphere fullerenes. Generally, according to the number of wall, CNT are divided into two basic types: single-walled carbon nanotubes (SWCNT) and multi-walled carbon nanotubes (MWCNT) [3, 8]. As shown in Fig. 2.1, SWCNT can be considered as a single graphene sheet rolled into a seamless cylinder, while, MWCNT consist of two or more concentric cylindrical shells of graphene sheets coaxially

arranged leading to a central hollow core through van der Waals forces between adjacent layers.

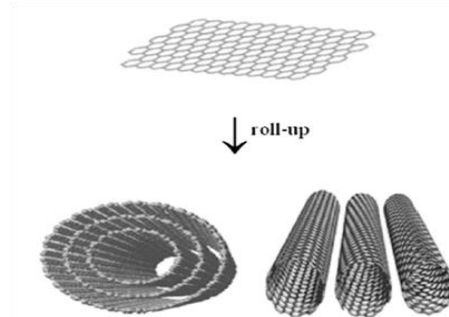


Fig. 2.1 Models of multi-walled CNT and single-walled CNT (reproduced from Ref. [9])

2.1.1 Structure of carbon nanotubes

As described in Fig. 2.1, the most general way to define the structure of CNT is considering CNT as rolled graphene sheet in a specific direction [10, 11]. According to the different rolling angle of the graphene sheet, there are three chiralities of CNT: armchair, zig-zag and chiral. The chiralities of nanotubes can be defined by a coordinate system with the unit vectors a_1 and a_2 , called “chiral vector”

$$\overrightarrow{C_h} = n\overrightarrow{a_1} + m\overrightarrow{a_2} \quad \text{Eq. 2.1}$$

where the integers (i.e. n,m) are the numbers of steps along the unit vectors ($\overrightarrow{a_1}$ and $\overrightarrow{a_2}$) of the hexagonal lattice (Fig. 2.2) [8, 12]. Using this (n, m) scheme, three types of CNT are identified: if n=m, the nanotubes are called as “armchair”; if n=0 or m=0, the nanotubes are called as “zig-zag”; otherwise, the CNT are implied as “chiral”.

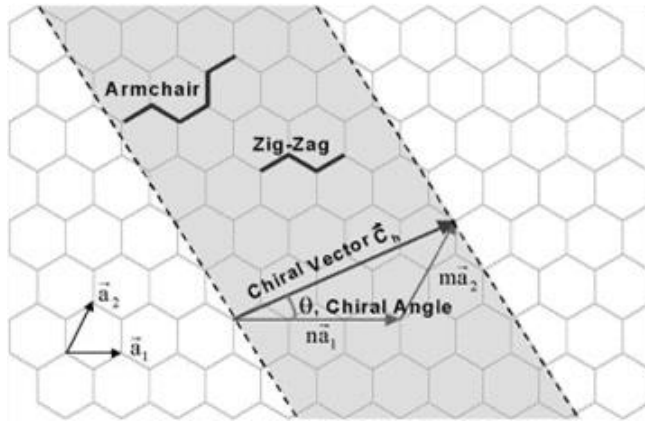


Fig. 2.2 Schematic diagram showing how a hexagonal sheet of graphite is “rolled” to form a carbon nanotube
(reproduced from Ref. [12])

The chiral angle, determining the degree of “twisting” of the tube, is defined as the angle (θ) between the vector \vec{C}_h and \vec{a}_1 and is given by:

$$\tan \theta = \sqrt{3} \frac{m}{2n+m} \quad \text{Eq. 2.2}$$

According to Eq. 2.2, the chiral angle for armchair nanotubes is 30° and the one for zig-zag tubes is 0° . If $0^\circ < |\theta| < 30^\circ$, CNT are chiral tubes. Additionally, if the inter-atomic spacing between carbon atoms is known, there is also a possibility to calculate the diameter of CNT (d) with the integers using the following equation:

$$d = \frac{\sqrt{3}}{\pi} l_{c-c} (n^2 + m^2 + nm)^{0.5} \quad \text{Eq. 2.3}$$

where $l_{c-c} = 0.14$ nm is the distance between two neighbor carbon atoms.

The chirality of CNT has a significant impact on their transport properties, especially on the electrical conductivity. In the case of SWCNT, when $(2n+m)$ is a multiple of 3, the nanotubes present a metallic conductivity with a band gap of 0 eV. Unfortunately, for MWCNT, the chiralities of each nanotube are various, so that, it is difficult to predict the physical properties of these tubes according to their chiralities.

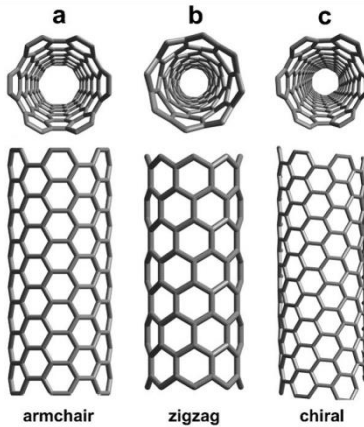


Fig. 2.3 Structures of CNT: (a) armchair nanotubes, (b) zig-zag nanotubes and (c) chiral nanotubes (reproduced from Ref. [13])

2.1.2 Fabrication methods of carbon nanotubes

In the last twenty years, three main techniques have been widely applied to produce CNT: arc discharge [3, 14, 15], laser ablation [16] and chemical vapor deposition (CVD) [11, 17, 18]. Each approach has its own characteristics. In this section, these three procedures for preparing CNT will be briefly described.

The carbon arc discharge method, initially used for producing C_{60} fullerenes, was applied to produce MWCNT by Iijima in 1991 [2]. It is the most common and perhaps easiest way to produce CNT. As depicted in Fig. 2.4, CNT are generated between two carbon electrodes under an inert atmosphere. The discharge vaporizes on the surface of one carbon electrode and forms a small rod-shaped deposit on the other electrode [19]. Producing CNT with high yield depends on several parameters including the uniformity of the plasma arc, the temperature of the deposit forming on the carbon electrode and the gas used (helium, argon, nitrogen, a mixture of hydrogen and nitrogen) as well as the pressure of gas. In order to obtain SWCNT, the electrodes are doped with a suitable catalyst, such as Ni-Co, Co-Y or Ni-Y [14, 19-21]. Using this method, CNT with less defects can be prepared, whereas the tubes are usually

entangled and heterogeneous with various lengths and diameters. Furthermore, this technique requires further purification to separate the CNT from the obtained solids and the residual catalytic metals are also found in the crude product.

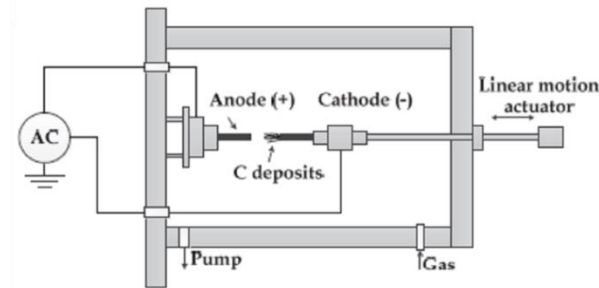


Fig. 2.4 Scheme of arc discharge method for preparing CNT (reproduced from Ref. [22])

Another method, laser ablation, was first used to synthesize CNT in 1996 with high purity (higher than 70%) [23]. In this method, graphite samples are evaporated by laser irradiation with a catalyst mixture of Co and Ni under flowing inert atmosphere at 1200 °C [14, 24]. The carbon products are swept by the flowing gas and deposit on a water-cooled collector [25]. Substantially, the system is treated in vacuum at 1000 °C in order to remove byproducts (C_{60} and other fullerenes). CNT with a diameter of 10-20 nm and a length of up to 100 μm appearing as a mat of “ropes” can be achieved using laser ablation. Each “CNT rope” consists of a bundle of single nanotubes which align along a common axis. The diameter and size distribution of CNT can be controlled by the temperature during growth procedure and the composition of catalyst.

Arc discharge and laser ablation are two principal approaches to produce CNT with high quality, however, the scale of both procedure is low and the obtained CNT are difficult to be purified because of the mixture of unwanted carbon impurities and metal species. In contrast to these two approaches, CVD method is a more practical way to produce CNT on a large scale, which has a higher potential for industrial production [26]. CVD procedure is realized by decomposing a gaseous or volatile compound of carbon onto a substrate in a tube reactor at

a certain temperature (between 600 °C and 1000 °C) [27]. The synthesized CNT are collected by cooling down the system at room temperature. During production, metallic nanoparticles do not only act as catalyst, but are also used as nucleation agents for nucleation and growth of CNT. Therefore, the deposition of catalysts on the substrate allows the formation of novel structures of carbon materials. Although CVD can offer industrial quantities of CNT with high purity and controllable structure, obtained CNT via CVD generally have a large amount of defects.

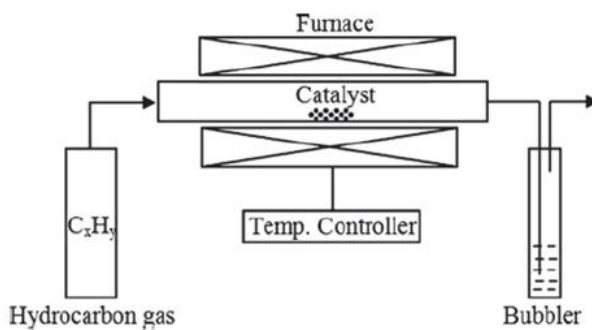


Fig. 2.5 Scheme of a chemical vapor deposition step of preparing CNT (reproduced from Ref. [23])

On the basis of CVD method, some implemented approaches are also used for synthesis of CNT. For example, one approach, called high pressure conversion of carbon monoxide (HiPco) [28], is applied to produce SWCNT using a floating catalyst during CVD procedure. Although the techniques of producing CNT have been developed for more than two decades, nevertheless, their industrial productions with high purity, uniformity and low cost are still issues needed to be improved.

2.1.3 Dispersion of carbon nanotubes

Although CNT are believed to open a new promising avenue in material science, unfortunately, there are still some troublesome issues leading to a gap between the high expectation and low practical achievement of materials containing CNT. The most significant

challenge of employing CNT is unsatisfied dispersibility of CNT in a matrix. The insufficient dispersion of entangled CNT considerably limits the performance of CNT on the performance of the. In this section, the dispersibility of CNT will be briefly described and the main techniques for improvement will be discussed.

2.1.3.1 Nature of dispersion problem for carbon nanotubes

To define the dispersibility of CNT, Ma et al. [29] gave a vivid impression on the different distribution behavior of some micro- and nano-filters in a matrix (see Fig. 2.6). The dispersion of Al_2O_3 and carbon fibers with micro-scale dimension (A and B in Fig. 2.6) is homogenous throughout the matrix. Consequently, the differentiation of individual particles in the matrix can be realized easily. On the contrary, when graphite nano-platelets and carbon nanotubes are filled into the same volume of matrix, it is hard for individual particles to be homogeneously dispersed (C and D in Fig. 2.6). Such agglomeration of particles, which results from the electrostatic interaction and van der Waals forces, leads to a more complicated situation to disperse nano-scale fillers in a real experiment than the one shown in the schematics.

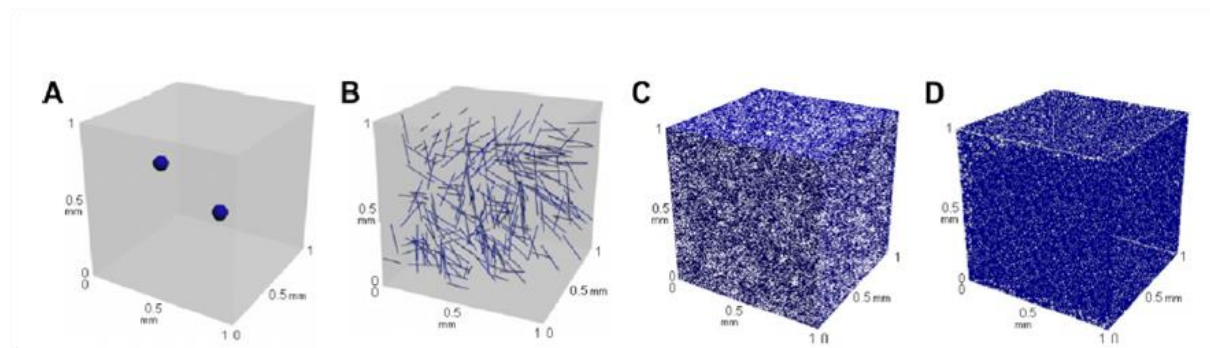


Fig. 2.6 Distribution of different fillers of the same loading in a reference volume of 1 mm^3
(A: Al_2O_3 particles; B: carbon fiber; C: graphite nano-platelets; D: CNT) (reproduced from Ref. [29])

Ma's work showed a fact that, the physical size of particles has a strong effect on the dispersion of CNT. Generally, as-produced CNT appear in bundles or entanglements

consisting of 50 to a few hundreds individual CNT because of van der Waals force. These kinds of bundles and agglomerates could diminish mechanical and electrical properties of composites as compared with theoretical predictions related to individual CNT. Therefore, how to incorporate CNT, or how to disentangle CNT, is the most significant challenge when applying CNT.

2.1.3.2 Techniques of dispersing carbon nanotubes

In order to improve the dispersibility of CNT, a series of techniques has been developed in the last two decades, such as ultrasonication, calendaring process, ball milling, mechanical stirring and extrusion [29]. The basic mechanism of these techniques is loading a mechanical energy or specific force onto the system to separate the individual tube from the agglomerates of CNT.

Among these approaches, ultrasonication might be the most frequently used and effective method to improve the dispersibility of CNT in liquids with a low viscosity. The principle of this technique is that when ultrasound propagates with a series of compression, the attenuated waves are induced in the molecules of the medium through which it passes. The production of these shock waves promotes the “peeling off” of individual nanoparticles located at the outer part of the nanoparticles bundles, or agglomerates. Subsequently, it results in the separation of individualized nanoparticles from the bundles. The standard laboratory sonicators (in a water bath) run at about 20-23 kHz with a power less than 100 W. Commercial probe sonicators have an adjustable amplitude ranging from 20% to 70% and a power of 100-1500 W. If the sonication treatment is excessive and/or too long, CNT can be easily and seriously damaged, especially when a probe sonicator is employed.

Calendering processing and ball mixing are two other kinds of mechanical ways to separate the bundles of aggregated CNT. The calendar, or commonly known as three roll mills, is a machine that employs the shear force created by rollers to mix, disperse or homogenize viscous materials (see in Fig. 2.7). In recent works, the utility of calendar to disperse CNT in polymer matrices has proved that this technique is a very promising approach to achieve a good dispersibility of CNT [30, 31]. A high shear stress is required to disentangle CNT bundles and distribute the CNT into polymer. Furthermore, a short residence time during the processing can limit the breakage of individual CNT. However, the smallest gap between the rollers ($1\text{-}5 \mu\text{m}$) is bigger than the diameter of individual CNT. Thus, calendaring is more suitable to separate large agglomerated CNT into small ones at a sub-microlevel, while only a small amount of individual tubes can be disentangled from large agglomerates [31].

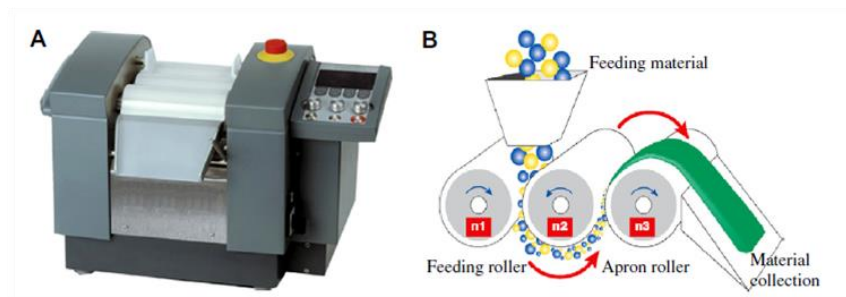


Fig. 2.7 Calendering machine used for particle dispersion into a polymer matrix (A) and corresponding schematic of processing (B) (reproduced from Ref. [29])

Ball milling is a type of grinding method to grind materials into extremely fine powder using in paints, pyrotechnics and ceramics. High quality ball mills can grind mixture particles into as small as 100 nm. Ball milling has been reported to successfully transform CNT agglomerates into nanoparticles [32] and to generate highly curved or closed shell carbon nanostructure from carbon graphite [33] as well as to modify the morphology of cup-stacked CNT [34].

2.1.4 Functionalization of carbon nanotubes

Besides of mechanical approaches mentioned in Section 2.1.3.2, surficial functionalization is one another efficient way to enhance the dispersibility of CNT in a polymeric matrix and the solubility in liquids. Furthermore, CNT with an appropriately functionalized layer present a better interaction with the surrounding matrix, so that, it is able to provide an efficient load transfer across the CNT/matrix interface. The techniques of modifying CNT are generally divided into covalent functionalization and non-covalent methods depending on the mechanism of the connection between functionalized component and the carbon atoms on the surface of CNT. As each approach has its advantages and drawbacks, it is of utmost importance to select proper methods according to the preparation conditions and expected properties of final composites.

2.1.4.1 Covalent functionalization

The inherent characteristics of CNT are pyramidization and misalignment of “ π -orbital” of sp^2 hybridized carbon atoms. The so-called covalent functionalization is based on the covalent linkage of functional entities onto the scaffold of CNT. Normally, this kind of modification happens at ends and defect sites of CNT or at the sidewall of nanotubes. Direct covalent sidewall functionalization involves a change of hybridization from sp^2 to sp^3 and a simultaneous loss of π -conjugation system on the graphene layer [35, 36]. Molecules with high chemical reactivity, like fluorine, are widely used to modify CNT by direct covalent functionalization [37, 38]. Besides, several replacements of the fluorine atoms have been also reported in literatures, such as amino, alkyl and hydroxyl groups [39, 40]. The defect functionalization is other usual method of covalent functionalization. The defects on CNT have several formats including opening ends, holes in the sidewalls, pentagon or heptagon

irregularities, and also oxygenated sites. Oxidization using strong acids (e.g., mixture of HNO_3 and H_2SO_4) is one typical and widely used approach to generate defects on the surface of nanotubes. After oxidization, the functional carboxylic acid or hydroxyl groups on CNT have a rich chemistry. Subsequently, such kind of CNT can be treated with a further chemical reaction (e.g., polymer grafting).

Regarding to functionalization of CNT with polymer, there are two main strategies to graft polymer on the surface of CNT, well known as “*grafting-to*” and “*grafting-from*” methods. The “*grafting-to*” approach is carried out between the readymade polymer with reactive end groups and carbon atom/grafted reactive group on the surface of CNT. This method does not only mean the covalent attachment but also include physical adsorption of the functional molecules. Macromolecules with nitroxyl and nitrine groups have been reported to have high grafting efficiencies on pristine CNT. When they are heated, polymer chains containing these functional groups are able to dissociate to generate polymer centered macroradicals, which can react with the graphitic structure of CNT. Qin et al. [41] reported that nitrine end-capped polystyrene with desired molecular weight was added to the surface of SWCNT via a cycloaddition reaction. The end-capped polymers with a 2,2,6,6-tetramethylpiperidine-1-oxy group (TEMPO) also have high reactivity with MWCNT by an addition reaction of the alkoxyamine-terminated precursors according to a radical mechanism [42]. The “living” polystyrene, poly(3-caprolactone) or their block copolymers end-capped by such TEMPO group can be grafted onto MWCNT through this method [43].

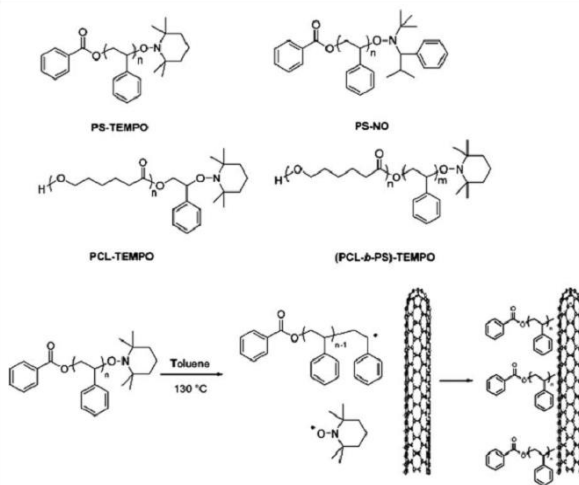


Fig. 2.8 Grafting of alkoxyamine end-capped copolymers onto MWCNT (reproduced from Ref. [43])

Additionally, creating suitable groups on the surface of CNT is a way to enhance or generate reactivity between CNT and the end-capped polymer chains. Oxidization is the most common approach to treat the MWCNT. For example, polymer-terminated amino or hydroxyl groups can link with the carboxylic acid group on the surface of CNT by amidation and esterification reaction. Refluxing the carboxylic acid groups functionalized CNT in neat SOCl_2 for an adequate time can convert the carboxylic acid group into acyl chlorides [44]. Then, the CNT with acyl chloride is possible to be covalently functionalized with several polymer chains, such as poly(propionyl-ethylenimine-*co*-ethylenimine) [45] and poly(styrene-*co*-aminomethylstyrene) [46], poly(amic acid) with bithiazole ring [47]. Dwyer et al. [48] used amino-terminated DNA to functionalize the open ends and defect sites of oxidized SWCNT, which realized a DNA-guided self-assembly process for CNT. Until now, many novel approaches of “grafting-*to*” method have been reported in literatures [49, 50].

However, although the “grafting-*to*” method is facile which only contains one step reaction involving MWCNT, a lower concentration of grafted polymer is a primary shortcoming for this method because of the limited reactivity of MWCNT. On the contrary, the “grafting-*from*” method offers an opportunity to functionalize CNT with high grafted content. The approach of

“grafting-from” means that reactive group is firstly covalently attached to the surface of CNT and then, the polymers are grown from the immobile reactive initiator on CNT. In 2003, Yao et al. [51] reported the approach of functionalizing CNT via a “*grafting-from*” approach for the first time. In their work, the alkyl bromides groups grafted on the surface of CNT were used as initiator for atom transfer radical polymerization (ATRP) of methyl methacrylate (MMA).

In the development of “*grafting-from*” approach, ATRP is one of the most effective methods to synthesize polymer from the immobile initiator on the surface of CNT with well controlled thickness of the functional polymer layer. Yan et al. [52, 53] gave a brief description of common procedure of functionalizing MWCNT via ATRP: (1) carbonyl chloride groups functionalized MWCNT (MWCNT-COCl) were prepared from the carboxyl-containing MWCNT (MWCNT-COOH) via reaction of thionyl chloride; (2) hydroxyl groups were introduced onto the surface of MWCNT by reaction of MWCNT-COCl with glycol, creating hydroxyl functionalized MWCNT (MWCNT-OH); (3) the initiator, 2-bromo-2-methylpropionyl bromide, was anchored onto the surface of MWCNT-OH to form MWCNT with immobile initiator (MWCNT-Br); (4) grafting polymerization of MMA was carried out from the immobile initiator on MWCNT-Br through ATRP reaction. The schematic representation of this procedure is given in Fig. 2.9. Due to the presence of CNT, ATRP processing is not a homogeneous polymerization. In order to control the growth of polymer chains and to monitor the polymerization kinetics, a tailored amount of free initiator was added to the system, which is sometimes called as “sacrificial initiator” in some publications. Lou et al. [54] fabricated polymer brushes by functionalizing SWCNT with poly(*n*-butyl methacrylate) (PnBMA). By means of methyl-2-bromopropionate as free initiator, the polymerization of PnBMA was well controllable with a linear increase of PnBMA content on SWCNT. Choi and his co-workers [55] proposed a method for the grafting of styrene from

SWCNT without previous acid treatment, which can protect from disruption of the graphitic structure of CNT during the acid treatment. In their work, hydroxyl groups were introduced on the surface of the SWCNT by the electrophilic addition of chloroform, followed by hydrolysis. Then, the initiator were anchored to the hydroxyl functionalized SWCNT and styrene was polymerized under ATRP conditions.



Fig. 2.9 Scheme of functionalizing MWCNT with PMMA via ATRP (reproduced from Ref. [52])

In addition, the self-condensing vinyl polymerization strategy combining monomer and inimer under ATRP condition was also reported to grow hyperbranched macromolecules on the surface of MWCNT. Anchoring initiator on MWCNT was carried out between MWCNT-COCl and excess of initiator components (2-hydroxyethyl-2-bromo-isobutyrate). Then, the hyperbranched macromolecules were covalently grafted on the surface of MWCNT by self-condensing vinyl polymerization of 2-((bromobutyryl)-oxy)ethyl acrylate via ATRP reaction [56].

As a novel development, Yoon et al. [57] applied a “grafting-from” approach combining surface-initiated and ring-opening polymerization to polymerize *p*-dioxanone. Using this method, they successfully obtained SWCNT functionalized with poly(*p*-dioxanone) from shorten SWCNT attached with 6-amino-1-hexanol.

2.1.4.2 Non-covalent functionalization

Although there are many successful examples of covalent functionalization of CNT, this method exhibits two major drawbacks. First of all, the sidewalls of CNT might be damaged by the created defects during the functionalization reaction, which could result in a negative effect on the mechanical properties and the disruption of π electrons system in CNT. Secondly, the concentrated acid or strong oxidants which are commonly used for oxidizing CNT are not environmentally friendly. Hence, many efforts have been made on developing physical functionalization of CNT which are convenient to fabricate CNT with low cost and less damage. Corresponding to covalent functionalization, this kind of physical method is also named as “non-covalent” functionalization.

Polymer wrapping and adsorption are two main strategies of non-covalent functionalization. The polymer wrapping is realized by the van der Waals interaction and π - π stacking between CNT and polymers which contain aromatic rings. In this case, poly(phenylene vinylene) and polystyrene are two typically suitable polymers [58, 59]. Sufficient stirring on the suspension of CNT in presence of polymer can lead to a wrapping process which promotes polymers to cover the surface of CNT. The efficiency of physical adsorption mainly depends on the properties of surfactants, medium chemistry and polymer matrix. Several researchers have contributed to study the effects of surfactants on the dispersibility and other properties of CNT [60-63]. Surfactants enwrapping the surface of nanotubes can effectively decrease the surface tension of CNT and prevent the formation of aggregates. As one essential element, surfactants are generally classified as several types, like non-ionic surfactants (e.g., polyoxyethylene octyl phenyl ether, nonylphenol ethoxylate), anionic surfactants (e.g., sodium dodecylsulfate, sodium dodecylbenzenesulfonate) as well as cationic surfactants (e.g., dodecyltri-methyl ammoniumbromide, 4-vinylbenzoate).

2.2 Atom transfer radical polymerization

Among several approaches for covalent functionalization of CNT, controlled radical polymerization (CRP) is generally used to realize the synthesis of polymer during functionalization. Compared to other kinds of techniques, CRP does not require elaborated setups and accepts higher levels of impurities. Moreover, the architecture and composition of the copolymers can be easily controlled. The commonly used methods of CRP include atom transfer radical polymerization (ATRP), reversible addition fragmentation chain transfer (RAFT) and nitroxide mediated radical polymerization (NMP). Because the catalysts are commercially available and relatively cheap, ATRP is more widely used than other kinds of methods [64]. In pioneering works, many scientific researchers successfully carried out ATRP with good controllability in the presence of CNT and the functionalized CNT have presented improved dispersibility in liquid solvents and polymer matrices [52, 53].

The mechanism of ATRP is depicted in Fig. 2.10. The radicals or active species are generated through a reversible redox reaction using a transition metal complex (M_i^n -Y/Ligand, where Y may be another ligand or the counterion) as catalyst. This metal catalyst undergoes an oxidation reaction with concomitant abstraction of a (pseudo) halogen atom (X) from a dormant species, R-X. This process is carried out with a constant activation “ k_{act} ” and deactivation “ k_{deact} ”. Polymer chains propagate by adding intermediate radicals to monomers in a manner similar to a conventional radical polymerization, with a constant rate k_p . Termination reaction (k_t) in ATRP occurs mainly through the radical coupling and disproportionation.

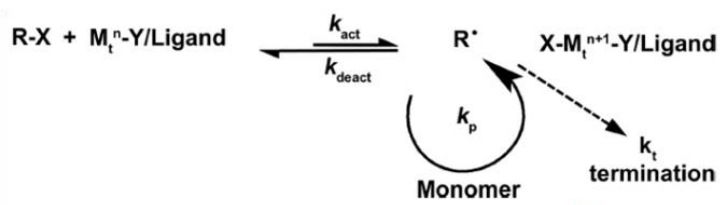


Fig. 2.10 Scheme of general mechanism of ATRP (reproduced from Ref. [65])

ATRP can be used for polymerizing several types of monomers including styrene, acrylates, methacrylates and acrylonitrile [66]. Successful ATRP reactions rely on the combination between the components and the polymerization condition. In absence of side reactions, the polymerization rate is determined by the equilibrium constant ($k_{eq} = k_{act} / k_{deact}$). Because of the unique intrinsic radical propagation rate of each monomer, it is necessary to adjust the concentration of propagating radicals and the rate of radical deactivation for maintaining the controllability of the polymerization.

In ATRP, alkyl halides (RX) are one kind of typical initiators. In order to obtain well-defined polymers with narrow molecular weight distribution, the halide groups (X) should rapidly and selectively migrate between the growing chains and the transition-metal complex. Alkyl halides with activating substituents on the α -carbon, such as carbonyl, allyl groups and polyhalogenated compounds, are the primary initiators in ATRP [65].

Regarding to the catalyst, copper salts are the most frequently used transition-metal catalyst in ATRP, which is advantageous compared to other kinds of transition metals, like molybdenum, chromium, rhenium etc. [65]. The solubility of transition-metal salt in the organic solvent media during the reaction depends on the ligand which is of primary importance for the reaction. Therefore, the catalyst system of ATRP usually consists of the ligands together with transition-metal salts. In reported works, nitrogen based ligands (e.g., N,N,N',N'',N''-pentamethyldiethylenetriamine (PMDETA) and 2,2'-bipyridine are two common types of ligands [67].

The rate of polymerization of ATRP can be expressed by Eq. 2.4 as following:

$$R_p = k_p[M][P\cdot] = k_p K_{eq} [M][I]_0 \times [M_t^n][X - M_t^{n+1}] \quad \text{Eq. 2.4}$$

The typical linear variation of conversion with time in semilogarithmic coordinates is shown in Fig. 2.11. This behavior indicates a constant concentration of propagating species during the reaction and a first-order kinetic of polymerization with respect to monomer. Generally, ATRP occurring under homogeneous conditions shows that the rate of polymerization is also first order with respect to initiator and the concentration of the transition-metal complex. The precise kinetic law for the deactivator is more complicated because of the spontaneous generation of deactivator. Radical termination occurs rapidly until sufficient amount of deactivator is generated and the radical concentration is low enough. Normally, termination occurs during the earliest stage of ATRP on the small fraction of polymer chains, while, the majority of the chains will continue to propagate. If a deactivator is added initially to the system, then the proportion of terminated chains can be effectively reduced.

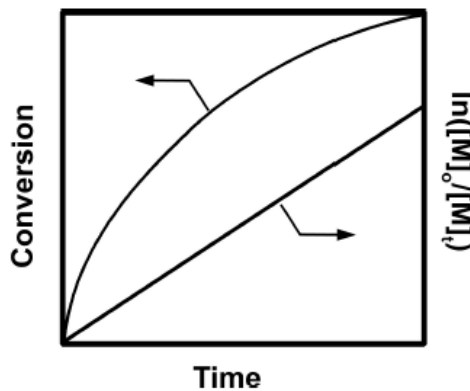


Fig. 2.11 Scheme of the dependence of the conversion as function of time on linear and semilogarithmic scale

(reproduced from Ref. [65])

ATRP can be run in either bulk, solution or heterogeneous systems (e.g., emulsion, suspension). However, solvent medium sometimes is necessary. Both of non-polar solvents (e.g., *p*-xylene, *p*-dimethoxy benzene, anisole, diphenyl ether) and some kinds of polar solvent

(e.g., ethylene carbonate and propylene carbonate) can be also utilized as ATRP medium [68]. The temperature is another significant factor which needs to be taken into account. At higher temperature, higher k_p/k_t ratios and better controllable reaction are observed. Furthermore, the solubility of the metal catalyst will increase with temperature. But, in the meantime, the decomposition of transition metal catalyst may take place at elevated temperatures and the chain transfer as well as other side reactions can occur at high temperatures. Therefore, in order to select the optimal temperature for ATRP, it has to take into account for the combination of the monomer, the catalyst, and the targeted molecular weight.

2.3 Immiscible polymer blends

Polymer blends or polymer mixtures represent one important class of materials, in which at least two polymers are mixed together to generate a new material with different properties. Blending may be the simplest and cheapest way to obtain polymeric materials with tailored properties. Since the middle of last century, large number achievements have been got in both scientific investigation and industrial application of polymer blends. . In particular, because of the combination of advantageous properties of each component, two-phase blends have attracted high attention in the last decades. In this section, the basis and some properties of polymer blends are briefly outlined.

2.3.1 Thermodynamics

For polymer blends, the most important characteristic property is the phase behavior. According to the phase behavior, polymers blends can be classified into three groups: miscible polymer blends (forming one phase), immiscible polymer blends (forming two or more phases) and partially miscible polymer blends (where the individual polymer reveal

some level of miscibility in the respective other phase). The relationship of free enthalpy governing the mixture of the components in blends is used to describe the phase behavior of the blends:

$$\Delta G_m = \Delta H_m - T\Delta S_m \quad \text{Eq. 2.5}$$

where ΔG_m is the free energy of the mixing, ΔH_m is the enthalpy of mixing and ΔS_m is the entropy of mixing. T denotes the temperature. If the two polymers are completely miscible, both of the following expressions must be satisfied:

$$\Delta G_m \leq 0 \text{ and } \frac{\partial^2 \Delta G_m}{\partial \phi^2} > 0 \quad \text{Eq. 2.6}$$

In the case of partially miscible blends, the second derivative of the free enthalpy is negative:

$$\Delta G_m < 0 \text{ and } \frac{\partial^2 \Delta G_m}{\partial \phi^2} < 0 \quad \text{Eq. 2.7}$$

For immiscible blends, the free enthalpy of mixing is positive:

$$\Delta G_m > 0 \quad \text{Eq. 2.8}$$

For low molecular weight materials, an increasing temperature drives ΔG_m to more negative values because of the increased $T\Delta S_m$ term. In the case of high molecular weight materials, the $T\Delta S_m$ term is small. Other factors, such as non-combinatorial entropy contributions and temperature dependent enthalpy values, dominate and lead to a reverse behavior, which means that miscibility decrease with increasing of temperature. Therefore, liquid-liquid and polymer-solvent mixtures generally have an upper critical solution temperature (UCST). While, for polymer-polymer mixtures, according to some mixing theories (e. g. “equation of state” approached by Flory [69, 70] and “lattice fluid” model by Sanchez [71, 72]), it is predicted that polymer-polymer blends which are miscible at lower temperatures are likely to exhibit phase separation at higher temperature. However, such lower critical solution temperature (LCST) behavior have been only proved in a few blending system which has either specific

interactions or differences in free volume, like poly(methyl methacrylate)/poly(styrene-*co*-acrylonitrile) (PMMA/SAN) [73], polystyrene/poly(vinyl methyl ether) (PS/PVME) [74, 75]. On the other hand, the classical Flory-Huggins theory shows an apposite prediction, in which UCST behavior is described as a common behavior in case of polymer-polymer mixtures. In practical experiments, UCST behavior generally occurs in the dispersive-force (van der Waals interaction) dominant systems and in the case with low molecular weight components [76]. The LCST and UCST behaviors are illustrated in Fig. 2.12.

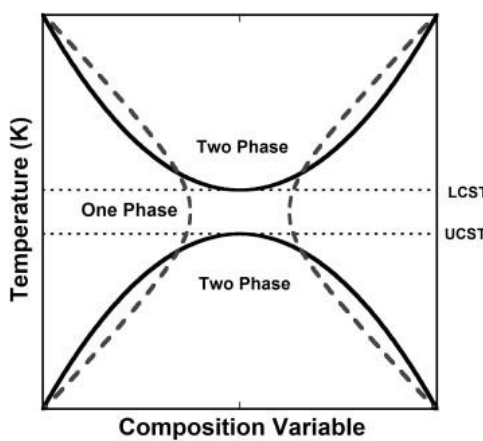


Fig. 2.12 Upper (UCST) and lower critical solution temperatures (LCST). UCST-type and LCST-type phase diagrams are depicted as solid curves with a one phase region between. The phase diagram where UCST and LCST overlap is shown as a dashed set of curves (reproduced from Ref. [69])

2.3.2 Flory-Huggins Theory

The most important theory for modeling the free energy of a binary polymer mixture is the Flory-Huggins theory. In this part, only the relevant results of this theory are discussed without going into details. A basic presumption of this theory is that the polymer chains of each component are distributed on a lattice with equal cell size, where each polymer segment covers exactly one lattice cell and all lattice positions are occupied. The key equation of this theory is:

$$\Delta G_m = RT \left(\frac{\phi_1}{N_1} \ln \phi_1 + \frac{\phi_2}{N_2} \ln \phi_2 + \phi_1 \phi_2 \chi_{12} \right) \quad \text{Eq. 2.9}$$

where R is the universal gas constant, N_i is polymerization degree of polymer i , ϕ_i is volume fraction of repeating segment i and χ_{12} is the Flory-Huggins interaction parameter. The first term in Eq. 2.9 denotes the mixing enthalpy and the latter two terms represent the combinatorial entropy of mixing. Generally, the molecular weight of the polymers in polymer blends is above 1 kg/mol so that the parameter N_i is large. Therefore, the entropy of mixing is rather small and can be neglected. Consequently, the mixing enthalpy is regarded as the main factor which controls the miscibility behavior of the blends. As discussed in Section 2.3.1, the critical conditions for phase separation satisfy the following equation:

$$(\partial^2 \Delta G_m / \partial \phi_2^2)_{p,T} = (\partial^3 \Delta G_m / \partial \phi_2^3)_{p,T} = 0 \quad \text{Eq. 2.10}$$

Thus, this condition leads to the critical binary interaction parameter $\chi_{12,cr}$:

$$\chi_{12,cr} \cong \frac{1}{2} \left(N_1^{-1/2} + N_2^{-1/2} \right)^2 \quad \text{Eq. 2.11}$$

Generally, the degree of polymerization of each component in blends is very high ($N_1, N_2 \rightarrow \infty$). Hence, the condition for obtaining miscibility reduces to:

$$\chi_{12} < \chi_{12,cr} = 0 \quad \text{Eq. 2.12}$$

As the interaction parameters of most polymer pairs are positive, immiscible blends are generally observed and only few miscible systems are known until now. Furthermore, although in many investigations researchers assumed the interaction parameters as constant, it is found that χ_{12} depends on many different factors such as temperature, molecular weight and pressure. Therefore, some miscible blends also can become partially miscible or even immiscible under specific conditions.

2.3.3 Compatibilization of immiscible blends

As described by the Flory-Huggins theory, the interaction parameter is generally positive. Thus, most polymer blends present immiscibility with coarse and unstable morphologies and poor adhesion at the interface. In order to overcome these problems, adding a small amount of a third ingredient has been proved as an effective way to modify the interfacial condition of the blends. These additives act as interfacial agent, called compatibilizer, which has been researched and widely used in industrial field for over twenty years [78]. A useful compatibilizer is helpful to obtain a tailored phase structure and also can improve the mechanical compatibility by enhancing the interfacial adhesion between the phases. According to the interaction between the compatibilizer and the components of the blends, there are two groups of strategies: non-reactive compatibilization and reactive compatibilization.

2.3.3.1 Non-reactive compatibilization

Generally, non-reactive compatibilizers are precisely tailored block- or graft copolymers, in which individual components are miscible with one of the components of the blends

The utility of block copolymers for compatibilizing immiscible blends has been known since the studies of Malau and his co-workers [79, 80]. The simplest example is to add diblock copolymers A-b-B into an immiscible blend of polymers A and B. For instance, the blends of polystyrene and poly(vinylpyridine) can be simply compatibilized by the block copolymers of polystyrene and polyvinylpyridine (PS-*b*-PVP). Another type of compatibilization is using C-*b*-D in the blends of A and B, where both the C-block and D-block show a negative enthalpy of mixing with polymer A and B, respectively. Due to the enthalpic driving force, individual

blocks of the compatibilizer can respectively stretch into their miscible phases of the blends and improve the stability of the interfacial area by reducing the coalescence of the dispersed phases. As shown in many previous works, the addition of PS-*b*-PMMA copolymers with defined composition successfully compatibilized the blends of poly(styrene-co-acrylonitrile) and poly(2,6-dimethyl-1,4-phenylene ether) (SAN/PPE) and remarkably enhance the load transfer between SAN and PPE [81-83]. In this system, the PS block shows an enthalpic favorable interaction with PPE, while PMMA is miscible with SAN (AN content is not higher than 30 wt%).

When block copolymers are used as compatibilizer, the molecular weight ratio between the blocks of copolymer and the components of blends plays an important role in the efficiency. Riess et al. [84] pointed out that when the molecular weight of the homopolymer component in the blends is so much higher than the one of the corresponding block in copolymers, the block copolymers cannot act as a compatibilizers. The work of Creton et al. [85] also demonstrated that, a block length should be higher than the average molecular weight of entanglements. Because only if the block segment completely permeate across the interface, compatibilizer can effectively strengthen the interfacial region (wet brush situation). Otherwise, the copolymers with short blocks cannot efficiently extend into the miscible phase in blends to achieve the compatibilization (dry brush situation). In subsequent studies, researches added one more block into the previous diblock to form triblock terpolymers to improve the compatibilization of diblock copolymers. It was observed that these “new” triblock terpolymers had better compatibilizing performance than the diblock substances. For example, SAN/PPE blends compatibilized with polystyrene-*block*-polybutadiene-*block*-poly(methyl methacrylate) triblock terpolymers (SBM) showed a higher toughness than the blends with polystyrene-*block*-poly(methyl methacrylate) (PS-*b*-PMMA) diblock copolymers.

Furthermore, the addition of a graft copolymer is an alternative to block copolymers. Although graft copolymers can be synthesized more easily by a free radical reaction, they are less efficient than block copolymers [86]. Like block copolymers, the molecular weights of graft copolymers also play a fundamental role.

2.3.3.2 Reactive compatibilization

The main method of reactively compatibilizing polymer blends involves *in situ* polymerization, where covalent bonding between constituents can generate grafting or block copolymers allowing for interfacial stabilization.

Before reaction, a reactive compound is not a real compatibilizer, as it tends to dissolve preferably in one phase during melt blending. After the reaction, the *in situ* formed graft or block copolymers contain chains which are identical to, or miscible with, the components of blends. When a C-X copolymer (where X is a reactive functional group and C is miscible with B) are added to the blends of A and B, the reactive copolymers can react with at least one of the components (i.e. A) and the *in situ* formed C-X-A copolymers can act as compatibilizer for the blends of A and B. One example of this compatibilizer is polyolefins grafted with maleic anhydride (MA). The MA group can react with the amine end groups of polyamides as well as the hydroxyl end groups of polyesters to yield the desired graft copolymers necessary for compatibilization, such as SAN/PA 6 blends reactively compatibilized by SAN-g-MA [87]. However, *in situ* compatibilization is applicable only to those systems in which at least one component contains functional groups that can interact with reactive compatibilization.

2.3.4 Rheological properties of phase separated blends

The rheological behavior of phase separated blends is significantly influenced by the morphology of the phase and shape changes in shear flow. The continuous phase of blend is determined by two important factors: the volume fraction and the viscosity of the component.

A high volume fraction and a low viscosity favor phase continuity. In the extreme case, a very low viscosity phase can form a continuous phase at very low volume fraction, like the blends involving PVC and ethylene copolymers [88]. An empirical relationship referring to the continuous phase structure bases on the viscosity/volume fraction ratio [89]: $\frac{\eta_1\phi_2}{\eta_2\phi_1}$.

The phase inversion point (equal continuity of both components) is where the expression is equal to 1 ($\eta_1/\eta_2 = \Phi_1/\Phi_2$). In the case of $\eta_1/\eta_2 > \Phi_1/\Phi_2$ (viscosity/volume fraction ratio < 1), the phase 1 is predicted as continuous phase; otherwise, continuity of phase 2 is expected. However, this expression is only a qualitative guide for predicting phase behavior. A lot of other expressions have also been proposed to predict the phase behavior as a function of viscosity and volume fraction [90]. It should be noted that other factors, such as melt elasticity and interfacial tension might be also important for the rheological behavior of the blends.

For phase separated polymers, there are several common mixing rules which can be employed to predict the viscos behavior of blends:

$$\text{Additivity model: } \eta_{blend} = \phi_1\eta_1 + \phi_2\eta_2 \quad \text{Eq. 2.13}$$

$$\text{Log additivity model: } \log \eta_{blend} = \phi_1 \log \eta_1 + \phi_2 \log \eta_2 \quad \text{Eq. 2.14}$$

$$\text{Fluidity model: } \frac{1}{\eta_{blend}} = \frac{\phi_1}{\eta_1} + \frac{\phi_2}{\eta_2} \quad \text{Eq. 2.15}$$

The additivity model and the fluidity model are similar to the parallel and series model for modulus data (in Section 2.2.4) and represent the upper and lower bound data for the viscosity

of phase separated blends. In the case of more viscous component with high volume fraction, the additivity model reflects the viscosity data. When less viscous component has a high volume fraction, the fluidity model is valid. The log additivity model should be used for the miscible system.

2.4 Polymer nano-composites with carbon nanotubes

Polymer composites, consisting of additives and polymer matrix, are believed to be one kind of significant materials with relatively inexpensive cost and good properties. Unlike traditional composites with micron-scale fillers, the properties of polymer composites with nanoscales fillers can be largely modified even at an extremely low loading of fillers because of the high surface to volume ratio. In addition to the inherent properties of polymer matrix, the behavior of composites with CNT also depends on several factors: synthesis and purification of CNT, the amount and the type of impurities from CNT product, diameter, length as well as aspect ratio of CNT; the orientation of CNT in polymer matrix; the interaction between CNT and polymer matrix. Since the first report on the preparation of a polymer composite with CNT was published in 1994 [91], a large number of studies paid their attention on understanding the structure-property of the composites and widening their application in different fields. This section gives a brief description of various fabrication techniques for polymer composites with CNT and the effect of CNT on these materials.

2.4.1 Fabrication of polymer composites with carbon nanotubes

Solution blending, melt blending and *in situ* polymerization are three groups of typical techniques to prepare polymeric composites with CNT.

Solution blending might be the most common approach for mixing polymer and nanotubes. One benefit of solution blending is that agitation of CNT in solution facilitates the de-aggregation and dispersion of nanotubes. The general processing of solution blending includes: dispersion of nanotubes in either a solvent or polymer solution by energetic agitation, mixing of CNT and polymer solution by energetic agitation and lastly, controlling evaporation of solvent leaving a composite film. The common approaches providing energy for agitation are magnetic stirring, shear mixing, reflux and ultrasonication. In the early work of Jin and coworkers [92], MWCNT were dispersed in chloroform by sonication for one hour and then, polyhydroxyaminoether was dissolved in the MWCNT suspension. Mixing was realized by applying a further sonication treatment. Then, the solution was poured in a Teflon® mould and dried at ambient conditions overnight. By this method, the composites with a high loading (up to 50 wt%) and a reasonably good dispersion were achieved. In subsequent studies, this technique has been continuously utilized with a very slight variation. Qian et al. [93] applied sonication to disperse catalytic MWCNT in toluene and then blended the suspension with a solution of polystyrene. After further mixing by sonication, the solution casting step was processed drop by drop. Ruan et al. [94] used a similar way to prepare composites. However, in their work, nanotubes were dispersed using magnetic stirring and sonication, whereas, refluxing was applied to mix MWCNT and polymer instead of sonication treatment. The key points of solution blending are the solubility of polymer in solvent and the efficient dispersion of CNT in the same solvent. The choice of solvent is generally determined by the solubility between the polymeric matrix and solvent. However, pristine nanotubes cannot be well-dispersed in most solvents. In order to overcome this problem, many works have discussed the approach to enhance the dispersibility of CNT in polymer solution and the pronounced improvement has been achieved by insistent effort from many scientists in the last two decades [95, 96]. This part of work has been briefly described in Section 2.1.4.2.

Another common way to prepare nanocomposites containing CNT is melt processing. Unlike solution blending which is restricted by the solubility of polymer, melt blending technique is suitable for most polymers, especially for dealing with composites based on thermoplastic polymers. This technique can be used when the polymers are softened by heating. Amorphous polymers are processed above their glass transition temperature while semi-crystalline polymers have to be heated above their melting temperature to achieve sufficient softening. One obvious advantage of melt blending is its facility which is more compatible with industrial production [97, 98]. Melt processing involves the melting of polymeric materials by heating approach to form a viscous liquid and the nanofillers are mixed into the melt polymer by shear mixing. The techniques used for preparing such bulk composites include compression moulding, extrusion, injection moulding, etc. However, compared to solution blending, melt compressing presents less influence on the dispersibility of nanotubes in a polymer matrix and it is limited to low concentration due to the high viscosities of composites containing high CNT loading [99]. An early study on melt mixing of MWCNT and polymer was reported by Jin et al. in 2001 [100]. The authors mixed poly(methyl methacrylate) (PMMA) with MWCNT in a laboratory mixing molder at 200 °C. The mixed samples were formed as specimens by melting compression. More successful examples of melt processing have been achieved in the following several years, for instance, CNT/polypropylene [101], CNT/polyimide [102], CNT/nylon-6 [103]. However, in some cases, shear mixing is tough in practice as the nanotube powder tends to stick to the walls of the mixing device. In order to solve this issue, a combination of solution and melt processing was introduced. Thostenson et al. [104] initially dispersed MWCNT in a solution of polystyrene in THF and subsequently, the dried films were cut up and extruded through a rectangular die. Cooper and his colleagues [105] mixed PMMA microspheres and SWCNT using a dry powder mixing method with a small amount of ethanol. Although PMMA were not dissolved, the spheres of PMMA were

coated by immobilized SWCNT. The dried mixture was molten in a twin screw compounder. Films of composites were obtained through a slit die of compounder and significant alignment of CNT was observed.

The last common preparing approach, called *in situ* polymerization, is also defined as one way to functionalize CNT which has been described in Section 2.1.4. This fabrication started from dispersing CNT in mixture of monomer and other reagents. Then the monomer was polymerized in presence of CNT. The obtained functionalized CNT can improve the initial dispersion of nanotubes in the selective solvents and consequently better dispersibility of CNT fillers can be achieved in the composites.

2.4.2 Properties of polymeric composites with carbon nanotubes

2.4.2.1 Rheological properties

The viscoelastic properties have practical influence on processing of materials and scientific importance as a probe of the dynamics and microstructure of composites. Fig. 2.14 shows a typical response of polymeric composites with CNT during a rheological measurement. At high frequencies, the response is not sensitive to the concentration of fillers, which indicates that the nanotubes only have low influence on the short-range polymer dynamics. While, an obvious transfer from liquid-like response to solid-like response occurs at low frequencies when the concentration of CNT increases in the composites. This phenomenon is consistent with earlier studies in silicate composites [106]. Applying a power law function to the G' vs nanotubes loading provides a rheological percolation threshold corresponding to the onset of solid-like behavior.

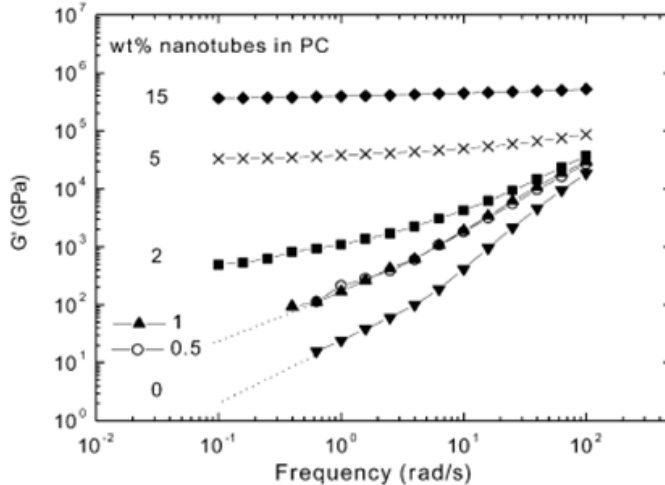


Fig. 2.13 Storage modulus G' of CNT filled polycarbonate at 260°C (reproduced from Ref.[107])

Similar to electrical percolation, rheological percolation is found to rely on the dispersion, aspect ratio and alignment of CNT. Mitchell et al.[108] enhanced the dispersion of CNT in polystyrene by functionalization and found that the rheological percolation threshold decreased from 3 wt% to 1.5 wt% using functionalized nanotubes. Furthermore, the data of G' at low frequencies of composites with functionalized SWCNT were higher than the ones with pristine nanotubes, demonstrating improved compatibility between the SWCNT and the polymer matrix and the better dispersion of the SWCNT.

Additionally, the work of Pötschke et al. [109] pointed out that temperature also has a strong influence on the rheological percolation threshold of CNT composites. Their results demonstrated that the percolation threshold of PC composites with SWCNT decreased from around 5wt% to 0.5wt% when the temperature was increased from 170°C to 280 °C. They attributed this rheological property to the superposition of the entangled polymer network and the combined nanotube-polymer network in the system rather than the nanotube network. Besides, the concentration of CNT required to form a reinforcing nanotube-polymer network is considered to be lower than the electrical percolation threshold. For example, in the case of PMMA composites with SWCNT, the rheological percolation threshold was found as 0.12 wt% which was considerably smaller than the one for electrical conductivity (0.39 wt%) [107].

2.4.2.2 Electrical conductivity

The electrically conductive behavior of polymer composites filled with CNT can be explained by the percolation theory. The electrical percolation threshold is a critical volume or weight fraction of CNT where the electrical conductivity of the composite suddenly increases by orders of magnitude. According to percolation threshold theory, the measured electrical conductivity of composites can be fitted with a power law function:

$$\sigma_{DC} = \sigma_0 \left(\frac{p_A - p_C}{1 - p_C} \right)^x \quad \text{Eq. 2.16}$$

where σ_{DC} is the measured electrical volume conductivity of composite and p_A is filler content (wt%) of CNT and p_C is the critical value of CNT content at percolation threshold as well as σ_0 and x are fit parameters. Compared to other kinds of nanofillers, extremely high aspect ratio and excellent electrical conductivity of CNT lead to a transformation from insulating polymer to a conductive composite at a very lower loading of fillers. Figure 2.14 gives the percolation threshold of CNT in different polymer matrices. For most polymer matrices, the percolation threshold values of CNT are generally below 5 wt% [29, 110-112]. However, the filler loading in a range of 10-50 wt% is necessary for the composites with other kinds of fillers, such as carbon black, carbon fibers, micrometer-scale metallic particles, to achieve the percolation threshold [29, 113, 114].

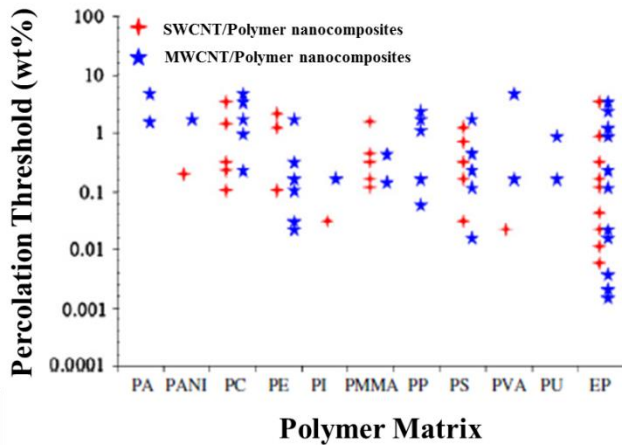


Fig. 2.14 Percolation threshold of CNT/Polymer nanocompositess based on different polymer matrices (reproduced from Ref. [110])

The percolation threshold for polymer composites with CNT depends on dispersion [115, 116], alignment [117], aspect ratio [116, 118] and degree of modification of CNT [119], polymer types [120] as well as processing methods of preparing composites [116]. Among these aspects, the formation of CNT-CNT network is one of the most important factors. Both agglomerated and dispersed CNT can form electrically conductive networks. A well dispersed structure of CNT is more or less beneficial for improving the electrical conductivity of composites [121-123]. However, it does not mean that the well dispersed CNT is necessary for an electrically conductive network. A continuously and loosely packed agglomeration of CNT is ideal state for enhancing the electrical conductivity. For instance, through confining CNT at the interface of polyethylene (PE) pellets via compression moulding, the critical value of CNT content at percolation threshold was achieved 0.1 vol% of CNT which was lower than the theoretical percolation threshold for composite with well dispersed CNT (see Fig. 2.15) [122].

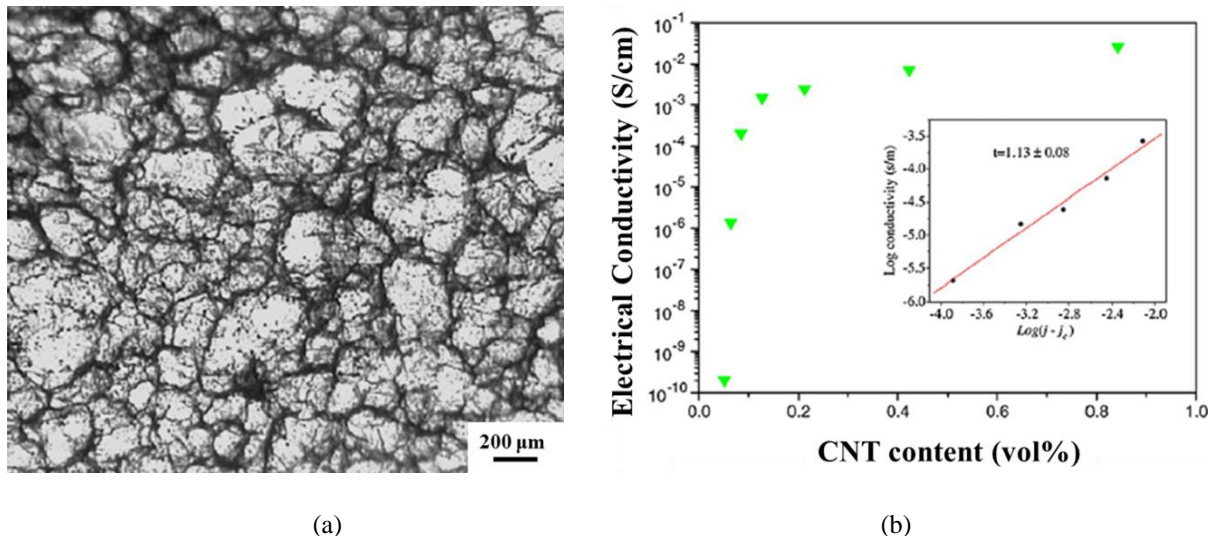


Fig. 2.15 Optical micrographs of compression molded CNT/PE composite film with CNT (a) and the electrical conductivity as a function of the CNTs content for CNT/PE composite (b) (reproduced from Ref. [122])

In addition, many previous studies showed that the functionalization of CNT has significant influence on the electrical conductivity of composites [29, 112, 124]. Appropriate modification can improve the dispersion of CNT and is helpful to form a network in composites, which leads to a decrease of the percolation threshold of composites. Nevertheless, excessive functionalization could introduce too many heterogeneous atoms on the surface of CNT, resulting in the perturbation of π electrons. Consequently, the intrinsic electrical properties of CNT are degraded. Furthermore, acid treatment for functionalization can severely damage and fragment CNT into short pieces with lower aspect ratio, which is also disadvantageous for electrical conductivity of CNT.

References

1. Radushkevich LV and Lukyanovich VM. Zh. Fizich. Khim (in Russian) 1952;26:88.
2. Iijima S. Nature 1991;354(6348):56 - 58.
3. Qian D, Wagner GJ, Liu WK, Yu M-F, and Ruoff RS. Applied Mechanics Reviews 2002;55(6):495 - 599.
4. Reich S, Thomsen C, and Maultzsch J. Carbon nanotubes: basic concepts and physical properties. New York: Wiley-VCH, 2004.
5. Coleman JN, Khan U, and Gun'ko YK. Advanced Materials 2006;18(6):689-706.

6. Koo J. *Polymer nanocomposites: processing, characterization, and Applications*. New York: McGraw Hill Professional, 2006.
7. Dresselhaus MS, Lin YM, Rabin O, Jorio A, Souza Filho AG, Pimenta MA, Saito R, Samsonidze G, and Dresselhaus G. *Materials Science and Engineering: C* 2003;23(1–2):129-140.
8. Dresselhaus MS, Dresselhaus G, and Saito R. *Carbon* 1995;33(7):883-891.
9. Simate GS, Cluett J, Iyuke SE, Musapatika ET, Ndlovu S, Walubita LF, and Alvarez AE. *Desalination* 2011;273(2–3):235-247.
10. Moniruzzaman M and Winey KI. *Macromolecules* 2006;39(16):5194-5205.
11. Dresselhaus MS, Dresselhaus G, and Avouris P. *Carbon nanotubes: synthesis, structure, properties, and applications*. Berlin: Springer, 2001.
12. Thostenson ET, Ren Z, and Chou T-W. *Composites Science and Technology* 2001;61(13):1899-1912.
13. Terrones M. *Annual Review of Materials Research* 2003;33(1):419-501.
14. Saito Y, Nishikubo K, Kawabata K, and Matsumoto T. *Journal of Applied Physics* 1996;80(5):3062-3067.
15. Li Z, Wei L, and Zhang Y. *Applied Surface Science* 2008;254(16):5247-5251.
16. Rinzler AG, Liu J, Dai H, Nikolaev P, Huffman CB, Rodríguez-Macías FJ, Boul PJ, Lu AH, Heymann D, Colbert DT, Lee RS, Fischer JE, Rao AM, Eklund PC, and Smalley RE. *Applied Physics A* 1998;67(1):29-37.
17. Queipo P, Nasibulin AG, Shandakov SD, Jiang H, Gonzalez D, and Kauppinen EI. *Current Applied Physics* 2009;9(2):301-305.
18. Huang ZP, Xu JW, Ren ZF, Wang JH, Siegal MP, and Provencio PN. *Applied Physics Letters* 1998;73(26):3845-3847.
19. Journet C, Maser WK, Bernier P, Loiseau A, Chapelle MLdl, Lefrant S, Deniard P, Lee R, and Fischer JE. *Nature* 1997;388(6644):756 - 758.
20. Bethune DS, Kiang CH, Devries MS, Gorman G, Savoy R, and Vazquez. J. *Nature* 1993;363:605 - 607.
21. Shi Z, Lian Y, Liao FH, Zhou X, Gu Z, Zhang Y, Iijima S, Li H, Yue KT, and Zhang S-L. *Journal of Physics and Chemistry of Solids* 2000;61(7):1031-1036.
22. Gore JP and Sane A. *Flame Synthesis of Carbon Nanotubes*: InTech, 2011.
23. Thess A, Lee R, Nikolaev P, Dai H, Petit P, Robert J, Xu C, Lee YH, Kim SG, Rinzler AG, Colbert DT, Scuseria GE, Tománek D, Fischer JE, and Smalley RE. *Science* 1996;273:483 - 487.
24. Zhang Y and Iijima S. *Applied Physics Letters* 1999;75(20):3087-3089.
25. Guo T, Nikolaev P, Thess A, Colbert DT, and Smalley RE. *Chemical Physics Letters* 1995;243(1–2):49-54.
26. Coleman JN, Khan U, Blau WJ, and Gun'ko YK. *Carbon* 2006;44(9):1624-1652.
27. Xie S, Li W, Pan Z, Chang B, and Sun L. *Materials Science and Engineering: A* 2000;286(1):11-15.
28. Chiang IW, Brinson BE, Huang AY, Willis PA, Bronikowski MJ, Margrave JL, Smalley RE, and Hauge RH. *Journal of Physical Chemistry B* 2001;105(35):8297-8301.
29. Ma P, Siddiqui NA, Marom G, and Kim J-K. *Composites Part A: Applied Science and Manufacturing* 2010;41(10):1345-1367.
30. Gojny FH, Wichmann MHG, Köpke U, Fiedler B, and Schulte K. *Composites Science and Technology* 2004;64(15):2363-2371.
31. Thostenson ET and Chou T-W. *Carbon* 2006;44(14):3022-3029.
32. Li YB, Wei BQ, Liang J, Yu Q, and Wu DH. *Carbon* 1999;37(3):493-497.
33. Gao B, Bower C, Lorentzen JD, Fleming L, Kleinhammes A, Tang XP, McNeil LE, Wu Y, and Zhou O. *Chemical Physics Letters* 2000;327(1–2):69-75.
34. Ma PC, Wang SQ, Kim J-K, and Tang BZ. *Journal of Nanoscience and Nanotechnology* 2009;9(2):749-753.
35. Niyogi S, Hamon MA, Hu H, Zhao B, Bhowmik P, Sen R, Itkis ME, and Haddon RC. *Accounts of Chemical Research* 2002;35(12):1105-1113.
36. Dyke CA and Tour JM. *The Journal of Physical Chemistry A* 2004;108(51):11151-11159.
37. Mickelson ET, Huffman CB, Rinzler AG, Smalley RE, Hauge RH, and Margrave JL. *Chemical Physics Letters* 1998;296(1–2):188-194.
38. Kelly KF, Chiang IW, Mickelson ET, Hauge RH, Margrave JL, Wang X, Scuseria GE, Radloff C, and Halas NJ. *Chemical Physics Letters* 1999;313(3–4):445-450.
39. Stevens JL, Huang AY, Peng H, Chiang IW, Khabashesku VN, and Margrave JL. *Nano Letters* 2003;3(3):331-336.
40. Hua ZQ and Jun CD. *Journal of Materials Science* 2004;39(5):1751-1757.
41. Qin S, Qin D, Ford WT, Resasco DE, and Herrera JE. *Macromolecules* 2004;37(3):752-757.
42. Wong SS, Joselevich E, Woolley AT, Cheung CL, and Lieber CM. *Nature* 1998;394:52-55.
43. Liu P. *European Polymer Journal* 2005;41(11):2693-2703.

44. Chen J, Hamon MA, Hu H, Chen Y, Rao AM, Eklund PC, and Haddon RC. *Science* 1998;282(5986):95 - 98.
45. Riggs JE, Guo Z, Carroll DL, and Sun Y-P. *Journal of the American Chemical Society* 2000;122(24):5879-5880.
46. Hill DE, Lin Y, Allard LF, and Sun Y. *International Journal of Nanoscience* 2002;1:213 - 221.
47. He B, Sun W, Wang M, Liu S, and Shen Z. *Materials Chemistry and Physics* 2004;84(1):140-145.
48. Dwyer C, Guthold M, Falvo M, Washburn S, Superfine R, and Erie D. *Nanotechnology* 2001;13(5):601-604.
49. Chen Q, Dai L, Gao M, Huang S, and Mau A. *The Journal of Physical Chemistry B* 2000;105(3):618-622.
50. Pantarotto D, Partidos CD, Graff R, Hoebeke J, Briand J-P, Prato M, and Bianco A. *Journal of the American Chemical Society* 2003;125(20):6160-6164.
51. Yao Z, Braidy N, Botton GA, and Adronov A. *Journal of the American Chemical Society* 2003;125(51):16015-16024.
52. Kong H, Gao C, and Yan D. *Journal of the American Chemical Society* 2003;126(2):412-413.
53. Kong H, Gao C, and Yan D. *Macromolecules* 2004;37(11):4022-4030.
54. Qin S, Qin D, Ford WT, Resasco DE, and Herrera JE. *Journal of the American Chemical Society* 2003;126(1):170-176.
55. Choi JH, Oh SB, Chang J, Kim I, Ha C-S, Kim BG, Han JH, Joo S-W, Kim G-H, and Paik H-j. *Polymer Bulletin* 2005;55(3):173-179.
56. Hong Ca, You YZ, Wu D, Liu Y, and Pan Cu. *Macromolecules* 2005;38(7):2606-2611.
57. Yoon KR, Kim W-J, and Choi IS. *Macromolecular Chemistry and Physics* 2004;205(9):1218-1221.
58. Mc Carthy B, Coleman JN, Czerw R, Dalton AB, Carroll DL, and Blau WJ. *Synthetic Metals* 2001;121(1-3):1225-1226.
59. Hill DE, Lin Y, Rao AM, Allard LF, and Sun Y-P. *Macromolecules* 2002;35(25):9466-9471.
60. Cui S, Canet R, Derre A, Couzi M, and Delhaes P. *Carbon* 2003;41(4):797-809.
61. Geng Y, Liu MY, Li J, Shi XM, and Kim JK. *Composites Part A: Applied Science and Manufacturing* 2008;39(12):1876-1883.
62. Grossiord N, Loos J, Regev O, and Koning CE. *Chemistry of Materials* 2006;18(5):1089-1099.
63. Vaisman L, Wagner HD, and Marom G. *Advances in Colloid and Interface Science* 2006;128-130(0):37-46.
64. Matyjaszewski K, Coca S, Gaynor SG, Wei M, and Woodworth BE. *Macromolecules* 1998;31(17):5967-5969.
65. Matyjaszewski K and Xia J. *Chemical Reviews* 2001;101:2929 - 2990.
66. Patten TE and Matyjaszewski K. *Advanced Materials* 1998;10(12):901-915.
67. Matyjaszewski K, Wei M, Xia J, and McDermott NE. *Macromolecules* 1997;30(26):8161-8164.
68. Matyjaszewski K, Patten TE, and Xia J. *Journal of the American Chemical Society* 1997;119(4):674-680.
69. Flory PJ, Orwoll RA, and Vrij A. *Journal of the American Chemical Society* 1964;86(17):3507-3514.
70. Flory PJ. *Journal of the American Chemical Society* 1965;87(9):1833-1838.
71. Sanchez IC and Lacombe RH. *The Journal of Physical Chemistry* 1976;80(21):2352-2362.
72. Lacombe RH and Sanchez IC. *The Journal of Physical Chemistry* 1976;80(23):2568-2580.
73. McMaster LP. *Macromolecules* 1973;6(5):760-773.
74. Bank M, Leffingwell J, and Thies C. *Macromolecules* 1971;4(1):43-46.
75. Kwei TK, Nishi T, and Roberts RF. *Macromolecules* 1974;7(5):667-674.
76. Ougizawa T, Inoue T, and Kammer HW. *Macromolecules* 1985;18(10):2089-2092.
77. Clark EA and Lipson JEG. *Polymer* 2012;53(2):536-545.
78. Barlow JW. *Makromolekulare Chemie. Macromolecular Symposia* 1993;70-71(1):235-244.
79. Molau GE. *Journal of Polymer Science Part A: General Papers* 1965;3(4):1267-1278.
80. Molau GE. *Journal of Polymer Science Part A: General Papers* 1965;3(12):4235-4242.
81. Gottschalk A, Mühlbach K, Seitz F, Stadler R, and Auschra C. *Macromolecular Symposia* 1994;83(1):127-146.
82. Auschra C and Stadler R. *Macromolecules* 1993;26(9):2171-2174.
83. Auschra C and Stadler R. *Polymer Bulletin* 1993;30(3):305-311.
84. Kohler J, Riess G, and Banderet A. *European Polymer Journal* 1968;4(1):173-185.
85. Creton C, Kramer EJ, Hui CY, and Brown HR. *Macromolecules* 1992;25(12):3075-3088.
86. Asakura J-I, Yoshihara M, and Maeshima T. *Journal of Polymer Science: Polymer Chemistry Edition* 1981;19(5):1269-1272.
87. Sailer C and Handge UA. *Macromolecular Symposia* 2007;254(1):217-225.
88. Robeson LM. *Polymer Blends: A Comprehensive Review*. Munich: Hanser Gardner Publ 2007.

89. Jordhamo GM, Manson JA, and Sperling LH. *Polymer Engineering & Science* 1986;26(8):517-524.
90. Pötschke P and Paul DR. *Journal of Macromolecular Science, Part C* 2003;43(1):87-141.
91. Ajayan P, Stephan O, Colliex C, and Trauth D. *Science* 1994;265:1212-1214.
92. Jin L, Bower C, and Zhou O. *Applied Physics Letters* 1998;73(9):1197-1199.
93. Qian D, Dickey EC, Andrews R, and Rantell T. *Applied Physics Letters* 2000;76:2868-2870.
94. Ruan SL, Gao P, Yang XG, and Yu TX. *Polymer* 2003;44(19):5643-5654.
95. Dufresne A, Paillet M, Putaux JL, Canet R, Carmona F, Delhaes P, and Cui S. *Journal of Materials Science* 2002;37(18):3915-3923.
96. Probst O, Moore EM, Resasco DE, and Grady BP. *Polymer* 2004;45(13):4437-4443.
97. Andrews R, Jacques D, Minot M, and Rantell T. *Macromolecular Materials and Engineering* 2002;287(6):395-403.
98. Breuer O and Sundararaj U. *Polymer Composites* 2004;25(6):630-645.
99. Lin B, Sundararaj U, and Pötschke P. *Macromolecular Materials and Engineering* 2006;291(3):227-238.
100. Jin Z, Pramoda KP, Xu G, and Goh SH. *Chemical Physics Letters* 2001;337(1-3):43-47.
101. Bhattacharyya AR, Sreekumar TV, Liu T, Kumar S, Ericson LM, Hauge RH, and Smalley RE. *Polymer* 2003;44(8):2373-2377.
102. Siochi EJ, Working DC, Park C, Lillehei PT, Rouse JH, Topping CC, Bhattacharyya AR, and Kumar S. *Composites Part B: Engineering* 2004;35(5):439-446.
103. Zhang WD, Shen L, Phang IY, and Liu T. *Macromolecules* 2003;37(2):256-259.
104. Thostenson ET and Chou TW. *Journal of Physics D: Applied Physics* 2002;35(16):77-80.
105. Cooper CA, Ravich D, Lips D, Mayer J, and Wagner HD. *Composites Science and Technology* 2002;62(7-8):1105-1112.
106. Krishnamoorti R and Giannelis EP. *Macromolecules* 1997;30(14):4097-4102.
107. Du F, Scogna RC, Zhou W, Brand S, Fischer JE, and Winey KI. *Macromolecules* 2004;37(24):9048-9055.
108. Mitchell CA, Bahr JL, Arepalli S, Tour JM, and Krishnamoorti R. *Macromolecules* 2002;35(23):8825-8830.
109. Pötschke P, Abdel-Goad M, Alig I, Dudkin S, and Lellinger D. *Polymer* 2004;45(26):8863-8870.
110. Bauhofer W and Kovacs JZ. *Composites Science and Technology* 2009;69(10):1486-1498.
111. Moisala A, Li Q, Kinloch IA, and Windle AH. *Composites Science and Technology* 2006;66(10):1285-1288.
112. Ma PC, Kim J, and Tang BZ. *Composites Science and Technology* 2007;67(14):2965-2972.
113. Zhang W, Dehghani-Sanij A, and Blackburn R. *Journal of Materials Science* 2007;42(10):3408-3418.
114. Li J, Sham ML, Kim J-K, and Marom G. *Composites Science and Technology* 2007;67(2):296-305.
115. Sandler JKW, Kirk JE, Kinloch IA, Shaffer MSP, and Windle AH. *Polymer* 2003;44(19):5893-5899.
116. Li J, Ma PC, Chow WS, To CK, Tang BZ, and Kim JK. *Advanced Functional Materials* 2007;17(16):3207-3215.
117. Du F, Fischer JE, and Winey KI. *Journal of Polymer Science Part B: Polymer Physics* 2003;41(24):3333-3338.
118. Bai JB and Allaoui A. *Composites Part A: Applied Science and Manufacturing* 2003;34(8):689-694.
119. Georgakilas V, Kordatos K, Prato M, Guldi DM, Holzinger M, and Hirsch A. *Journal of the American Chemical Society* 2002;124(5):760-761.
120. Ramasubramaniam R, Chen J, and Liu H. *Applied Physics Letters* 2003;83(14):2928-2930.
121. Tiusanen J, Vlasveld D, and Vuorinen J. *Composites Science and Technology* 2012;72(14):1741-1752.
122. Gao J, Li Z, Meng Q, and Yang Q. *Materials Letters* 2008;62(20):3530-3532.
123. BP G. *Macromol Rapid Commun* 2010;31(3):247-257.
124. Ma PC, Tang BZ, and Kim J-K. *Carbon* 2008;46(11):1497-1505.

Chapter 3

Experimental Part

3.1 Materials

Commercial poly(styrene-*co*-acrylonitrile) (SAN, Luran® 358N) was provided in granular form by BASF SE (Ludwigshafen, Germany). The content of acrylonitrile was 25 wt%. Poly(2,6-dimethyl-1,4-phenylene ether) (PPE, PX100F) powder was supplied by Mitsubishi Engineering Plastics Europe (Düsseldorf, Germany). The properties of as-received materials are listed in Table 3.1. Irganox 1010 and Irgafos 168 (Sigma Aldrich, Schnelldorf, Germany) were used as stabilisers for PPE during melt processing at a concentration of 0.1 wt% with respect to the total amount of SAN and PPE. The weight ratio of Irganox 1010 to Irgafos 168 was 2.

Table 3.1 Molecular weights and thermal characterization as well as the viscosities of used SAN and PPE

Substance	Grade	Average molecular weight ^(a) [kg/mol]		PDI ^(a)	T_g ^(b) [°C]	η_0 ^(c) [Pas]
		M_n	M_w			
SAN	Luran® 358N	83	161	1.95	108	900
PPE	PX 100F	12	28	2.42	213	45600

(a) The molecular weight was determined by gel permeation chromatography

(b) The T_g of polymers was detected by differential scanning calorimetry

(c) The viscosity at zero shear rate was determined by analysis of shear oscillations at low frequencies at 260°C.

Pristine multi-walled carbon nanotubes (MWCNT), amino functionalized MWCNT (MWCNT-NH₂) and hydroxyl-functionalized MWCNT (MWCNT-OH) were obtained from FutureCarbon GmbH (Bayreuth, Germany) with a purity of >90 % and a diameter of ~15 nm. The length of MWCNT was in the range of 10-50 µm. The number of walls of MWCNT was about 10 and the specific surface area of MWCNT was about 250 m²/g.

Methyl methacrylate (MMA, ≥99%), styrene (≥99%), 2-bromo-2-methylpropionyl bromide (2BriBr, 99%), ethyl 2-bromoisobutyrate (EBiB, 99%), triethyl amine (TEA, ≥99.5%), dimethylaminopyridine (DMAP, 97%), copper (I) bromide (Cu(I)Br, 99%), copper (I) chloride (CuCl, ≥99%), copper (II) chloride (CuCl₂, ≥99%), N, N, N', N', N-pentamethyl diethylenetriamine (PMDETA, 97%), diethyl ether (≥99%), furfuryl alcohol (≥98%), tetrahydrofuran (THF), chloroform (≥99%) and anisole were used as received. All the reagents were purchased from Sigma-Aldrich (Schnelldorf, Germany).

3.2 Functionalization of MWCNT by “grafting-from” method via ATRP

3.2.1 Anchoring initiator on the surface of MWCNT

The procedure of anchoring initiator onto MWCNT-NH₂ followed the work reported by Ryu et al. [1]. It is noteworthy that the scale of the reaction was significantly increased in order to prepare sufficient amount of nanotubes in one batch for melt processing step. In our up-scaled reaction, 9.6 g as-received MWCNT-NH₂ were dispersed in THF (1.156 L) by treating in an ultrasonication bath for 5 min (Bandelin SONOREX, frequency of 35 KHz, 160 W). Then, the suspension was vigorously stirred under argon flow and 40 ml TEA was dropwise added. Afterwards, oxygen was purged out from the reactor by switching between the vacuum and the argon flow for thrice. Subsequently, the anchoring reaction was produced after injecting a diluted solution of 2BriBr (32 ml) in THF (160 ml) at 0 °C. The mixture was still kept stirring at such low temperature for 2 hours and warmed up at ambient temperature for 48 hours. When the reaction was completed, the black product was separated and washed by chloroform for several times until no green filtrate was observed. Lastly, the obtained MWCNT with initiator (MWCNT-Br) was dried in an oven under vacuum at room temperature for one week.

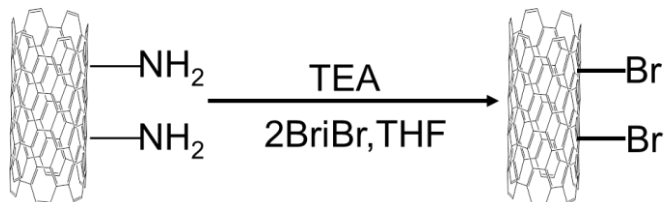


Fig. 3.1 Scheme of anchoring initiator on the surface of MWCNT-NH₂

Similar procedure was applied in anchoring initiator on hydroxyl functionalized MWCNT (MWCNT-OH), except for the use of a mixture of DMAP and TEA as catalyst instead of

TEA. The experimental scheme is shown in Fig. 3.2. In the following text, the notation of MWCNT-Br will be used to indicate all the MWCNT with initiator including the ones prepared either from MWCNT-NH₂ or from MWCNT-OH.

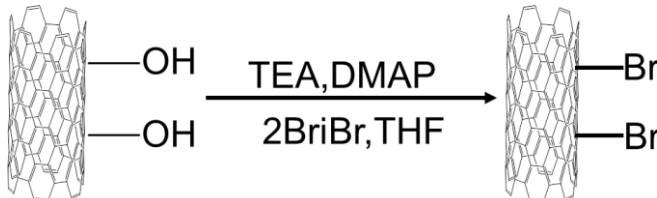


Fig. 3.2 Scheme of anchoring initiator on the surface of MWCNT-OH

3.2.2 Functionalization of MWCNT with homopolymers via ATRP

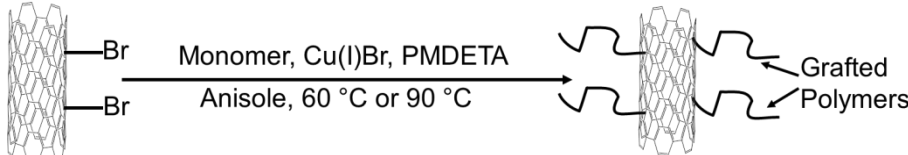


Fig. 3.3 Scheme of functionalizing MWCNT with homopolymers via ATRP

The functionalization of MWCNT with polystyrene was carried out following the work of Albuerne et al. [2]. In a typical reaction, 2 g MWCNT-Br, 97 ml styrene (0.848 mol), 24 ml anisole (25 % v/v with respect to the monomer) and 0.2 mol% of Cu(I)Br (with respect to the monomer) were dispersed in a glass flask under argon. 1 mol% of EBiB (with respect to the molar amount of initiator on MWCNT) was added drop by drop as sacrificial initiator. The system was vigorously stirred by means of a magnet for 1 hour. Then, 0.2 mol% of PMDETA (with respect to the monomer) was added and the flask was transferred into an oil bath at 90 °C. In order to obtain PS with different molecular weight, separate reactions were carried out for desired reaction time under the same parameters, respectively. When the reaction was completed, the mixture was diluted with THF and precipitated in methanol. The precipitated

product was filtered and dried for 48 hours under vacuum. Then, functionalized MWCNT with PS (MWCNT-PS) were again dispersed in THF and filtered. This procedure was repeated until no traces of polymer were collected from the filtered solution by precipitation in methanol. The conditions of functionalizing MWCNT with polystyrene are listed in Table 3.2. The functionalized MWCNT were dried in a vacuum oven at room temperature for one week before filling in polymer blends.

Table 3. 2 Experimental conditions employed for functionalizing MWCNT with polystyrene

Code	[Br] [mmol/g]	Monomer : initiator [molar ratio]	CuBr:PMDETA:Initiator [molar ratio]	Temperature [°C]	Reaction time
MWCNT-PS-12	0.379	500:1	1:1:1	90	12 h
MWCNT-PS-24	0.379	500:1	1:1:1	90	24 h
MWCNT-PS-48	0.379	500:1	1:1:1	90	48 h

The functionalization of MWCNT with PMMA used similar procedure in the case of MWCNT-PS. Owing to the relative high kinetic constant, lower temperature and shorter reaction time were utilized for polymerization of MMA. The optimized reaction conditions for polymerizing PMMA via ATRP in the presence of MWCNT are listed in Table 3.3.

Table 3.3 Experimental conditions employed for functionalizing MWCNT with poly(methyl methacrylate)

Code	[Br] [mmol/g]	Monomer: initiator [molar ratio]	CuBr:PMDETA:Initiator [molar ratio]	Temperature [°C]	Reaction time
MWCNT-PMMA-0.5	0.433	1000:1	1:1:1	60	0.5 h
MWCNT-PMMA-1	0.433	1000:1	1:1:1	60	1 h
MWCNT-PMMA-3	0.433	1000:1	1:1:1	60	3 h

3.2.3 Functionalization of MWCNT with P(MMA-*co*-S) random copolymers via ATRP

The procedure for functionalization of MWCNT with P(MMA-*co*-S) random copolymers (MWCNT-*CO*-X, where X is the reaction time) via ATRP is similar to the one for preparing MWCNT-PS described in Section 3.2.2. The detailed conditions are given in Table 3.4.

 Table 3.4 Experimental conditions employed for functionalizing MWCNT with P(MMA-*co*-S)

Code	[Br] [mmol/g]	Monomer : initiator ^(a)	MMA: Styrene ^(a)	CuCl: CuCl ₂ ^(a)	Copper salts : PMDETA: Initiator ^(a)	Temperature [°C]	Reaction time
MWCNT- <i>CO</i> -3	0.403	800:1	1:1	0.8:0.2	1:1:0.25	125	3 h
MWCNT- <i>CO</i> -4	0.403	800:1	1:1	0.8:0.2	1:1:0.25	125	4 h
MWCNT- <i>CO</i> -5	0.403	800:1	1:1	0.8:0.2	1:1:0.25	125	5 h
MWCNT- <i>CO</i> -6	0.403	800:1	1:1	0.8:0.2	1:1:0.25	125	6 h
MWCNT- <i>CO</i> -7	0.403	800:1	1:1	0.8:0.2	1:1:0.25	125	7 h

(a) The ratios among components are molar ratios

In a typical reaction, 500 mg MWCNT-Br were dispersed in a liquid mixture of 8.7 ml MMA, 9.3 ml styrene and 18 ml anisole. After being treated by ultrasonication for 5 minutes (Bandelin SONOREX, frequency of 35 kHz, 160 W), 0.5 mol% copper salts (with respect to the total amount of monomers, including CuCl and CuCl₂ with a weight ratio of 0.8 to 0.2) were added. Then, the system was vigorously stirred under argon atmosphere for one hour. Once 0.5 mol% PMDETA (with respect to the total amount of monomers) were fed, the flask was rapidly moved into an oil bath at a temperature of 125 °C. After a desired time, the product was precipitated in methanol and washed with THF for several times to dissolve the free polymers which were unanchored on MWCNT. Before filling into the polymeric matrix, the functionalized MWCNT were dried in an oven under vacuum at room temperature for one week. In order to obtain functionalized MWCNT with different molecular weight of copolymers, most reaction parameters in different reactions were unaltered, whereas, the time of each reaction varied.

3.3 Functionalization of MWCNT by “grafting-to” method via Diels-Alder reaction

3.3.1 Synthesis of furfuryl-2-bromoisobutyrate

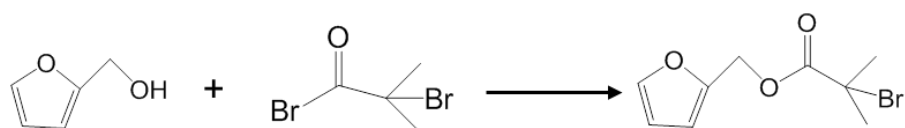


Fig. 3.4 Scheme of synthesis of furfuryl-2-bromoisobutyrate

The procedure was started from anchoring initiator onto furfuryl alcohol through typical esterification reaction between alcohol and acid bromide, following the work of Munirasu et al. [3]. During the synthesis of furfuryl-2-bromo isobutyrate, 10 ml of furfuryl alcohol (116 mmol), 9.7 ml of TEA and 350 ml of dried diethyl ether were taken into a round bottom flask. Then, the flask was cooled down below 0 °C by emerging into an ice bath. After the temperature became stable, a mixture of 17.5 ml of 2-bromo isobutyryl bromide and 50 ml diethyl ether was dropwise added into the flask. The system was vigorously stirred for 24 hours at room temperature. Afterwards, the liquid raw product was washed with water and passed through basic aluminum column. Lastly, the obtained product was dried with magnesium sulfate.

3.3.2 Synthesis of furfuryl-capped polymers via ATRP

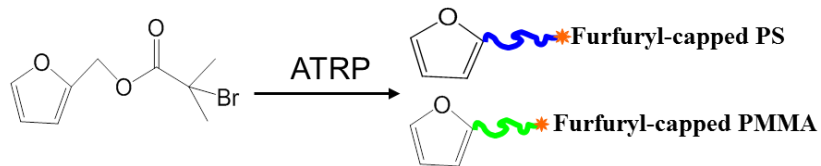


Fig. 3.5 Scheme of synthesis furfuryl-capped polymer via ATRP

The polymerization of monomers on furfuryl-based initiator followed similar procedure to the one of grafting homopolymers on MWCNT via ATRP which has been described in Section 3.2.2. For synthesis of furfuryl-capped polystyrene (Fp-PS), furfuryl-2-bromo isobutyrate, styrene, anisole and CuBr were added in a round bottom flask with a certain molar ratio. Then, the flask was purged with argon flow for one hour and PMDETA was fed into the system by syringe. During the whole procedure, the system was vigorously stirred. After a

desired reaction time, Fp-PS was obtained by precipitating the substance into methanol. Before reacting with MWCNT, the products were dried in a vacuum oven under room temperature for 48 hours. Polymerization of furfuryl-capped MMA (Fp-PMMA) was carried out under similar conditions. The reaction conditions are listed in Table 3.5.

Table 3.5 Experimental conditions employed for synthesizing furfuryl-capped polymers

Monomer	Monomer : initiator [molar ratio]	Initiator: CuBr: PMDETA [molar ratio]	Temperature [°C]
Styrene	150	1:1:1	90
MMA	150	1:1:1	60

3.3.3 Functionalization of MWCNT via Diels-Alder reaction

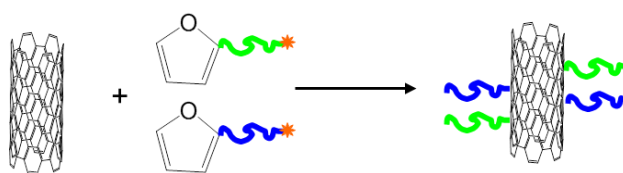


Fig. 3.6 Scheme of functionalization of MWCNT via Diels-Alder reaction

In a typical reaction, 0.5 g pristine MWCNT were dispersed in 200 ml DMP and treated in an ultrasonication bath for 30 min (Bandelin SONOREX, frequency of 35 kHz, 160 W). Then, 250 mg Fp-PMMA and 250 mg Fp-PS were fed into the suspension under vigorously stirring. After being purged by argon flow for one hour, the flask was emerged into an oil bath at 80 °C for 24 hours. The raw product was washed by THF for several times until no excessive polymer can be collected from the filtrate. Lastly, the obtained MWCNT were dried in a vacuum oven at room temperature for one week.

3.4 Preparation of SAN/PPE composites containing functionalized MWCNT with polystyrene



Fig. 3.7 Scheme of preparation of SAN/PPE blends filled with MWCNT-PS

The preparation of the SAN/PPE blends with MWCNT was divided into two steps which are shown in Fig. 3.7. Firstly, MWCNT were pre-mixed with SAN using solution casting. The given amount of MWCNT was dispersed in chloroform and treated by ultrasonic probe (Bandelin SONOPULS, frequency of 20 kHz, 60 W) for 30 min and ultrasonic bath (Bandelin SONOREX, frequency of 35 kHz, 160 W) for 1 hour, respectively. Then, the MWCNT suspension was mixed with an SAN solution in chloroform. The concentration of dissolved SAN was 5 wt% in chloroform. The concentration of MWCNT with respect to SAN was 2.5 wt% so that the concentration of MWCNT should be 1 wt% in the SAN/PPE 40/60 blend. After stirring vigorously for 24 hours, the suspension was directly cast in Teflon® moulds and kept on the heating plate at 40 °C for 1 day. Subsequently, the cast material was dried under vacuum at 40 °C for one more day. In order to sufficiently evaporate the solvent, the pre-mixed SAN composites with MWCNT were cut into small particles by an electrical grinder. Before melt processing, the pre-mixed particles were dried under vacuum at 80 °C for two weeks.

The composites based on SAN/PPE were prepared by blending the pre-mixed SAN/MWCNT powder with PPE through melt extrusion. Prior to blending, the obtained SAN/MWCNT

powder and PPE powder were dried at 80 °C under vacuum for at least 12 hours. The components were melt-blended in a micro-compounder with a filling volume of 15 cm³ (DSM Xplore, Geleen, Netherlands) at 300 °C. The speed of revolutions was 100 rpm and the mixing time was set to 5 minutes. The specimens for morphological and rheological measurements were prepared by using a micro-injection moulding machine with a filling volume of 12 cm³ (DSM Xplore, Geleen, Netherlands). The temperature in the injection chamber was 280 °C and the mould temperature was set to 100 °C. The pressure for shooting was set to 4 bar for 4 seconds. A pressure of 6 bar for 4 seconds was set for the holding process.

The neat SAN/PPE blend was prepared under the same conditions of melt processing as described above. Furthermore, the specimens of SAN/MWCNT composites were also fabricated by a similar procedure but under different conditions. In the case of SAN/MWCNT composites, the temperature for extrusion was 220°C. In the injection chamber, it was 200 °C and the mould temperature was set to 100 °C. Except of these parameters, the other conditions were the same as the ones for preparing the composites based on SAN/PPE blends.

3.5 Preparation of SAN/PPE composites containing functionalized MWCNT with random copolymers

The preparation of SAN/PPE composites containing functionalized MWCNT with copolymers started directly from mixing the suspension of MWCNT with both SAN and PPE together in chloroform without a pre-mixing step. However, before solution blending,

MWCNT fillers still needed to be treated by sonication to get a better dispersion in the solvent. The procedures of solution casting and melt processing were the same as the preparation of blending composites with MWCNT-PS which is described in Section 3.3.

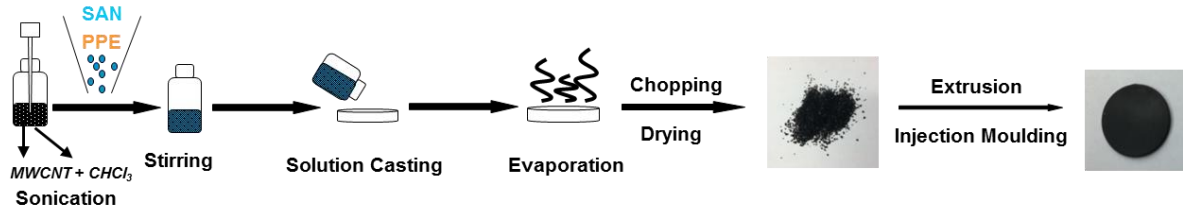


Fig. 3.8 Scheme of preparation of SAN/PPE blends filled with MWCNT-CO

3.6 Characterization

3.6.1 Differential scanning calorimetry

The glass transition temperature T_g of SAN and PPE was measured by differential scanning calorimetry (DSC) using a Netzsch DSC Phoenix. The equipment was calibrated using indium and cyclohexane. Standard aluminum pans of 50 μl were used to encapsulate the sample. The mass of the samples was approximately 10 mg. The samples were first heated up to 250 °C, cooled down to 25 °C, and heated up again to 250 °C for the second circle. All measurements were done under nitrogen atmosphere at a constant heating and cooling rate of 10 °C/min. The T_g value was determined based on inflection temperature of the second heating cycle.

3.6.2 Nuclear magnetic resonance spectroscopy

Nuclear magnetic resonance spectroscopy ($^1\text{H-NMR}$) was carried out using a Bruker AV-300

(Bruker BioSpin Co. Ltd, Karlsruhe, Germany) at 300 MHz. The solvent for measurements was CDCl₃. In case of detect of functionalized MWCNT, the measured polymer were the free polymers in the system which were not grafted on the surface of nanotubes.

3.6.3 Gel permeation chromatography

The average molecular weights of the neat polymer components and the grafted polymers were characterized by gel permeation chromatography (GPC) and analysis by a UV detector using THF as a solvent and standard polystyrene (PS) as calibration.

3.6.4 Thermal gravimetric analysis

Thermal gravimetric analysis (TGA) was carried out using a TGA device Netzsch TG209 F1 Iris (Netzsch-Gerätebau GmbH, Selb, Germany). The measurements were conducted at constant argon flow with a flow rate of 20 ml/min. The temperature range was 25 °C to 1000 °C, and the heating rate was 10 °C/min.

3.6.5 Fourier transform infrared spectroscopy

The Fourier transform infrared spectra (FT-IR) measurements were carried out using a Bruker Equinox 55 (Bruker Optics, Ettlingen, Germany). The MWCNT samples were carefully dispersed in potassium bromide (KBr) and compressed into pellets under high loading. The content of carbon nanotubes in KBr pellets was 0.1 wt% in the case of pristine MWCNT and MWCNT-NH₂ as well as MWCNT-Br, while, the concentration was 0.5 wt% in the case of

functionalized MWCNT with polymers. The infrared spectra were recorded in a spectral range of 600-3200 cm⁻¹ with a spectral resolution of 1 cm⁻¹.

3.6.6 Transmission and scanning electron microscopy

The morphological properties of composites were characterized by transmission electron micrographs (TEM) using a Tecnai G2 F20 (FEI) operated at an acceleration voltage of 200 kV in bright field mode. Ultrathin sections with a thickness of about 50 nm-100 nm were cut at room temperature from the injection-molded round disks for rheological experiments by means of a Leica Ultracut UCT microtome (Leica Microsystems, Wetzlar, Germany) equipped with a diamond knife. As the high stiffness of MWCNT, some micrographs show stripes from the cutting direction of the diamond knife. These stripes were removed by eliminating the respective signals in the Fourier transformation of the image and then back transforming to the filtered image following a procedure described by Michler [4].

Scanning electron microscopy (SEM) was utilized to determine the miscibility of SAN and grafted PS with high molecular weight. The experiment was carried out with a LEO Gemini 1550VP from Zeiss. The extruded sample was broken under liquid nitrogen condition. Then the sample was sputtered with a Pt layer with a thickness of 1.5 nm for analysis of the cross section.

3.6.7 Rheological measurement

The rheological properties of materials were analyzed using the rotational rheometer ARES

(Rheometrics Scientific, Piscataway, USA) in parallel-plates configuration. The diameter of the samples was 20 mm and the gap was 1.6 mm. In order to minimize thermal degradation, all measurements were performed in a nitrogen atmosphere. The temperature for all tests was 260 °C. The time for annealing the samples was 8 minutes before each test. The thermal stability was characterized by dynamic time sweeps at an angular frequency ω of 0.5 rad/s and a strain amplitude γ_0 of 10%. The storage and loss moduli as well as complex viscosity were measured as a function of angular frequency in a range of 0.01-100 rad/s starting at the largest frequency. Prior to these measurements, dynamic strain sweeps were carried out in the range of 1-10% at an angular frequency of 10 rad/s in order to determine the linear viscoelastic region.

3.6.8 Dielectric spectroscopy

Broadband dielectric measurements were performed using an alpha-AN high resolution dielectric analyzer (Novocontrol Technologies GmbH, Hundsangen). The samples had a disk-like shape with a diameter of 25 mm and a height of approx. 1.57 mm. Two platinum electrodes with diameters of 20 mm and 30 mm were used for the measurements. No additional support for the electrical contact like conductive silver was used. At each temperature, 49 different frequencies in the range of 10^7 Hz to 10^{-3} Hz were measured.

References

1. Ryu J, Ramaraj B, and Yoon KR. Surface and Interface Analysis 2009;41(4):303-309.
2. Albuerne J, Boschetti-de-Fierro A, and Abetz V. Journal of Polymer Science Part B: Polymer Physics 2010;48(10):1035-1046.

Chapter 3

3. Munirasu S, Albuerne J, Boschetti-de-Fierro A, and Abetz V. Macromolecular Rapid Communications 2010;31(6):574-579.
4. Michler GH. Electron Microscopy of Polymers. Berlin Heidelberg: Springer, 2008.

Chapter 4

Functionalization of carbon nanotubes

4.1 Introduction

Although CNT open a promising potential of novel composites with good properties, aggregation of pristine MWCNT originating from the strong π - π stacking interactions between graphene sheets weakens the performance of materials [1, 2]. To solve this issue, modification on the surface of CNT is an effective way to improve the dispersibility of CNT and the affinity between CNT and polymer matrices. Moreover, functionalization is one possible approach to tuning the localization of CNT in multi-phase blends by introducing desired polymer groups. Grafting methods for functionalizing CNT are generally classified into two approaches: “*grafting-from*” and “*grafting-to*” polymerization.

The main advantage of the “*grafting-from*” method is the possibility to obtain functionalized CNT with high concentration of grafted polymer [3]. Controlled radical polymerization is one of most effective and widely used techniques to realize the “*grafting-from*” method, such as the atom transfer radical polymerization (ATRP) reaction. The details of ATRP have been discussed in Chapter 3. Owing to the good controllability, various molecular weights of polymer can be grafted on MWCNT by adjusting the reaction of ATRP. Up to now, several works have reported successful functionalization of MWCNT via ATRP, especially in the cases of grafting polystyrene (PS) and poly(methyl methacrylate) (PMMA) [4-7].

In contrast to the “*grafting-from*” method, the way of “*grafting-to*” could be more facile with one-step reaction in presence of CNT. Diels-Alder (DA) cycloaddition reaction is one of them which can be carried out without byproduct and catalyst. The possibility of the DA reaction for modifying CNT was first reported in 2002 and has been confirmed by experimental results [8]. Munirasu et al. [9] investigated the application of DA reaction on various carbonaceous materials, including single-walled and multi-walled carbon nanotubes as well as carbon fiber. Moreover, the nanotubes were used as both diene and dienophile in company with suitable functional compounds. However, due to the limited reactivity of MWCNT, the extent of functionalization via DA is still not as high as the one prepared by “*grafting-from*” method.

In present chapter, the functionalization of multi-walled carbon nanotubes (MWCNT) by both “*grafting-from*” and “*grafting-to*” will be presented. The “*grafting-from*” functionalization started from anchoring initiator on MWCNT. PS and PMMA were polymerized from the anchored initiators via ATRP reaction under appropriate conditions, respectively. The influence of reaction time on the molecular weight of grafted polymer will be discussed. Besides of homopolymers, MWCNT were also functionalized with random copolymers containing both styrene and MMA units. Furthermore, at the end of this part, an initial attempt of functionalizing MWCNT via DA reaction will be presented.

4.2 Results and discussion

4.2.1 Anchoring Initiator onto the surface of MWCNT

Anchoring initiator onto MWCNT can be realized using two typical kinds of functionalized MWCNT: hydroxyl functionalized MWCNT (MWCNT-OH) and amino functionalized MWCNT (MWCNT-NH₂). In order to select the more suitable kind of MWCNT, anchoring

reactions were carried out in both cases under similar and optimized conditions obtain comparable results. Only the concentrations of reactive group (hydroxyl and amino group) were different since the commercial products were used as-received. Considering the low reactivity of MWCNT, an excess amount of 2BriB ($3.3 \mu\text{L}/\text{mg}$, respect to amount of MWCNT) was used for the reactions compared to the concentration of reactive group on MWCNT. Table 4.1 lists the concentration of initiator on different MWCNT after anchoring reaction, which were estimated from TGA results (see Fig. 4.1).

Table 4.1 Reaction conditions and concentrations of anchored initiator on MWCNT

Code	Scale [mg]	$[2\text{BriB}]^{\text{(a)}}$ [ml/g]	$[\text{OH}] \text{ or } [\text{NH}_2]^{\text{(b)}}$ [mmol/g]	$[\text{Br}]^{\text{(b)}}$ [mmol/g]
MWCNT-OH-Ini	1200	3.33	0.447	0.07
MWCNT-NH ₂ -Ini	1200	3.33	0.577	0.453

(a) The concentration of 2BriB (ml) respect to MWCNT (mg)

(b) The content of initiator on MWCNT was calculated according to TGA results

From the results, it indicates the fact that, although the reaction conditions are similar, the concentration of initiator in the case of MWCNT-OH is lower in contrast to the tubes with amino group. The main reason should be attributed to the much lower reactivity of hydroxyl group than the amino group [10]. Furthermore, in the as-received commercial products, the concentration of hydroxyl group is not as high as the amino group on the surface of MWCNT, which also can decrease the efficiency of MWCNT-OH in the reaction. Albuerne et al. [5] systematically studied the functionalization of commercial MWCNT supplied by FutureCarbon GmbH. In their work, the concentration of anchored initiator was found to increase with the concentration of 2BriB used in the reaction. The highest concentration they obtained was 0.240 mmol/g using a large amount of 2BriB ($5.4 \mu\text{L}/\text{mg}$, respect to amount of MWCNT). This value is lower than the results of anchoring initiator onto MWCNT-NH₂.

Based on these results, the MWCNT-NH₂ is selected to be used as immobile initiator substance in this work, which can prepare functionalized MWCNT with high density initiator.

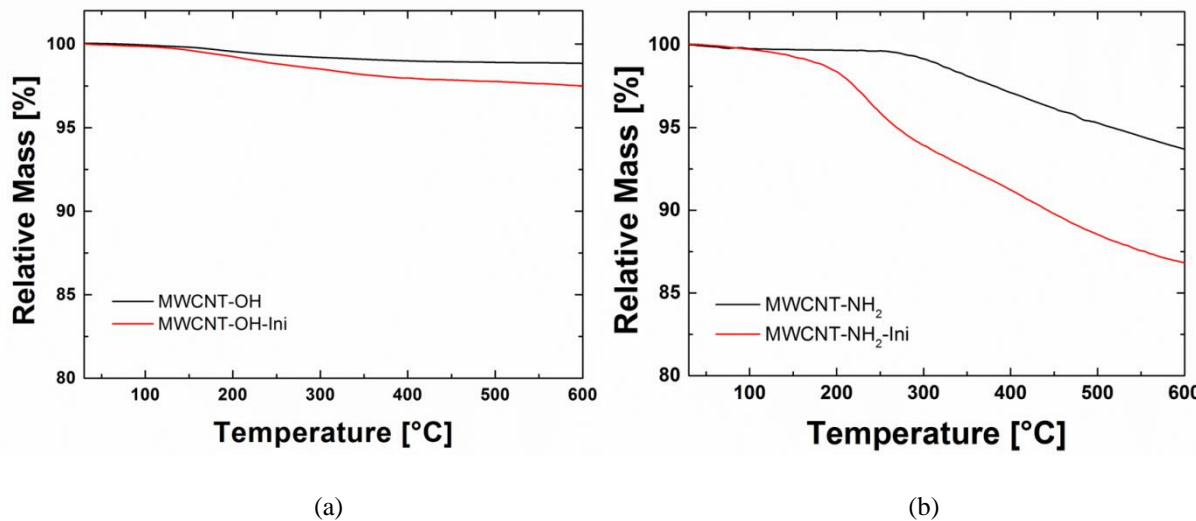


Fig. 4.1 TGA results of anchoring initiator onto MWCNT-OH (a) and MWCNT-NH₂ (b)

In many previous studies, the reactions for functionalization of MWCNT via ATRP were just carried out at small scales (generally about dozens of milligram). However, the required amount of MWCNT for preparing standard specimens for several measurements, e.g., rheological measurement and dielectric spectroscopy, are quite larger than the outcome from a small lab-scale in previous works. Therefore, an up-scaling of functionalization reactions is necessary for further preparation of composites. Table 4.2 shows the conditions and obtained initiator concentration of reactions for anchoring initiator at different scales. From these data, the concentration of the amino groups shows a significant influence on the concentration of anchored initiator. Under the same reaction condition, when the concentration of amino groups is in the range of 0.5 to 0.7 mmol/g, a relatively high density of initiator can be achieved. On the other hand, if the concentration of amino groups is higher than 0.7 mmol/g, MWCNT with a low concentration of initiator would be obtained. For instance, in the case of MWCNT-NH₂-Ini-2, the density of anchored initiator is 0.210 mmol/g, of which functionalized MWCNT are prepared from the as-received MWCNT-NH₂ with 0.779 mmol/g amino group. Compared to this sample, MWCNT-NH₂-Ini-1 with higher concentration of

initiator (0.453 mmol/g) is prepared from as-received MWCNT-NH₂ which only 0.577 mmol/g amino group. Similar phenomenon was also described in the work of Majeed [11], where MWCNT-NH₂ supplied from FutureCarbon GmbH were used. Based on these results, we consider that it probably exists a density limitation of anchored initiator. The excessive amino group might be hindered by the anchored initiator group, so that, the utilization coefficient of amino group is reduced when the concentration of amino group is relatively high (higher than ~0.6 mmol/g).

Table 4.2 Anchoring initiator on MWCNT-NH₂ with different reaction scales

Code	Scale [g]	[2BriB] ^(a) [ml/g]	[TEA] ^(b) [ml/g]	[NH ₂] ^(c) [mmol/g]	[Br] ^(c) [mmol/g]
MWCNT-NH ₂ -Ini-1	1.2	3.33	4.17	0.577	0.453
MWCNT-NH ₂ -Ini-2	1.2	3.33	4.17	0.779	0.210
MWCNT-NH ₂ -Ini-3	2.4	3.33	4.17	0.779	0.219
MWCNT-NH ₂ -Ini-4	9.6	3.33	4.17	0.627	0.433
MWCNT-NH ₂ -Ini-5	9.6	3.33	4.17	0.644	0.379
MWCNT-NH ₂ -Ini-6	9.6	3.33	4.17	0.644	0.403

(a) The concentrations of 2BriB (ml) respect to MWCNT (g);

(b) The concentrations of TEA (ml) respect to MWCNT (g);

(c) The content of amino group and initiators on MWCNT were determined by TGA results.

On the other hand, the reaction presents more or less reproducible when the amino density is constant. As seen in the Table 4.2, the concentrations of initiator in the sample of MWCNT-NH₂-Ini-2 and MWCNT-NH₂-Ini-3 are very close to each other, which were prepared from the same batch of as-received MWCNT-NH₂ with the same density of amino groups on the tubes. This stability is constant even when the reaction scale is increased (see sample MWCNT-NH₂-Ini-5 and MWCNT-NH₂-Ini-6).

4.2.2 Functionalization of MWCNT with polystyrene

The reaction for functionalizing MWCNT with polystyrene (PS) was carried out under optimized conditions which are described in Chapter 3. Figure 4.2 gives the TGA results of functionalized MWCNT and also the DTG curve of two kinds of functionalized MWCNT with PS. The peaks of the DTG curves are located between 330 °C and 470 °C and approximately constant mass occurs above 500 °C. Thus, the mass loss of grafted polymer is determined by the data in the temperature range from 100 °C to 550 °C for each sample. In the case of pristine MWCNT, the weight loss slightly increased and no pronounced and clear characteristic peak could be seen in the DTG curve. Therefore, we only present the DTG of functionalized MWCNT with polystyrene. In Fig 4.2 (a), the received MWCNT-NH₂ show a weight loss of 5.9 wt% corresponding to a concentration of amino groups of 6.4 mmol/g on the surface of MWCNT. After the anchoring process, 0.379 mmol/g (11.6 wt%) initiator was successfully bound to the MWCNT. As the reaction time is too short to get long polymer chains, the weight loss of MWCNT-PS-12 is only 14 wt% which is a very slight enhancement from MWCNT-Br. After 24 hours, the contents of grafted PS remarkably increase. In case of functionalized MWCNT with a relatively low molecular weight of PS (21 kg/mol), the content of grafted polymer is 28 wt% with respect to the total weight of functionalized MWCNT. When molecular weight of grafted polymer increases to 73 kg/mol, the weight loss considerably attains to 76 wt%. Moreover, the polymerization presents a good controllability with a narrow PDI (approx. 1.1) in each sample. It is also noteworthy that, the ratio of weight loss to molecular weight is 1.30×10^{-5} in the case of MWCNT-PS-24, while, the value of MWCNT-PS-48 is 1.04×10^{-5} . Thus, the content of grafted polymer presents proportional increment with the molecular weight to same extent.

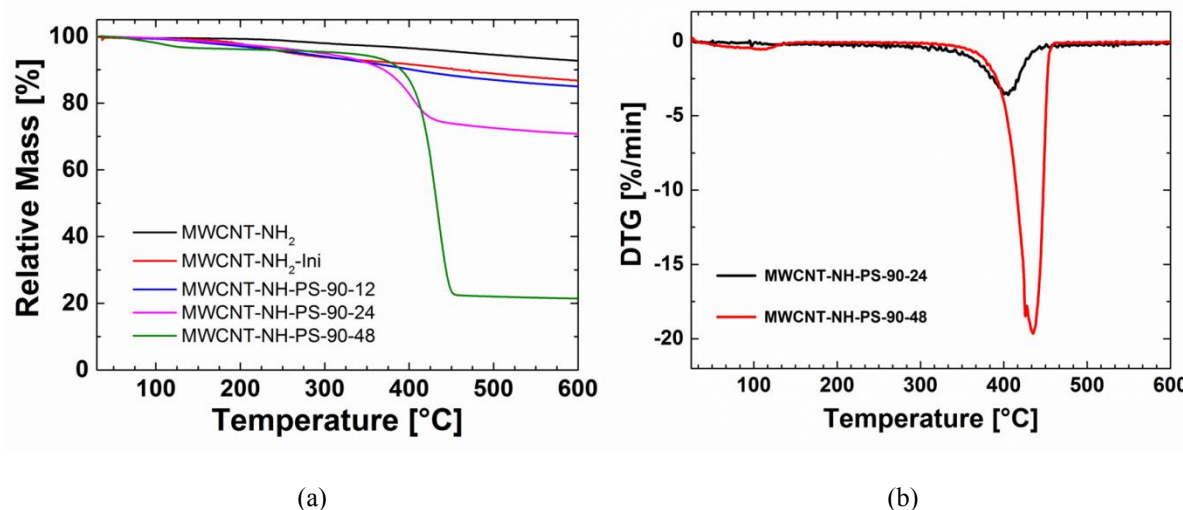


Fig. 4.2 TGA and DTG results of functionalization of MWCNT-NH₂ via ATRP

The properties of obtained functionalized MWCNT with PS are summarized in Table 4.3. Compared to other available monomers for ATRP, styrene shows a slower polymerization rate. After 12 h, no polymer powder is obtained by precipitation. However, due to the well construability of the reaction, different molecular weights of PS could be synthesized on MWCNT by adjusting the time for ATRP. Polymers with low molecular weight of 21 kg/mol are obtained after 24 h. The molecular weight increases with reaction time to 73 kg/mol in the case of MWCNT-NH-PS-48.

Table 4.3 Summary of MWCNT functionalized with polystyrene

Codes	[Br] ^(a) [mmol/g]	Time [hours]	Weight loss ^(a) [wt%]	M_n ^(b) [kg/mol]	PDI ^(b)	Weight loss/ M_n [wt% / g/mol]
MWCNT-PS-12	0.379	12	14	--	--	--
MWCNT-PS-24	0.379	24	28	21.0	1.08	1.30×10^{-5}
MWCNT-PS-48	0.379	48	76	73.0	1.13	1.04×10^{-5}

(a) The content of initiators and grafted polymers on MWCNT were estimated by TGA results

(b) The molecular weight and PDI of grafted polymers were determined by GPC

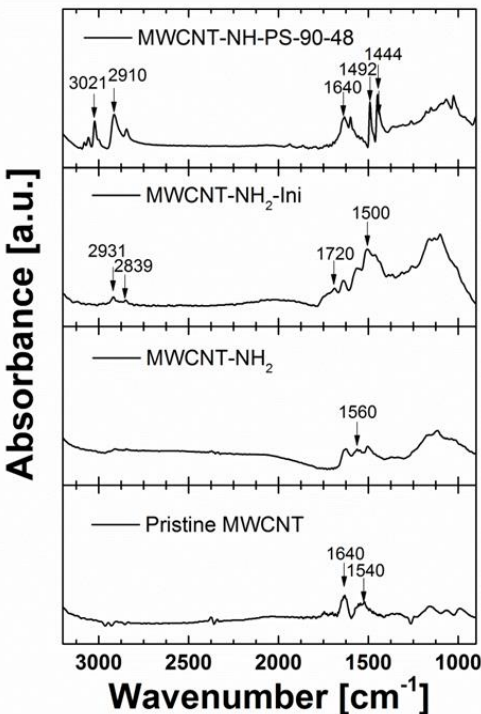


Fig. 4.3 FT-IR spectra of pristine MWCNT and different functionalized MWCNT

FT-IR spectra of pristine MWCNT and functionalized MWCNT are presented in Fig. 4.3. Compared to pristine MWCNT, the typical signals for aromatic systems ($900\text{-}1200\text{ cm}^{-1}$) are detected in all spectra of the functionalized MWCNT samples, which results from the covalent functionalization on the surface of the tubes [12]. The signal between 1650 cm^{-1} and 1540 cm^{-1} are attributed to the C=C stretching mode of aromatic ring [5, 13, 14]. In contrast to pristine MWCNT, an additional peak locating at 1560 cm^{-1} corresponding to the amine group is observed in the spectra of MWCNT-NH₂ [15]. After anchoring the initiator, the -CH stretching peaks from alkyl chains at $2931\text{ cm}^{-1}\text{--}2839\text{ cm}^{-1}$ and the -C=O stretching peak from the ester linkage at 1720 cm^{-1} appear, which reveal the presence of a 2BriB group on the surface of MWCNT [16]. The PS component is determined by the characteristic peaks at $3100\text{--}2800\text{ cm}^{-1}$ corresponding to the stretching vibration of C-H, the signals at $1500\text{--}1638\text{ cm}^{-1}$ resulting from the unsaturation sites in the benzene ring as well as the peaks at 1492 cm^{-1} and 1444 cm^{-1} attributing to both of stretching vibration of aromatic ring and the deformation

vibration of $-\text{CH}_2$ [5]. Based on the FT-IR spectra, we can conclude that the MWCNT are successfully functionalized.

4.2.3 Functionalization of MWCNT with PMMA

In this work, a similar procedure of functionalizing MWCNT via ATRP is also adopted to modify MWCNT with PMMA. In contrast to styrene, MMA displays a higher kinetic constant of polymerization. Thereby, a higher dilution and a low catalyst concentration are used in this case.

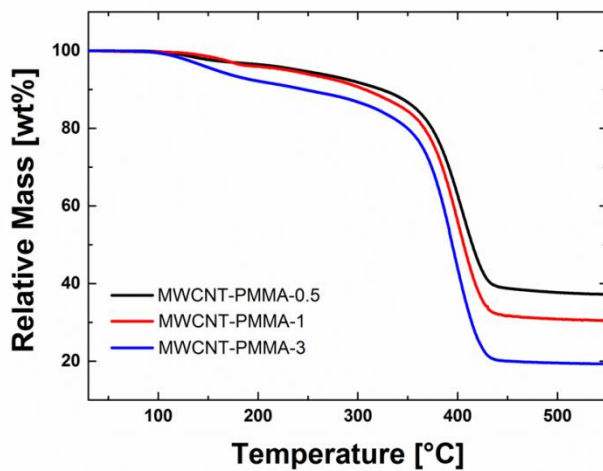


Fig. 4.4 TGA results of functionalized MWCNT with PMMA

PMMA with different molecular weights are grafted onto the surface of MWCNT by varying the time for ATRP reaction. The molecular weights and the contents of grafted PMMA in each sample are listed in Table 4.4. Different from the polymerization of PS, PMMA chains with a molecular weight of 19 kg/mol are obtained just after 30 min. With the extension of reaction time, the molecular weights of grafted PMMA increase. As a result, the contents are also enhanced with the change of molecular weight, as the densities of initiator on MWCNT are the same in each sample.

Table 4. 4 Summary of functionalized MWCNT with polystyrene

Codes	[Br] (a) [mmol/g]	Time [h]	Weight loss ^(a) [wt%]	M_n ^(b) [kg/mol]	PDI ^(b)
MWCNT-PMMA-0.5	0.433	0.5	62	19.0	1.03
MWCNT-PMMA-1	0.433	1	69	23.6	1.04
MWCNT-PMMA -3	0.433	3	80	43.6	1.12

(a) The content of initiators and grafted polymer on MWCNT were estimated by TGA results

(b) The molecular weight and PDI of grafted polymer were determined by GPC

4.2.4 Functionalization of MWCNT with P(MMA-*co*-S) copolymers

Because the difference of reactivity between MMA and styrene is quite large in the ATRP reaction, selecting appropriate parameters which are suitable for both monomers is of utmost importance to get success in polymerization of P(MMA-*co*-S) copolymers with random sequence of monomers. In many works, the polymerization of MMA via ATRP was set up at a temperature equal or lower than 90 °C. Nevertheless, styrene presented a very low conversion at these temperatures. By comparing the polymerization of styrene at 90 °C and 125 °C, respectively, Liu et al. [17] pointed out that a higher temperature (125 °C) and the use of specific catalysts should be the optimum conditions for both MMA and styrene, which were also suitable for synthesizing P(MMA-*co*-S) copolymers. Therefore, in our work, we adapted this high temperature for the ATRP reaction and utilized a similar catalyst system of CuCl/CuCl₂/PMDETA. The advantage of using mixed copper salts was to overcome the comparably fast propagation of MMA by the deactivating effect from Cu²⁺ [18] and the halogen exchange between R-Br and CuCl [19-21].

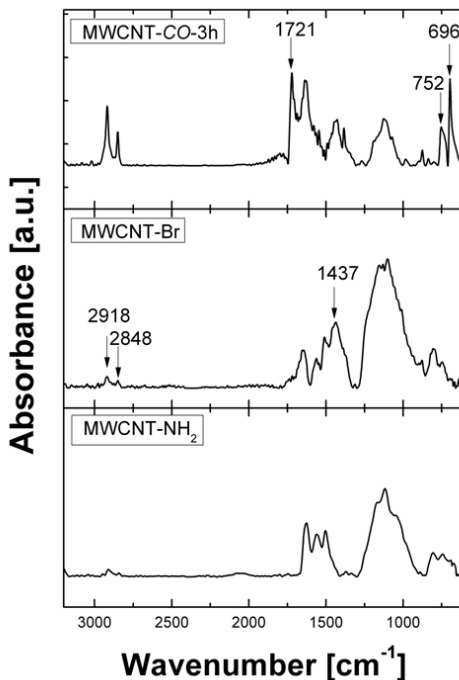


Fig. 4.5 FT-IR spectra of functionalized MWCNT

Figure 4.5 shows the FT-IR spectra of functionalized MWCNT. For as-received MWCNT-NH₂, the characteristic peaks of amino groups are observed at 1626 cm⁻¹ and 1502 cm⁻¹ corresponding to N-H deformation [15, 22]. However, many authors also attributed the absorption in the range of 1650 cm⁻¹-1540 cm⁻¹ to the C=C stretching mode of the aromatic ring from CNT [5, 13, 14]. The broad band locating from 900 cm⁻¹ to 1200 cm⁻¹ is typical for aromatic systems, which commonly appears in the spectra of covalently functionalized MWCNT [12]. In the case of MWCNT-Br, the presence of initiator is confirmed by the peaks of C-H deformation of alkyl chains at 1437 cm⁻¹. Moreover, signals from stretching of alkyl also appear at 2919 cm⁻¹ and 2848 cm⁻¹ [22], which also proves the existence of the initiator group on MWCNT. In the spectrum of functionalized MWCNT with copolymer (MWCNT-CO-3h), the characteristic peaks from the tubes become weaker. Meanwhile, pronounced signals from grafted polymers are shown with a strong intensity. Successful functionalization of MWCNT with copolymers are determined by the C=O stretching peaks at 1721 cm⁻¹ presumably from ester linkage in MMA units [23] and strong peaks at 752 cm⁻¹ and 696 cm⁻¹

designated to the out-of-plane bending vibrations of five –CH- groups in aromatic ring and the out-of-plane skeleton bending vibration of entire aromatic ring and, respectively, from styrene units [24, 25].

The controllability of ATRP reactions for functionalization is examined by investigating the products obtained with different reaction times. Figure 4.6 shows the TGA results of functionalized MWCNT with copolymers prepared by different reaction times. The as-received MWCNT-NH₂ had a small weight loss of 5.9 wt% corresponding to a concentration of amino groups of 0.64 mmol/g. After the attachment with 2BriB, the weight loss increases to 12.3 wt%, implying a successful grafting of initiator on the surface of MWCNT with a concentration of 0.403 mmol/g. In the case of functionalized MWCNT with copolymers, the content of grafted copolymers increases from 30 wt% to 80 wt% with a change of total monomer conversion from 35% to 66% (see Fig. 4.6(b)). These data reveal that the content of grafted copolymers on MWCNT can be adjusted by varying the reaction time or the monomer conversion, which is consistent with the results of functionalizing MWCNT with homopolymers via ATRP [4, 26].

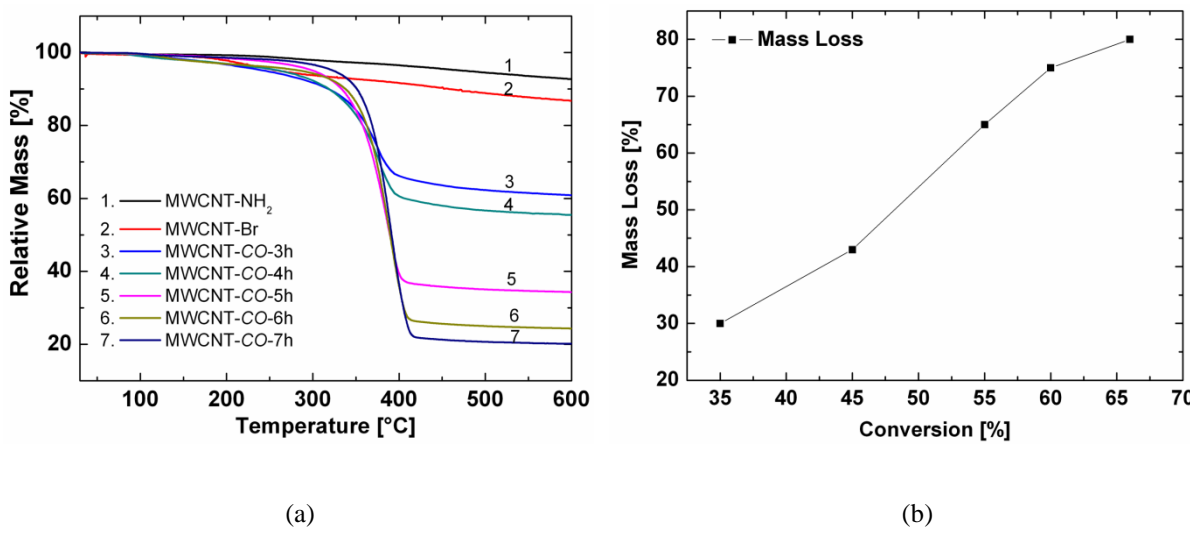


Fig. 4.6 TGA curves of MWCNT-NH₂, MWCNT-Br and functionalized MWCNT with P(MMA-*co*-S) copolymers prepared with different reaction times (a) and the content of grafted P(MMA-*co*-S) copolymers as a function of the total monomer conversion (b)

The number-average molecular weight and the PDI as a function of total monomer conversion are shown in Fig. 4.7. The relationship between the conversion of the total monomers and the molecular weight of copolymers is approximately linear. Furthermore, the PDI remain very low (in a range of 1.59 to 1.67) in the obtained conversion range. These characteristics are in agreement with kinetics of normal ATRP reactions in homogenous systems without nanoparticles [27] and are also observed in functionalization of MWCNT reported by other researchers [4]. Based on the aforementioned results, it can be concluded that the ATRP reactions to synthesize P(MMA-*co*-S) copolymers in the presence of MWCNT are characterized by a good controllability under the used conditions. The properties of obtained functionalized MWCNT are summarized in Table 4.5.

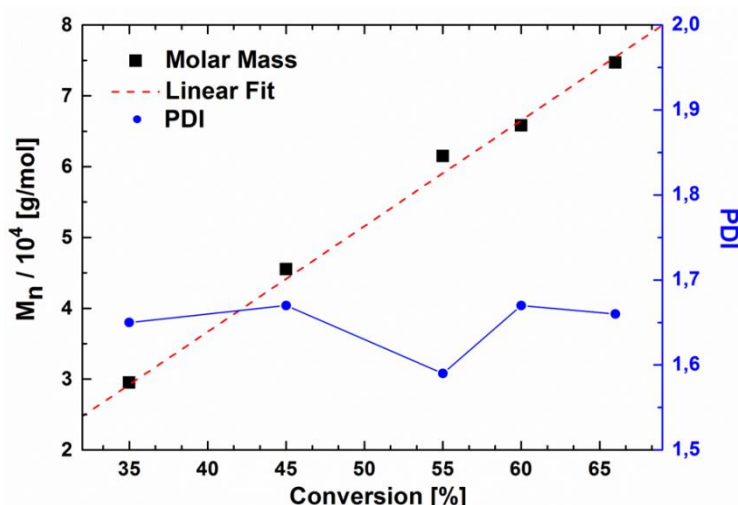


Fig. 4.7 Number-average molecular weight of P(MMA-*co*-S) copolymers (M_n) and polydispersity index (PDI) as a function of total monomer conversion

Table 4.5 Summary of characterization of functionalized MWCNT with copolymers

Sample	Conversion of total monomers ^(b) [%]	Content of grafted polymers ^(c) [wt%]	$M_n^{(d)}$ [kg/mol]	PDI ^(d)	Fraction of PS ^(e) [%]
MWCNT-CO-3h	35	30	29.5	1.65	56%
MWCNT-CO-4h	45	43	45.5	1.67	57%
MWCNT-CO-5h	55	65	61.5	1.59	56%
MWCNT-CO-6h	60	75	65.8	1.67	56%
MWCNT-CO-7h	66	80	74.7	1.66	56%

(a) The conversion of total monomer mixture was determined by gravimetric weighting

(b) The content of grafted polymer was estimated from the TGA results

(c) The number average molecular weight and polydispersity index of free polymer in the system were measured by GPC

(d) The fraction of polystyrene component in P(MMA-*co*-S) copolymers was calculated according to the spectra of ¹H-NMR

(e) The fraction of polystyrene component in P(MMA-*co*-S) copolymers was calculated based on the ¹H-NMR spectra

The compositions of the grafted copolymers were determined from the ¹H-NMR spectra of the obtained free polymers during the ATRP reaction. Signals of the main chains and the pendant groups in all spectra are broad and differ significantly from the ones of homopolymers of PMMA and PS [27], illustrating that the obtained polymers are neither block copolymers nor mixture of homopolymers but random copolymers. The compositions of P(MMA-*co*-S) copolymers can be calculated based on the relative areas of aromatic protons (I_1 , 6.5-7.25 ppm) corresponding to the styrene units and aliphatic proton region (I_2 , 0.3-3.7 ppm) of both units, styrene and MMA units, according to the following equation [27, 28]:

$$\phi_{PS} = \frac{I_1/5}{I_1/5 + (I_2 - 3I_1/5)/8} \quad \text{Eq. 4.1}$$

where ϕ_{PS} is the molar fraction of styrene units in the copolymers. The calculated composition of each grafted copolymer prepared with different reaction times are also listed in Table 4.5.

The results show that the compositions of the copolymers do not depend on the time of polymerization. In fact, the styrene fraction is about 56% in each sample, i.e. slightly larger than the methyl methacrylate fraction. This indicates an almost azeotropic copolymerization, which agrees well with the equal molar concentrations of the comonomers and the similar copolymerization parameters of MMA ($r_1=0.46$) and styrene ($r_2=0.52$) [29].

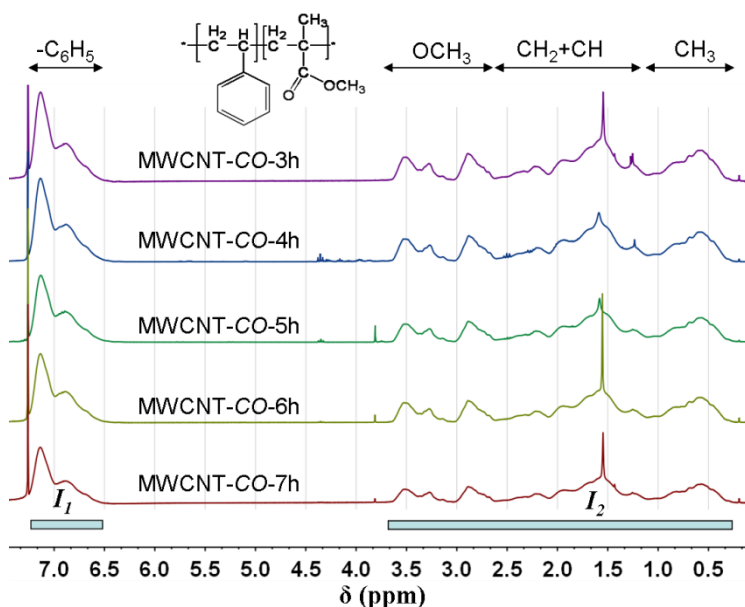


Fig. 4.8 ^1H -NMR spectra of functionalized MWCNT prepared at different reaction times in CDCl_3 at 25°C

4.2.5 Functionalization of MWCNT via Diels-Alder reaction

Although the “*grafting-from*” method described in former sections provides an efficient approach to obtain functionalized MWCNT with high density of grafted polymer, the procedure of preparation is complicated by means of running a series of reactions in the presence of MWCNT. More important, these reactions could generate considerable amount of byproducts, so that, extensively cleaning is required. As one alternative method, Diels-Alder (DA) cycloaddition reaction can realize the functionalization under mild conditions without byproduct. Munirasu et al. [9] showed that several carbon materials including CNT can

behave as both diene and dienophile in DA reaction with suitable opponent partners. In their work, MWCNT were attached with furfuryl-based initiator and then PS was grafted on MWCNT via “*grafting-from*” method through ATRP reaction. Later on, Bernal et al. [30] developed a simple and scalable “*grafting-to*” approach to modify pristine MWCNT with polystyrene-based furfuryl substance. Functionalization of MWCNT via DA reaction was carried on between the high reactivity of furfuryl-capped polymers (diene) and MWCNT (dienophile) at high temperature (80°C).

In present work, both furfuryl-capped PMMA and furfuryl-capped PS will take part into the reaction simultaneously at the initial stage of DA reaction. Individual MWCNT with two kinds of polymer chains is expected to attain a Janus structure on the surface of MWCNT. First of all, the furfuryl alcohol is anchored with the initiator for ATRP. The proposed structures of the substance are confirmed by $^1\text{H-NMR}$ measurements. As shown in Fig. 4.9, after anchoring initiator, a strong peak belonging to the proton of methyl group originating from 2BriB appears at 1.92 ppm, while, the signals at 3.73 ppm corresponding to the protons of hydroxyl group in furfuryl alcohol disappear. Furthermore, the signal relating to the methylene group is shifted from 4.48 ppm to 5.15 ppm due to the change of structure. Based on the comparison of these spectra, it demonstrates that the initiator is successfully anchored to the furfuryl compound.

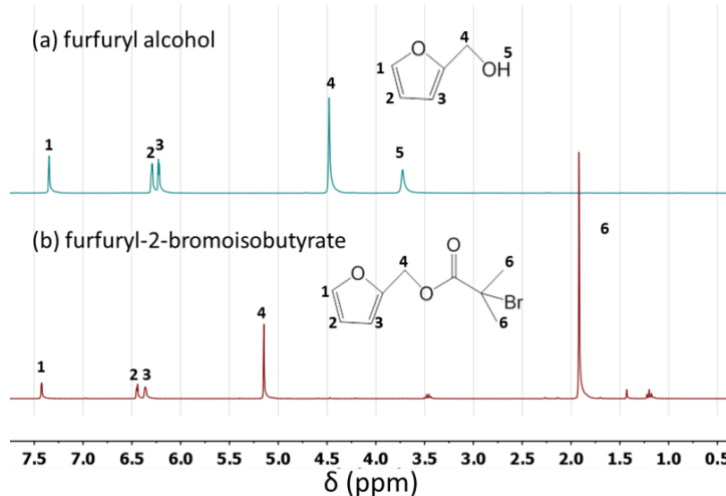
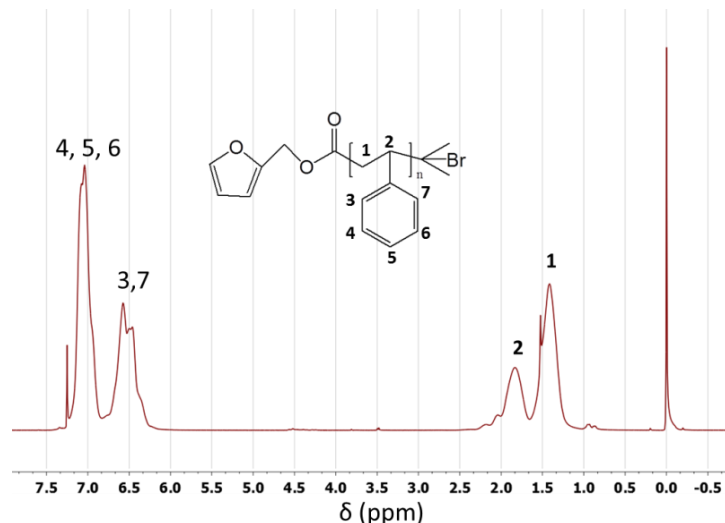
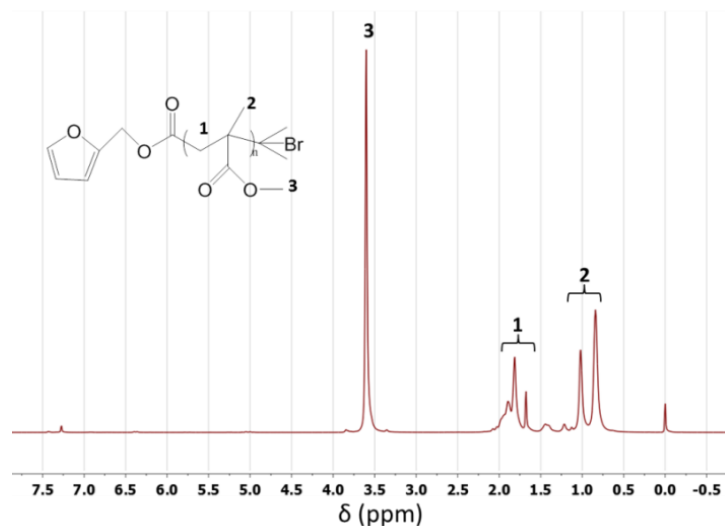


Fig. 4.9 ^1H -NMR spectrum of furfuryl alcohol (a) and furfuryl-2-bromoisobutyrate (b)

PS and PMMA are synthesized via ATRP using furfuryl-2-bromoisobutyrate as initiator. Figure 4.10 gives the ^1H -NMR spectrum of each kind of furfuryl-capped polymers. The characteristic signals of PS and PMMA are all observed in the spectra, implying the existence of proposed polymer chains capped with furfuryl unit. In Fig 4.10(a), the aromatic ring in styrene unit is determined from the peaks at 7.04 ppm and 6.57 ppm. The signals at 1.82 ppm and 1.41 ppm are respectively attributed to the protons of methine and methylene group of the backbone of PS. For furfuryl-capped PMMA, the resonance signals can be assigned as follows: the protons of oxymethyl group at 3.60 ppm, the methylene protons at 1.81–1.68 ppm and the signals at 1.02 – 0.84 ppm corresponding to the methyl unit. Through adjusting the reaction time of ATRP, furfuryl-capped polymers with different molecular weights are attained. Table 4.6 gives the reaction conditions and molecular weights of obtained furfuryl-capped polymers.



(a)



(b)

Fig. 4.10 ¹H-NMR spectra of furfuryl-capped PS (a) and furfuryl-capped PMMA (b)

Table 4.6 Reaction conditions and molecular weights of furfuryl-capped polymers

Code	Temperature [°C]	Reaction Time	$M_n^{(a)}$ [kg/mol]	PDI ^(a)
Fp-PMMA-1	60	25 min	53	1.12
Fp-PMMA-2		15 min	14	1.69
Fp-PS-1		20 h	27	1.11
Fp-PS-2	90	18 h	20	1.06
Fp-PS-3		8 h	8	1.06

(a) The molecular weight and PDI of furfuryl-capped polymers were determined by GPC

Functionalization of MWCNT with both PS and PMMA were realized by applying DA reaction which involved pristine MWCNT as dienophile and furfuryl-capped polymers as diene. Several DA reactions were carried out with a constant ratio between polymers and MWCNT. Moreover, the feed ratio of PMMA to PS was also the same in each reaction (see Table 4.7). From the results of TGA, it is shown that the content of grafted polymers increase with the molecular weights of furfuryl-capped polymer. However, the increase is not strictly proportional to the change of molecular weight. For instance, sample DA1 contains so much higher molecular weights of both PMMA and PS than the ones in sample DA2. Nevertheless, the diversity of final content of grafted polymer on MWCNT between DA1 and DA2 is only less than 2 wt%. Similar phenomenon is observed when only the molecular weight of used PS compound is changed (see DA2 and DA3). It seems that MWCNT with high molecular weight polymers have relative low density of functionalization on the surface of MWCNT. This might be explained by the fact that long chains of grafted polymer could form entanglements in the system which could more or less hamper another free furfuryl-capped polymer in the medium to contact with MWCNT. Hence, an appropriate molecular weight of readymade polymer is a very important aspect for obtaining relative high density of grafted polymer on MWCNT.

Another important phenomena observed in this study is that the content of grafted polymer is significantly lower than the value we obtained through “grafting-from” polymerization. This property is mainly caused by the limited reactivity of MWCNT in DA reaction. In contrast to single-walled nanotubes, MWCNT has more defects on their surface, which is disadvantageous for their reactivity in DA reaction [9, 31]. Until now, only a few approaches have been reported to improve the reactivity of pristine MWCNT, nevertheless, the conditions of most methods are harsh, e.g., utilizing microwave to provide high energy [32] and running the reaction under high pressure [33]. One facile way is to increase the reaction temperature. Therefore, one reaction at 100 °C was attempted in this work and the content of grafted polymer is found to increase from 4.9 wt% to 6.7 wt%.

Table 4.7 Reaction conditions of DA reactions and the contents of grafted polymer on the surface of functionalized MWCNT

Sample	Weight ratio [MWCNT:Polymer]	Weight ratio (PMMA:PS)	Temperature [°C]	Molecular weights of used polymers [kg/mol] ^(a)		Content of grafted polymer [wt%] ^(b)
				PMMA	PS	
DA1			80	53	27	8.8
DA2			80	14	20	7.3
DA3	1 : 50	1 : 1	80	14	8	4.9
DA4			100	14	8	6.7

(a) The molecular weights of used furfuryl-capped polymers were determined by GPC

(b) The contents of grafted polymer on MWCNT were detected by TGA

The existence of PMMA and PS on the surface of MWCNT is detected by FTIR (see Fig. 4.11). Through comparing the spectra of functionalized MWCNT and pristine MWCNT, characteristic signals of both kinds of grafted polymers are determined in the case of functionalized MWCNT. The peaks locating in the range of 3006 cm⁻¹~2959 cm⁻¹ corresponding to -CH stretching vibration from alkyl chains [22]. The signals from 1250 cm⁻¹ to 1022 cm⁻¹ are attributed to the ester bond stretching vibration implying the existence of

PMMA [34]. The PS chains are determined by the signal at 759 cm^{-1} and 695 cm^{-1} owing to the stretching vibration of aromatic ring from the styrene unit [24, 25].

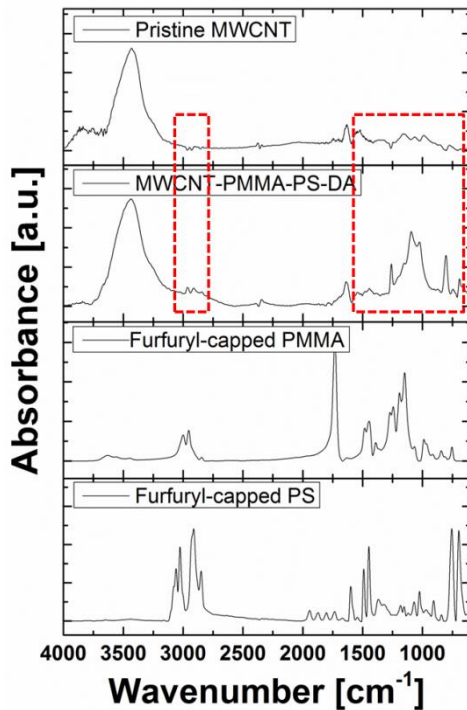


Fig. 4.11 FT-IR spectra of furfuryl-capped PS, furfuryl-capped PMMA, functionalized MWCNT with both PMMA and PS as well as pristine MWCNT

4.3 Conclusions

Surface functionalization of MWCNT was started from anchoring the initiator on MWCNT-OH and MWCNT-NH₂. Owing to the high density of reactive groups from the commercial product and the better reactivity than hydroxyl group, MWCNT-NH₂ with high concentration of amino group was selected to prepare functionalized MWCNT via “grafting-from” method.

The homopolymers of PS and PMMA were synthesized from the immobile initiator on the surface of MWCNT via ATRP reaction. Through controlling the reaction time, different molecular weights of homopolymers were obtained. With the constant density of initiator, the content of grafted polymers on MWCNT proportionally changed with the increase of

molecular weights. In case of functionalized MWCNT with random copolymer, MMA and styrene with a specific mole ratio were fed into the system together at the beginning of the reaction. Comparing the results obtained from different batches of reaction, the fractions of copolymer were found to be constant with the variation of reaction time. Additionally, signals of the main chains and the pendant groups in all the $^1\text{H-NMR}$ spectra were broad and significantly different from the either kind of homopolymers. Thus, it could be concluded that the grafted copolymer was neither block copolymers nor mixture of homopolymers but with random structure. Like grafted homopolymers, the molecular weights of grafted copolymers were also increased with the enhancement of reaction time. Good controllability of ATRP reaction for grafting was characterized by the proportional increase of polymer content and molecular weights with the conversion of total amount of monomers.

Furthermore, this work also attempted to functionalize MWCNT via “*grafting-to*” method through DA reaction. Both of PS and PMMA were polymerized via ATRP from the initiator anchored with furfuryl group. The functionalization was completed via DA reaction in presence of MWCNT, using furfuryl-capped polymers as diene and MWCNT as dienophile. The grafted content on MWCNT was found to increase with the molecular weight of readymade furfuryl-capped polymer. However, polymers with excessively high molecular weight could form entanglement and decrease the possibility of free furfuryl-capped polymer to anchor on the surface of MWCNT. Although functionalization of MWCNT via DA reaction was facile and without byproducts, the limited reactivity of MWCNT in mild conditions led to very low grafted content on MWCNT.

References

1. Wang M, Pramoda KP, and Goh SH. Polymer 2005;46(25):11510-11516.
2. Albuerne J, Boschetti-de-Fierro A, Abetz C, Fierro D, and Abetz V. Advanced Engineering Materials 2011;13(8):803-810.

3. Ryu J, Ramaraj B, and Yoon KR. *Surface and Interface Analysis* 2009;41(4):303-309.
4. Gao C, Muthukrishnan S, Li W, Yuan J, Xu Y, and Müller AHE. *Macromolecules* 2007;40(6):1803-1815.
5. Albuerne J, Boschetti-de-Fierro A, and Abetz V. *Journal of Polymer Science Part B: Polymer Physics* 2010;48(10):1035-1046.
6. Qin S, Qin D, Ford WT, Resasco DE, and Herrera JE. *Macromolecules* 2004;37(3):752-757.
7. Kong H, Gao C, and Yan D. *Journal of the American Chemical Society* 2003;126(2):412-413.
8. Lu X, Tian F, Wang N, and Zhang Q. *Organic Letters* 2002;4(24):4313-4315.
9. Munirasu S, Albuerne J, Boschetti-de-Fierro A, and Abetz V. *Macromolecular Rapid Communications* 2010;31(6):574-579.
10. Bernad A, Nieto MA, Vioque A, and Palacián E. *Biochimica et Biophysica Acta (BBA) - Protein Structure and Molecular Enzymology* 1986;873(3):350-355.
11. Majeed S. Thesis of Ph. D work 2013:70-71.
12. Zenkel C, Albuerne J, Emmler T, Boschetti-de-Fierro A, Helbig J, and Abetz V. *Microchimica Acta* 2012;179(1-2):41-48.
13. Wang TL and Tseng CG. *Journal of Applied Polymer Science* 2007;105(3):1642-1650.
14. Osswald S, Havel M, and Gogotsi Y. *Journal of Raman Spectroscopy* 2007;38(6):728-736.
15. Wang S, Liang Z, Liu T, Wang B, and Zhang C. *Nanotechnology* 2006;17(6):1551-1557.
16. Lee YW, Kang SM, Ro YK, Chi YS, Choi I, Hong SP, Yu BC, Paik HJ, and Yun WS. *Macromolecular Research* 2005;13(4):356-361.
17. Liu H, O'Mahony CT, Audouin F, Ventura C, Morris M, and Heise A. *Macromolecular Chemistry and Physics* 2012;213(1):108-115.
18. Becer CR, Hoogenboom R, Fournier D, and Schubert US. *Macromolecular Rapid Communications* 2007;28(10):1161-1166.
19. Dayananda K and Dhamodharan R. *Journal of Polymer Science Part A: Polymer Chemistry* 2004;42(4):902-915.
20. Matyjaszewski K, Wang JL, Grimaud T, and Shipp DA. *Macromolecules* 1998;31(5):1527-1534.
21. Sun X, Zhang H, Huang X, Wang X, and Zhou Q-F. *Polymer* 2005;46(14):5251-5257.
22. Lee YW, Kang S, Yoon K, Chi Y, Choi I, Hong SP, Yu BC, Paik HJ, and Yun W. *Macromolecular Research* 2005;13(4):356-361.
23. Baskaran D, Dunlap JR, Mays JW, and Bratcher MS. *Macromolecular Rapid Communications* 2005;26(6):481-486.
24. Yang JC, Jablonsky MJ, and Mays JW. *Polymer* 2002;43(19):5125-5132.
25. Wang Y, Teng X, Wang J, and Yang H. *Nano Letters* 2003;3(6):789-793.
26. Du B, Hande UA, Majeed S, and Abetz V. *Polymer* 2012;53(24):5491-5501.
27. Kotani Y, Kamigaito M, and Sawamoto M. *Macromolecules* 1998;31(17):5582-5587.
28. Brar AS and Puneeta. *Journal of Polymer Science Part A: Polymer Chemistry* 2006;44(6):2076-2085.
29. Young L. In: Brandrup J and Immergut E, editors. *Polymer Handbook*. New York: Wiley, 1989.
30. Bernal MM, Liras M, Verdejo R, López Manchado MA, Quijada-Garrido I, and París R. *Polymer* 2011;52(25):5739-5745.
31. Chang CM and Liu YL. *Carbon* 2009;47(13):3041-3049.
32. Delgado JL, de la Cruz P, Langa F, Urbina A, Casado J, and Lopez Navarrete JT. *Chemical Communications* 2004;0(15):1734-1735.
33. Ménard-Moyon C, Dumas F, Doris E, and Mioskowski C. *J Am Chem Soc* 2006;128(46):14764-14765.
34. Balamurugan A, Kannan S, Selvaraj V, and Rajeswari S. *Trends in Biomaterials and Artificial Organs* 2004;18(1):41-45.

Chapter 5

SAN/PPE 40/60 blend filled with functionalized MWCNT with polystyrene: Influence of molecular weight of grafted polystyrene on localization of MWCNT and the properties of its composites

5.1 Introduction

Blending of polymers is a well-established effective and beneficial approach to provide novel materials which combine the advantageous properties of each component [1, 2]. Because of the high molecular weight and their unfavourable interaction, most polymer pairs are immiscible so that their blends form a multi-phase structure with a weak interfacial adhesion. Therefore, a large number of studies pay their attention on improving the properties of immiscible blends by means of adding a third polymeric component or fillers.

In the last decade, increasing interest has focused on immiscible blends filled with carbon nanotubes (CNT), which are considered as one of the most promising filler due to their outstanding properties [3]. In contrast to the composites based on homopolymers, the situation in multi-phase blends is more complicated. Beside of factors observed in homopolymer system (e.g. the dispersibility of CNT and the interaction between CNT and matrices), another effects could be also influence the end-use properties of composites based on multi-phase blends. The localization of CNT might be one of the most important factors and attracts lots

of attention in recent researches. It has been well known that, if CNT are selectively dispersed in one phase of binary blend, the conductivity of the material can be increased with lower CNT loading than the case in homopolymer because of the so-called “double percolation” effect [4, 5]. Additionally, localization of MWCNT also presents important effect on the morphology of immiscible blends [6].

However, the localization at the interface should be an ideal state to maximize the advantages of CNT. Thus, tuning the localization of MWCNT in binary blends is essential to achieve optimum performance of composites. Unfortunately, due to the extremely high aspect ratio and cylindrical shape and different affinity with specific polymer, CNT are difficult to be confined at the interface but preferentially choose to disperse in one phase which has a better affinity with them. Is there any strategy can be used to manage the localization of CNT to our desired place? The work of Chui et al. provided one possible solution by introducing polymer on the surface of nanoparticles [7]. In their work, gold nanoparticles were located at the interface of PS-PVP lamellar diblock copolymer after functionalizing with PS and the distance of migration was influenced by the molecular weight of grafted polymer.

Up to now, there have been some successful examples of using anisotropic nanofillers as a third component to improve the morphology and properties of binary blends [8-12], however, no investigation has been reported on SAN/PPE blends filled with CNT. In this chapter, SAN/PPE blend filled with MWCNT-PS will be discussed. The weight ratio of SAN and PPE was 40 to 60, in which optimum properties were reported [13]. The functionalized nanotubes will be pre-mixed with the SAN phase which is not miscible with grafted PS. After extrusion, the grafted PS are expected to provide a driving force to promote MWCNT transferring from SAN phase to PPE phase. The influence of molecular weight of grafted PS on the localization of MWCNT in SAN/PPE 40/60 blend will be studied. In order to understand further the

microstructural changes of composites due to the addition of functionalized MWCNT, the linear viscoelastic behavior of the composites with various MWCNT will be also investigated.

5.2 Results and discussion

5.2.1 Characteristics of the used MWCNT fillers in SAN/PPE 40/60 blend

The characteristics of used MWCNT in SAN/PPE blend are listed in Table 5.1 and the details of measurements and analyses have been presented in Chapter 3 and Chapter 4. For minimizing the effect from other aspects, various kinds of MWCNT-PS were prepared from one batch of MWCNT-Br with constant concentration of initiator on the surface (0.379 mmol/g). Two types of MWCNT-PS with different molecular weight of grafted PS were utilized to study the influence of molecular weight on the localization of MWCNT in blend and the properties of composites. The notation for these functionalized MWCNT is MWCNT-PS_y^x, where x is the content of PS on MWCNT and y is the molecular weight of polystyrene.

Table 5.1 Summary of the used pristine and functionalized MWCNT in SAN/PPE blends

Codes	Weight loss ^(a) [wt%]	M_n ^(b) [kg/mol]	PDI	Weight loss/ M_n [wt% / g/mol]
MWCNT	---	---	---	---
MWCNT – PS ₂₁ ²⁸	28	21	1.08	1.30×10^{-5}
MWCNT – PS ₇₃ ⁷⁶	76	73	1.13	1.04×10^{-5}

(a) The content of grafted polymer was estimated by TGA results.

(b) The molecular weight and PDI of free PS polymerized in the presence of MWCNT were detected by GPC using polystyrene standards as calibration.

5.2.2 Morphological properties of composites with MWCNT fillers

5.2.2.1 Morphology of SAN/MWCNT composites

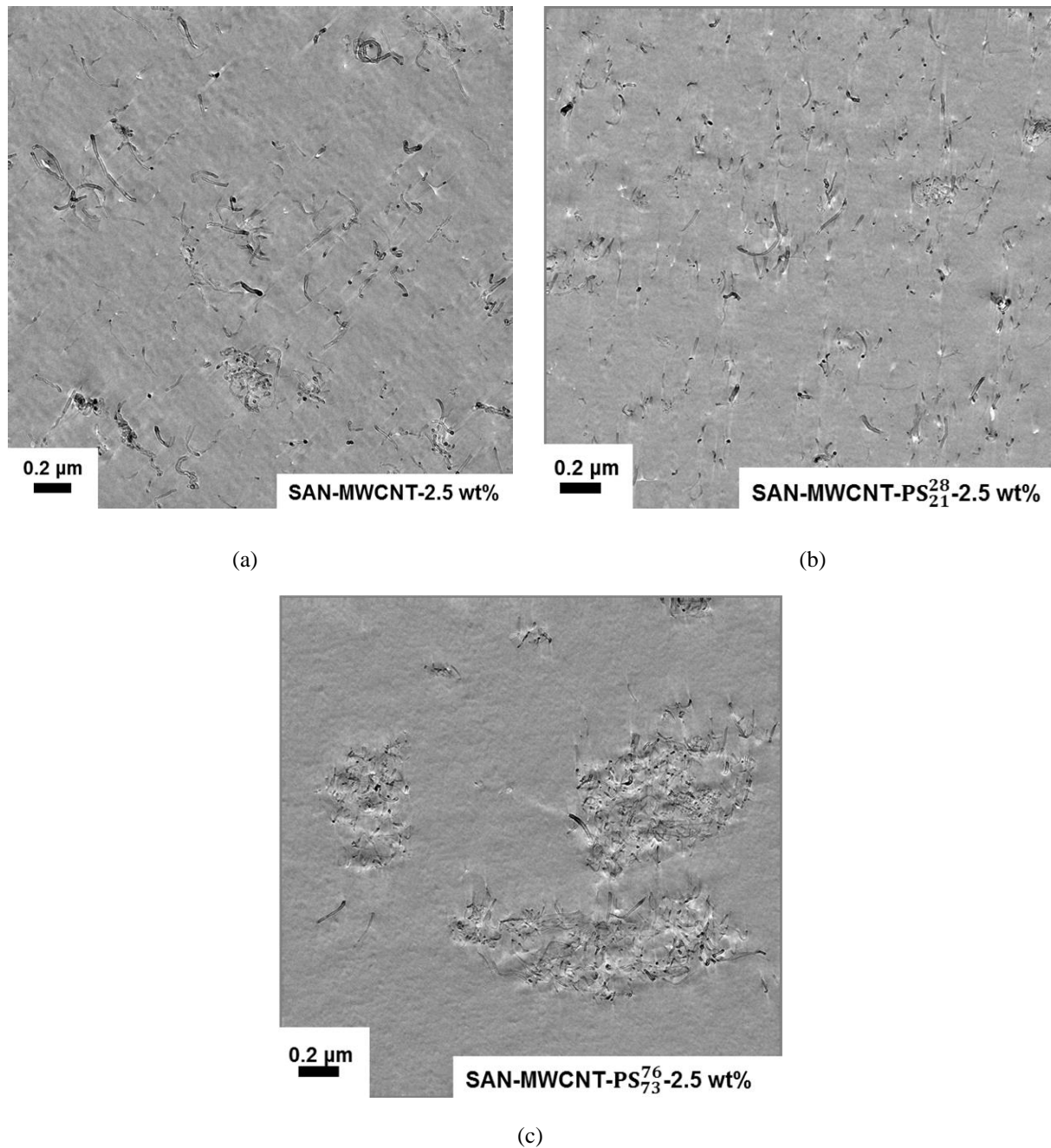


Fig. 5.1 TEM micrographs of SAN composites with various MWCNT fillers: SAN composites with pristine MWCNT-2.5 wt% (a); SAN composites with MWCNT – PS₂₁²⁸-2.5 wt% (b); SAN composites with MWCNT – PS₇₃⁷⁶-2.5 wt% (c).

The dispersion of MWCNT fillers in SAN is analyzed by TEM. The objective is to study the influence of functionalized PS on the dispersibility of MWCNT in SAN. As shown in Fig. 5.1(a), a large fraction of pristine MWCNT is agglomerated, while, some individual nanotube are dispersed well in the matrix. In contrast, MWCNT – PS₂₁²⁸ present a better dispersibility than the pristine ones. However, it is interesting that with the increase of the molecular weight of grafted PS, the functionalized MWCNT tend to aggregate again (see in Fig. 5.1(c)). Furthermore, the size of agglomerates in case of MWCNT – PS₇₃⁷⁶ is larger than the inhomogeneous aggregates of pristine MWCNT. Such phenomenon might be attributed to the variation of miscibility between SAN and grafted PS with the molecular weight of PS. Since the T_g of SAN and PS do not differ much, we determined the miscibility of SAN and grafted PS with high molecular weight by scanning electron microscopy (SEM). The free PS polymerized from sacrificial initiator was blended with SAN by extrusion under the same condition used for preparing MWCNT composites. The ratio of SAN to PS in the SAN/PS blend was 92 to 8 which is equal to the one between SAN and the grafted PS on the surface of MWCNT. In the SEM micrographs (Fig. 5.2), phase separation of SAN and PS is pronounced, revealing the immiscibility between SAN matrix and the grafted PS with high molecular weight. A similar effect was reported by Haase et al. [14].

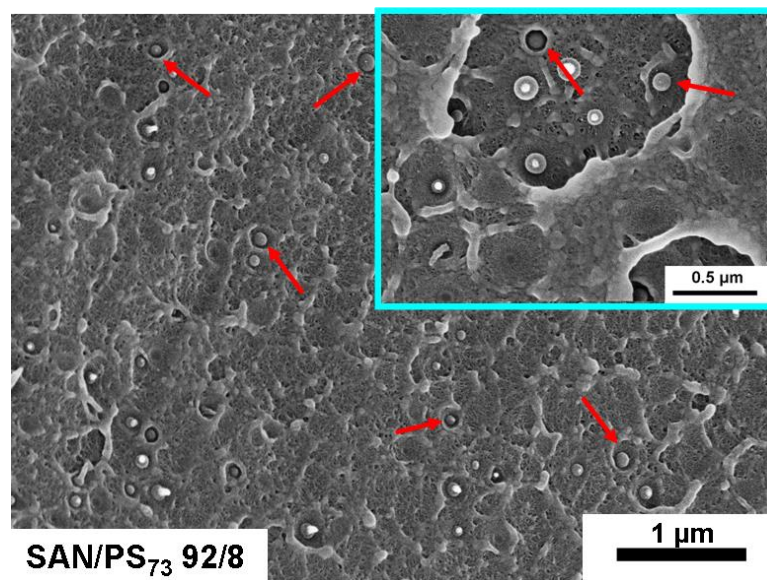
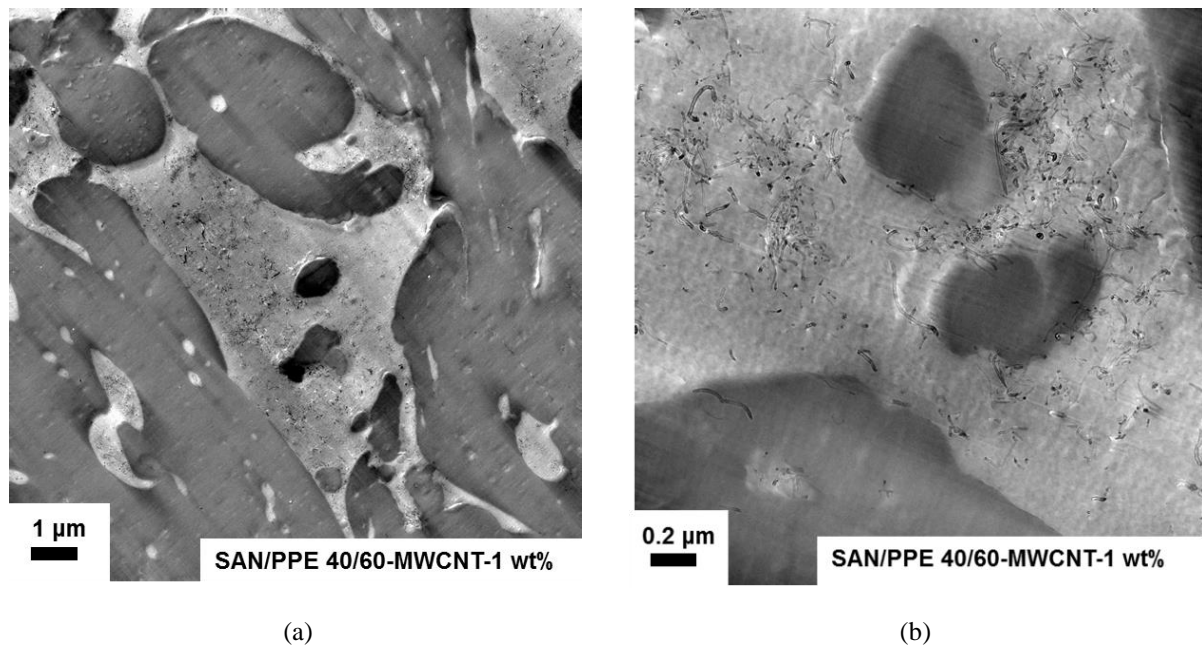


Fig. 5.2 SEM micrograph of SAN/PS₇₃ 92/8 blends. The arrows indicate the PS drops in the SAN matrix

5.2.2.2 Morphology of SAN/PPE 40/60 blend filled with MWCNT



(a)

(b)

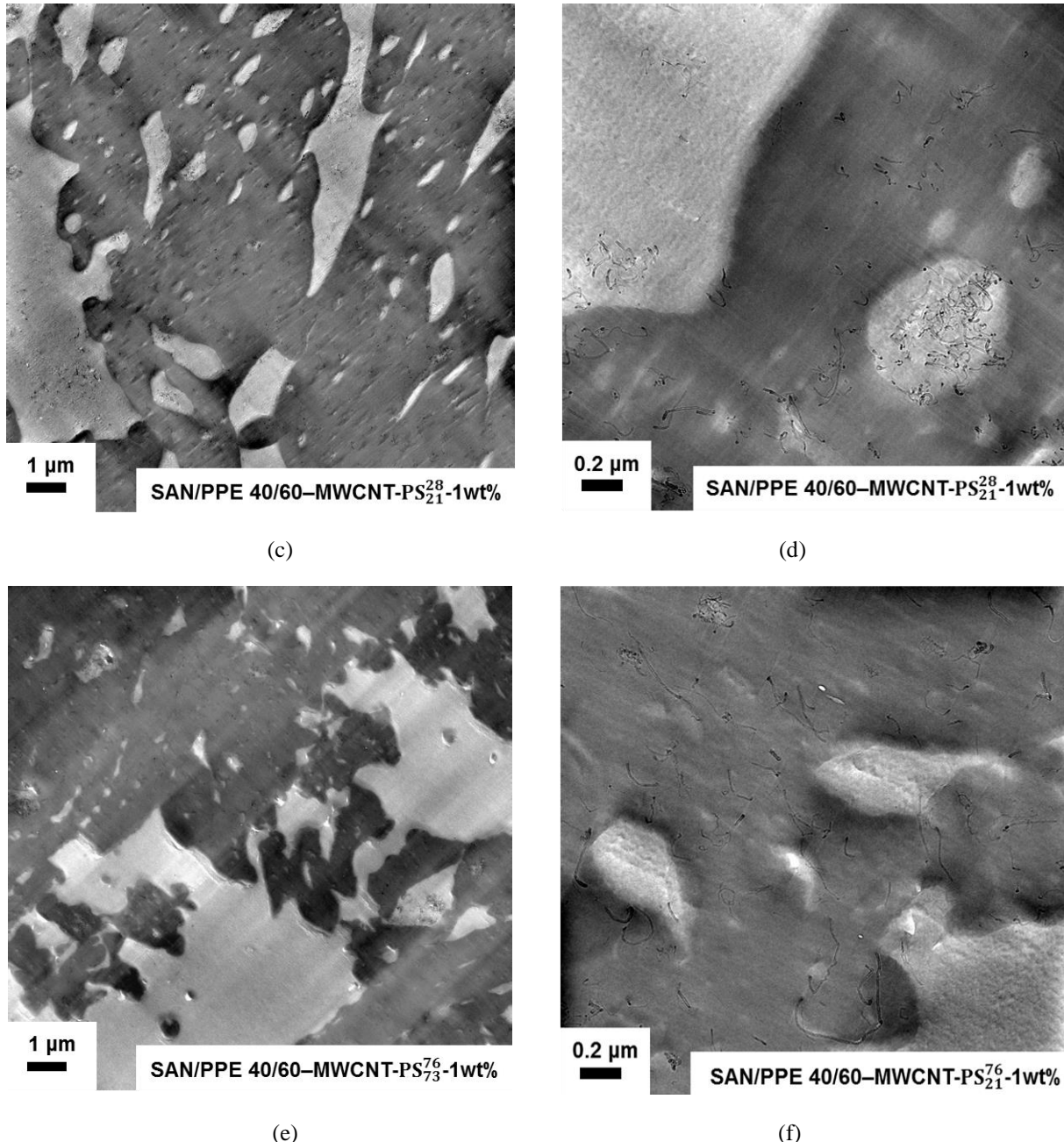


Fig. 5.3 TEM micrographs of SAN/PPE 40/60 blend filled with various MWCNT having different surface functionalization: SAN/PPE-MWCNT-1 wt% (a-b); SAN/PPE-MWCNT-PS₂₁²⁸ -1 wt% (c-d); SAN/PPE-MWCNT-PS₇₃⁷⁶ -1 wt% (e-f).

TEM micrographs of SAN/PPE 40/60 blend filled with MWCNT are shown in Fig. 5.3. The PPE phase appears in black and the bright phase corresponds to SAN in the micrographs. For composites with pristine MWCNT (see Figs. 5.3(a) and (b)), most of nanotubes are observed in the SAN phase with remarkable agglomerates. Only few individual tubes appear near the boundary or in the PPE phase by accident which is shown in Fig. 5.3(b) with high

magnification. The pre-mixing procedure with SAN should be one important reason why localization of MWCNT mainly concentrates in the SAN phase. Moreover, it is also known from the previous study that MWCNT in binary blend tend to be located in the phase which has a higher affinity with them or possess a lower viscosity [15]. Thus, these two factors could also have more or less effect on the localization of nanotubes. However, since the existence of pre-mixing procedure, the situation becomes complicate. The influence of affinity and viscosity on the localization of pristine MWCNT in SAN/PPE 40/60 blend will be discussed in Chapter 6 of this dissertation, where no pre-mixing step is used during the preparation for composites.

After functionalizing with polystyrene, a large amount of functionalized MWCNT migrate from the SAN phase into the PPE phase (see Figs. 5.3 (c) and (d)). In contrast to the morphology of SAN/PPE-MWCNT, the grey regions of the SAN phase in SAN/PPE 40/60-MWCNT-PS₂₁²⁸ become brighter, indicating a decreasing amount of MWCNT in the SAN phase. In Fig. 5.3(d), it clearly shows that MWCNT disperses well in the PPE phase and a few of nanotubes can be found at the interface of the blend. Since the surface of functionalized MWCNT have been covered by the grafted PS, the driving force of MWCNT migration could be attributed to the excellent thermodynamic miscibility between PPE and PS in case of any composition. However, with low molecular weight of grafted PS, the content of polymer on MWCNT is limited, so that, the driving force is not sufficient for migration with high extent. In addition, MWCNT in the pre-mixed SAN phase is random dispersed. Thus, the localization of MWCNT in SAN/PPE-MWCNT-PS₂₁²⁸ does not present strictly uniform. Furthermore, some bundles with big size which might need higher driving force to migrate still remain inside the SAN phase.

When a strong driving force is obtained in the case of MWCNT-PS₇₃⁷⁶ due to the increment of molecular weight of grafted PS, most of the functionalized MWCNT are selectively located in

the PPE phase (see Figs 5.3(e) and (f)). Only very few MWCNT can be seen in the SAN region. Moreover, pronounced agglomerates observed in the pre-mixed SAN phase (Fig. 5.2(c)) disappear in case of SAN/PPE-MWCNT-PS₇₃⁷⁶. The migrated MWCNT in the PPE phase perform a good dispersibility (Fig. 5.3(f)). This phenomenon is in agreement with the beneficial effect of grafting groups on the dispersibility of nanotubes.

5.2.3 Rheological properties of composites with MWCNT fillers

5.2.3.1 Thermal stability of neat SAN and PPE

Prior to study the liner viscoelastic properties, the thermal stability of the components in blend is investigated by dynamic time sweep tests which were carried out at a low frequency ($\omega = 0.5 \text{ rad/s}$). The time for the measurements was 5000 s which is long enough to guarantee a sufficient stability for the frequency sweep.

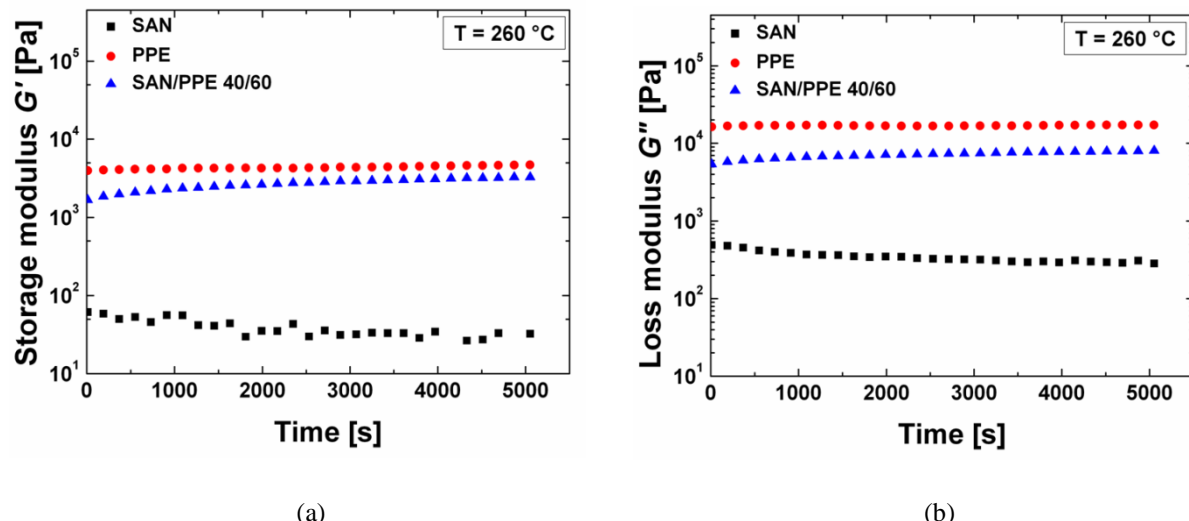


Fig. 5.4 Storage modulus G' (a), loss modulus G'' (b) of SAN and PPE as a function of time at 260 °C.

The constant values of G' and G'' in Fig 5.4 indicate a good stability of SAN and PPE during the whole time of measurement. A small scattering of G' of SAN in Fig. 5.4 (a) should result

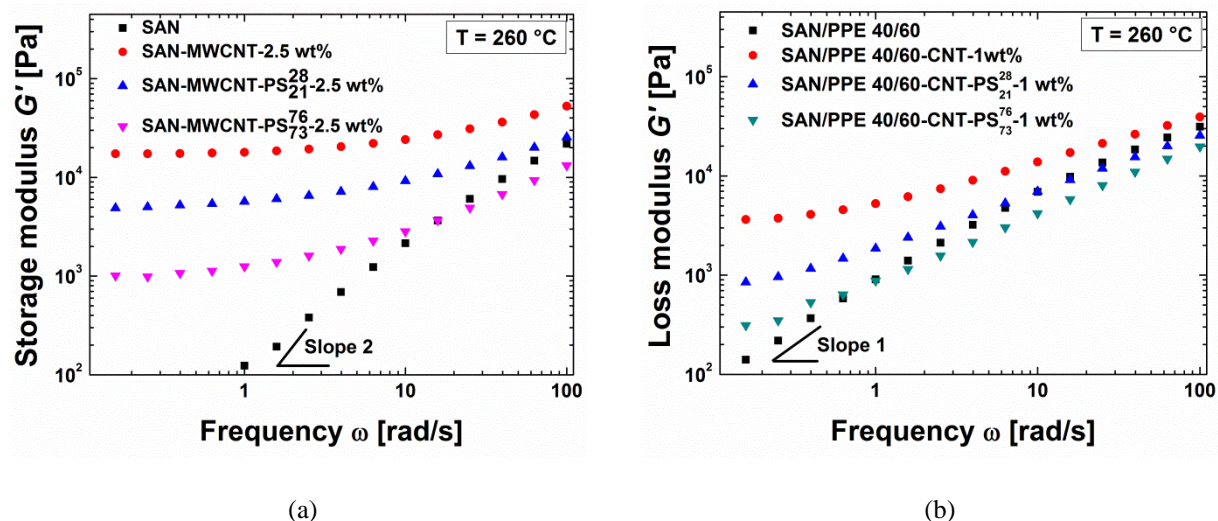
from the resolution of the device. The molecular weights of the polymers before and after measurement of the raw materials are listed in Table 5.2. From the data, it can be seen that the molecular weight of PPE significantly increases after melt processing. This phenomenon is in agreement with a previous investigation [16] and can be explained by the further chain growth originating from the ending hydroxyl group of PPE at the high processing temperature.

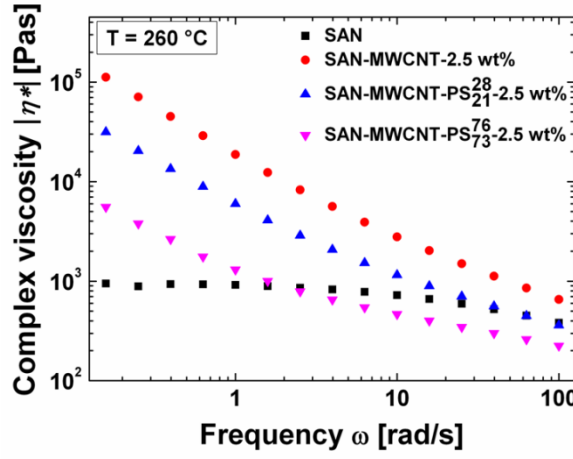
Table 5. 2 Summary of molecular weight (g/mol) of SAN and PPE at different processing steps (as determined by size exclusion chromatography calibrated to polystyrene) ^(a)

Materials	Raw material			After melt processing			After the measurement		
	M_w [kg/mol]	M_n [kg/mol]	PDI	M_w [kg/mol]	M_n [kg/mol]	PDI	M_w [kg/mol]	M_n [kg/mol]	PDI
SAN	161	83000	1.95	138	53000	2.61	149000	68000	2.21
PPE	28	12000	2.42	40	18000	2.19	46000	19000	2.44

(a) The molecular weight and PDI of free PS polymerized in the presence of MWCNT were detected by GPC using polystyrene standards as calibration.

5.2.3.2 Linear viscoelastic properties of neat SAN and pre-mixed SAN composites with MWCNT





(c)

Fig. 5.5 Storage modulus G' (a), loss modulus G'' (b) and complex viscosity $|\eta^*|$ (c) of SAN and its pre-mixed SAN/MWCNT composite as a function of angular frequency at 260°C.

The rheological properties of neat SAN and its composites with various MWCNT fillers are presented in Fig. 5.5. For neat SAN, the storage and loss modulus increase with angular frequency ω . Typical terminal behavior exhibits at low frequencies, revealing a full relaxation of SAN chains. After adding MWCNT fillers, the terminal behavior disappears and the dependence of G' and G'' on angular frequency ω becomes weak. This remarkable non-terminal behavior caused by the fact that CNT-CNT interactions start to dominate when the MWCNT loading is sufficiently high in the system (2.5 wt%). Such plateaus of G' and G'' versus frequency at low frequencies are in consistent with other polymer composites with MWCNT [17-19]. Complex viscosities of SAN and its composites shown in Fig. 5.5 (c) demonstrate a transition from a liquid-like to a solid-like behavior. The neat SAN displays a typical Newtonian plateau within the measured frequency range, whereas, the composites with MWCNT exhibit a strong shear thinning effect.

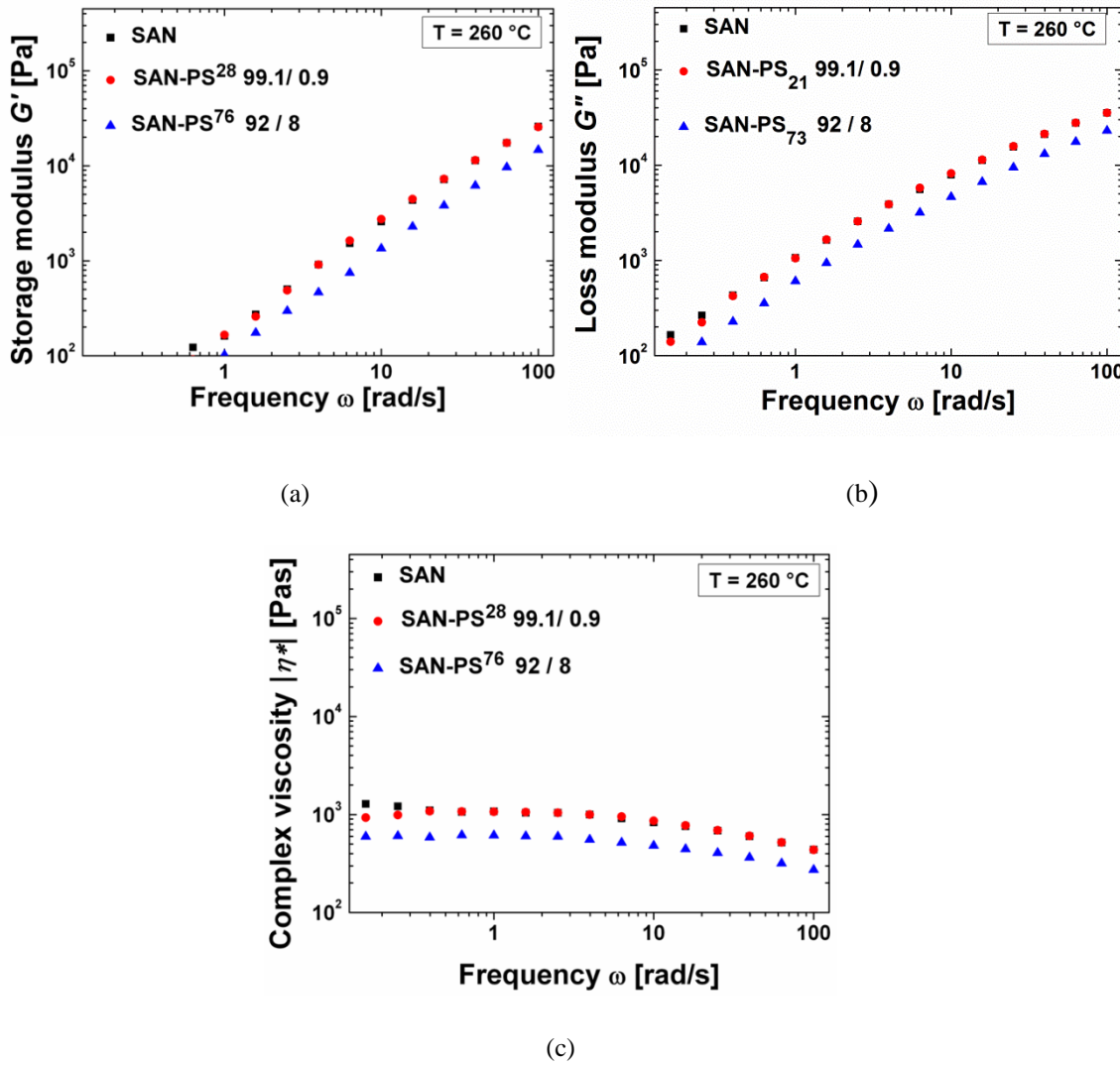


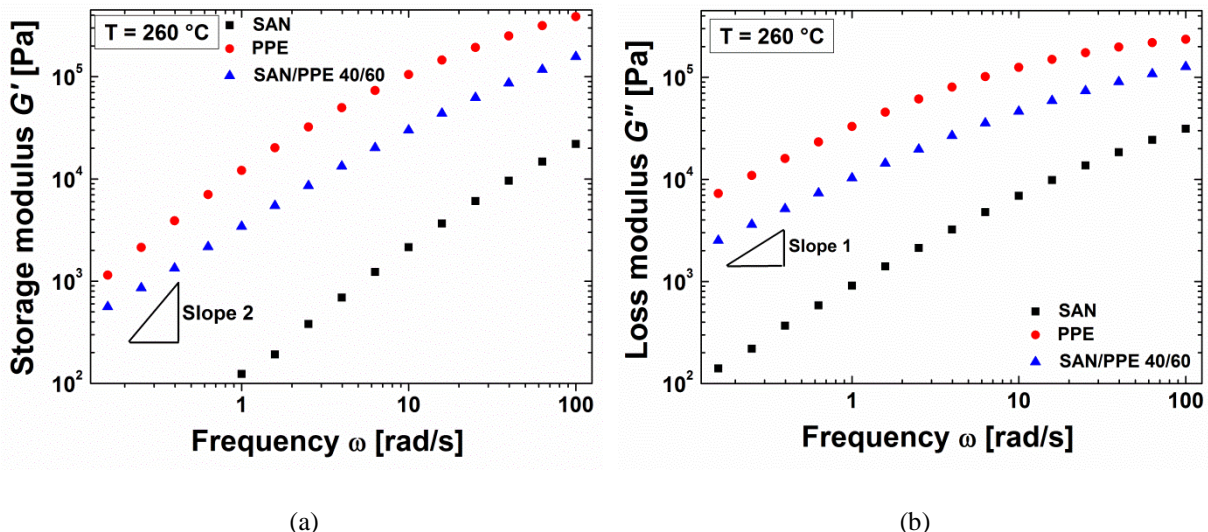
Fig. 5.6 Storage modulus G' (a), loss modulus G'' (b) and complex viscosity $|\eta^*|$ (c) of SAN/PS blends as a function of angular frequency at 260°C.

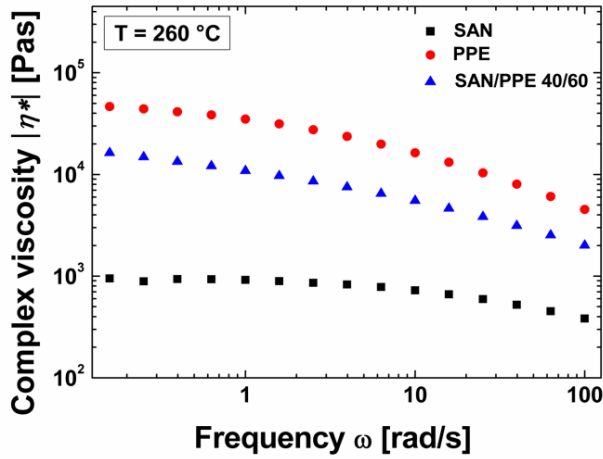
Interestingly, the dynamic moduli and the complex viscosity of the composites decrease in the presence of grafted polymer on the surface of MWCNT. The reduction of the dynamic moduli and complex viscosity most probably are caused by the grafted PS, which has a relatively low viscosity. Moreover, the effect is mostly pronounced in the case of SAN-MWCNT-PS⁷⁶, in which functionalized MWCNT possesses higher molecular weight of grafted PS. As we observed in the TEM micrographs (Fig. 5.1(c)), a high content of immiscible PS leads to agglomeration of MWCNT and no CNT-CNT network is formed in this case. Consequently, the effect of MWCNT is significantly weakened. On the other hand, it is also considered that the grafted PS could have a soften effect on the rheological properties of composites. In order

to determine the effect of PS, the rheological properties of SAN/PS are detected as shown in Fig. 5.6. The PS component is the free polymers synthesized from the sacrificial initiator. The composition of these SAN/PS blends is equal to the composition of SAN composites with functionalized MWCNT with PS. Comparing the data between neat SAN and SAN/PS blends, it shows that the high molecular weight of PS have pronouncedly softening effect on SAN component with lower dynamic moduli and the complex viscosity of SAN-PS₇₃ 92/8.

5.2.3.3 Linear viscoelastic properties of SAN/PPE 40/60 composites with various MWCNT

Fig. 5.7 gives the rheological properties of neat SAN, PPE and SAN/PPE 40/60 blend. SAN and PPE predict a typical terminal behavior with the scaling relations $G'' \propto \omega$ and $G' \propto \omega^2$. It indicates fully relax of neat homopolymers. The slope of G' of SAN/PPE 40/60 blends at low frequencies is smaller than 2. This behavior due to the interfacial tension reflects the phase separation in immiscible blend [18, 20].

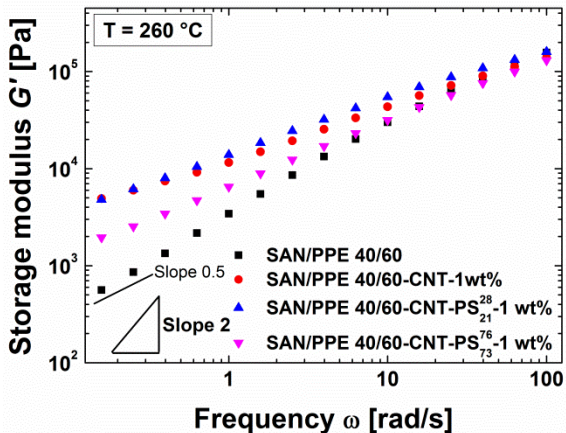




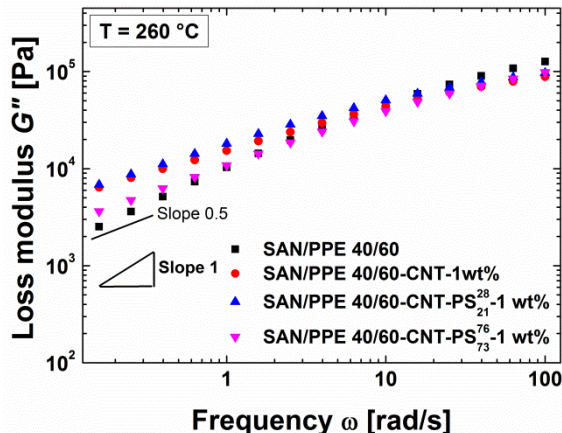
(c)

Fig. 5.7 Storage modulus G' (a), loss modulus G'' (b) and complex viscosity $|\eta^*|$ (c) of neat SAN, PPE and SAN/PPE 40/60 as a function of angular frequency at 260°C.

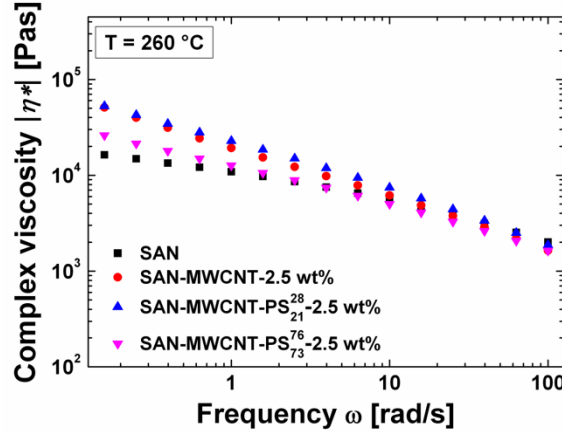
The rheological properties of SAN/PPE composites with MWCNT fillers are presented in Fig. 5.8. The results of the neat blends are also shown for comparison. Due to the elasticity of CNT and the elastic CNT-CNT interaction, the presence of MWCNT enhances the moduli and complex viscosity of SAN/PPE 40/60 blend. The reduced slopes at low frequencies also reflect the effect of stiff MWCNT. Meanwhile, the complex viscosity of the blends is increases at low frequencies in case of pristine MWCNT. As the loading of MWCNT in SAN/PPE blends is lower than the one in SAN/MWCNT composites, the effect of MWCNT in the SAN/PPE blend shown is not as pronounced as the one in the SAN matrix.



(a)



(b)



(c)

Fig. 5.8 Storage modulus G' (a), loss modulus G'' (b) and complex viscosity $|\eta^*|$ (c) of SAN/PPE 40/60 and its composites with different MWCNT fillers as a function of angular frequency at 260 °C.

However, in contrast to the composites with pristine MWCNT, the dynamic moduli and the complex viscosity of SAN/PPE 40/60-MWCNT-PS₇₃⁷⁶ composites are dramatically decreased. As shown in TEM micrographs (Fig. 5.3), that these functionalized MWCNT are mainly located in the PPE phase. Hence, the soften effect of grafted PPE occurring in the PPE phase should be considered as the reason leading to the decrease of rheological values in case of SAN/PPE composites [21]. On the other hand, the composite of SAN/PPE 40/60-MWCNT – PS₂₁²⁸ performs a quite similar behavior to the material with pristine MWCNT. In this composite, MWCNT are scattered in both SAN and PPE phase, so that, MWCNT cannot form effective network for rheological performance. Furthermore, the low molecular weight of grafted PS results in a low concentration of PS with respect to the amount of blend (0.4 wt%). In contrary, the value in SAN/PPE 40/60-MWCNT-PS₇₃⁷⁶ is 3wt%. Thus, the grafted PS also shows a weak influence on the properties of composites. Considering these two facts, it is not hard to understand the fact SAN/PPE 40/60-MWCNT – PS₂₁²⁸ perform similar properties to the composites with pristine MWCNT.

5.3 Conclusions

SAN/PPE composites with various MWCNT were prepared by melt processing. Prior to melt blending, MWCNT fillers were pre-mixed with SAN via solution casting. From TEM microscopies, it shown that pristine MWCNT dispersed with small size of agglomerates in SAN matrix. With higher molecular weight of grafted PS, functionalized MWCNT were found to aggregate again with large size because of the immiscibility between SAN and the grafted PS. For rheological properties, the composites with MWCNT presented a pronounced “solid-like” behavior owing to the high loading of fillers (2.5 wt%). The dynamic moduli of G' and G'' as well as the complex viscosity of SAN decreased with increment of molecular weight of grafted PS on MWCNT due to the softening effect of grafted PS and the dispersion of MWCNT in the matrix.

Then, the SAN/PPE 40/60 composites filled with 1 wt% of MWCNT were prepared by blending the SAN/MWCNT composites with PPE powder. In the blends, pristine MWCNT selectively stayed in the pre-mixed SAN phase, whereas, the functionalized MWCNT tended to migrate to the PPE phase driven by the miscibility between PPE and grafted PS on the surface of MWCNT. The extent of migration strongly depended on the molecular weight of the grafted PS. Rheological results reflected the influence of molecular weight of grafted PS on the microstructure and Linear viscoelastic properties of the composites. When functionalized MWCNT contain a high molecular weight of polystyrene (73 kg/mol), most of the nanofillers migrated into the PPE phase, leading to a decrease of both dynamic moduli and complex viscosity. On the other hand, functionalized MWCNT with a lower molecular weight PS (21 kg/mol) show a similar rheological behavior of the blends as pristine MWCNT because of the absence of CNT-CNT network and the low concentration of PS (0.4 wt%) in the blends.

References

1. Paul DR. *Polymer blends*. New York: Academic Press, 1978.
2. Utracki LA. *Polymer Alloys and Blends: Thermodynamics and Rheology*. München: Hanser Publisher, 1989.
3. Iijima S. *Nature* 1991;354(7):56-58.
4. Baughman RH, Zakhidov AA, and Heer WA. *Science* 2002;297(5582):787-792.
5. Meincke O, Kaempfer D, Weickmann H, Friedrich C, Vathauer M, and Warth H. *Polymer* 2004;45(3):739-748.
6. Liu XQ, Yang W, Xie BH, and Yang MB. *Materials & Design* 2011;34:355-362.
7. Chiu JJ, Kim BJ, Kramer EJ, and Pine DJ. *Journal of the American Chemical Society* 2005;127(14):5036-5037.
8. Khatua BB, Lee DJ, Kim HY, and Kim JK. *Macromolecules* 2004;37(7):2454-2459.
9. Ray SS and Bousmina M. *Macromolecular Rapid Communications* 2005;26(20):1639-1646.
10. Ray SS, Pouliot S, Bousmina M, and Utracki LA. *Polymer* 2004;45(25):8403-8413.
11. Chow WS, Mohd-Ishak ZA, Karger-Kocsis J, Apostolov AA, and Ishiaku US. *Polymer* 2003;44(24):7427-7440.
12. Wu DF, Wu LF, Zhang M, Zhou WD, and Zhang YS. *Journal of Polymer Science Part B: Polymer Physics* 2008;46(12):1265-1279.
13. Ruckdäschel H, Sandler JKW, Altstädt V, Schmalz H, Abetz V, and Müller AHE. *Polymer* 2007;48(9):2700-2719.
14. Haase A, Hesse P, Brommer L, Jacobs O, Abetz C, Handge UA, Boschetti-de-Fierro A, and Abetz V. *Macromolecular Materials and Engineering* 2012;n/a-n/a.
15. Wu D, Zhang Y, Zhang M, and Yu W. *Biomacromolecules* 2009;10(2):417-424.
16. Schmidt LR. *Journal of Applied Polymer Science* 1979;23(8):2463-2479.
17. Bose S, Bhattacharyya AR, Kodgire PV, Misra A, and Pötschke P. *Journal of Applied Polymer Science* 2007;106(6):3394-3408.
18. Graebling D, Muller R, and Palierne JF. *Macromolecules* 1993;26(2):320-329.
19. Amr IT, Amer AA, P ST, Harthi MA, Girei SA, Sougrat R, and Atieh MA. *Composites Part B: Engineering* 2011;42(6):1554-1561.
20. Bousmina M. *Rheologica Acta* 1999;38(3):251-254.
21. PrestJr WM and Porter RS. *Journal of Polymer Science Part A: Polymer Physics* 1972;10(9):1639-1655.

SAN/PPE 40/60 blend filled with functionalized MWCNT with P(MMA-*co*-S) random copolymers: Influence of molecular weight of grafted polymer on localization of MWCNT and the properties of its composites

6.1 Introduction

In Chapter 5, we observed a fact that migration of MWCNTs could be controlled by the molecular weight of grafted polymer on their surface owing to the specific thermodynamic relationship between grafted polymer and the polymer component in blends. However, by means of this method only a tendency of migration was observed. Main fraction of MWCNT still cannot be confined at the interface. In this chapter, we utilized an alternative approach, i.e. introducing random copolymers, to adjust the localization of nanotubes in binary blends.

Many experimental and theoretical results have demonstrated the possibility of using random copolymers which contain the same monomeric or miscible units as the blend components as compatibilizers in immiscible blends [1-4]. Lee et al. [1] chose random copolymer of styrene and methyl methacrylate (SMMA) with 70 wt % of styrene as compatibilizer for PMMA/PS binary blends. TEM micrographs clearly demonstrated that SMMA copolymer moved to the

interface of PMMA/PS blends during melt mixing and formed encapsulating layers. This localization and encapsulation of random copolymer were supported by their theoretical calculation of spreading coefficients. Furthermore, the authors extended their investigation to other blend systems by replacing one or both of blend components with corresponding miscible components. Similar encapsulations of random copolymer were also observed in several binary blends, such as in the poly(phenylene oxide)/polycarbonate (PPO/PS) blends compatibilized with SMMA. Besides, Kulasekere et al. [5] found that, although the random copolymer of PMMA and PS (P(MMA-*co*-S)) with 68 wt% of styrene was not miscible with either PS or PMMA, such kind of copolymer can markedly broaden the interface between PS and PMMA and significantly improve the toughness of PMMA/PS blends. Based on these previous works, random copolymers locating at the interface show ability to enhance the interfacial adhesion [3, 5, 6] and reduce the interfacial tension between blend phases [7]. Furthermore, compared to block or graft copolymers, synthesis of random copolymers is more facile and less expensive [6].

In the present study, considering block copolymers containing methyl methacrylate and styrene units are confirmed to be a good compatibilizer for poly(styrene-*co*-acrylonitrile)/poly(2, 6-dimethyl-1, 4-phenylene ether) (SAN/PPE) blends [8-10], random copolymer containing MMA and styrene units is selected to functionalize the surface of MWCNT in order to tuning the localization of nanotubes in SAN/PPE blends. The polymerization of random copolymer was realized via atom transfer radical polymerization (ATRP), of which details have been described in Chapter 4. Before analyzing experimental results, the localization of MWCNT in SAN/PPE blends will be predicted by thermodynamic calculation. The influence of molecular weight of grafted polymer on the localization of MWCNT and the morphological properties of composites will be investigated by analyzing

the TEM microscopies. In order to further understand the microstructural change of the composites, rheological and dielectric properties of composites are also studied in this chapter.

6. 2 Results and discussion

Two specifically functionalized MWCNT containing different molecular weights of grafted P(MMA-*co*-S) copolymers were selected to prepare SAN/PPE composites. For comparison, the composites with pristine MWCNT were also studied. The used MWCNT fillers for preparing SAN/PPE composites are listed in Table 6.1.

Table 6.1 Properties of selected functionalized MWCNT in SAN/PPE composites

Code	M_n ^(a) [kg/mol]	Content of grafted copolymers ^(b) [wt%]	Fraction of PS ^(c) [%]
SAN/PPE-MWCNT	---	---	---
SAN/PPE-MWCNT-CO-L	29.5	30	56
SAN/PPE-MWCNT-CO-H	74.7	80	56

(a) The molecular weights of grafted copolymer were detected by GPC

(b) The contents of grafted copolymer were determined by TGA

(c) The fraction of component in copolymer was calculated according the results form $^1\text{H-NMR}$

6.2.1 Morphology of SAN/PPE 40/60 blend filled with MWCNT

6.2.1.1 Theoretical prediction of the localization of pristine MWCNT in the SAN/PPE blends

Regarding to the state of pristine MWCNT in immiscible blends, the selectivity of MWCNT localization is generally explained as a result of thermodynamic equilibrium of the MWCNT fillers in the blends, which can be described by the wetting coefficient ω_α [11-14]. The

wetting coefficient is defined as a simple mathematical function of interfacial tension [15] and can be adapted to SAN/PPE blends as:

$$\omega_\alpha = \frac{\gamma_{CNT-SAN} - \gamma_{CNT-PPE}}{\gamma_{SAN-PPE}} \quad \text{Eq. 6.1}$$

where γ are the interfacial tensions between the different components. Three cases can be distinguished: If $\omega_\alpha > 1$, CNT are predicted to be in the second named polymer phase (PPE); If $\omega_\alpha < -1$, CNT are assumed to locate in the first named phase (SAN); If $-1 < \omega_\alpha < 1$, CNT are presumed to concentrate at the interface between the two polymeric components.

The interfacial tension between different materials can be calculated based on the surface tension of each component using the harmonic-mean equation [16]:

$$\gamma_{12} = \gamma_1 + \gamma_2 - 4\left(\frac{\gamma_1^d \gamma_2^d}{\gamma_1^d + \gamma_2^d} + \frac{\gamma_1^p \gamma_2^p}{\gamma_1^p + \gamma_2^p}\right) \quad \text{Eq. 6.2}$$

and the geometric-mean equation [16]

$$\gamma_{12} = \gamma_1 + \gamma_2 - 2\left(\sqrt{\gamma_1^d \gamma_2^d} + \sqrt{\gamma_1^p \gamma_2^p}\right) \quad \text{Eq. 6.3}$$

where γ_1, γ_2 are the surface tension of the components 1 and 2; γ_1^d, γ_2^d are the dispersive parts of the surface tension of components 1 and 2; γ_1^p, γ_2^p are the polar parts of the surface tension of the components 1 and 2. The harmonic-mean equation is considered to be more suitable for low-tension materials and the geometric one is valid to estimate the surface tension between high-tension materials and low-tension materials.

The values of surface tension of SAN, PPE and MWCNT at 260 °C are listed in Table 6.2. Because of the high viscosity of PPE, no literature has reported experimental data of the surface tension of PPE in the melt. In this text, we estimated the surface tension of pure PPE at high temperature according to the theoretical study of Everaert et al. [17].

Table 6.2 Surface tension of the polymers and MWCNT at 260 °C

Material	Total surface tension [γ , mJ·m ⁻²]	Dispersive surface tension [γ^d , mJ·m ⁻²]	Polar surface tension [γ^p , mJ·m ⁻²]	Reference
MWCNT	27.8	17.6	10.2	[18]
MWCNT	45.3	18.4	26.7	[19]
SAN	29.5	22.4	7.1	[11]
PPE	28.4	22.2	6.2	[17], [20]

Table 6.3 Interfacial tensions at 260 °C calculated from harmonic and geometric mean equations

Material	Interfacial tension according to harmonic-mean equation [mJ·m ⁻²]	Interfacial tension according to geometric-mean equation [mJ·m ⁻²]
SAN/PPE	0.06	0.04
SAN/MWCNT [18]	1.13	0.58
SAN/MWCNT [19]	11.72	6.44
PPE/MWCNT [18]	1.51	0.80
PPE/MWCNT [19]	13.10	7.32

Two different values of surface tension are widely accepted for MWCNT [11, 21, 22]. Nuriel et al. [18] measured the surface tension of MWCNT with a diameter of approx. 30 nm. The values from their study are 45.3 mJ·m⁻² for the total surface tension, while, 18.4 mJ·m⁻² and 26.9 mJ·m⁻² for dispersive and polar surface tension, respectively. Barber et al. [19] applied atomic force microscopy and a Wilhelmy balance method to quantify the contact angle between MWCNT and different organic liquids. The measured nanotubes were grown by arc-discharge with a diameter of approx. 20 nm. The total surface tension of MWCNT in their study was 27.8 mJ·m⁻² with a dispersive component of 17.6 mJ·m⁻² and a polar component of 10.2 mJ·m⁻². Since the diameter of MWCNT varies, these two typical data are both adapted in our estimation. On the basis of these data, the calculated interfacial energies are listed in Table 6.3 and the corresponding wetting coefficient values are given in Table 6.4.

Table 6.4 Wetting coefficient estimated according to the harmonic-mean and the geometric-mean equations

System	ω_α [harmonic-mean equation]	ω_α [geometric-mean equation]
SAN/PPE/MWCNT [18]	-6.33	-5.50
SAN/PPE/MWCNT [19]	-23.00	-22.00

It can be seen in Table 6.4 that the wetting coefficient is negative in all cases, because the interfacial energies between SAN and MWCNT are lower than the ones involving PPE. This marginal difference of the interfacial energies should be sufficient to promote the location of MWCNT in the preferable phase in thermodynamic equilibrium [23]. Consequently, according to the aforementioned estimation, the localization of MWCNT in SAN/PPE blends is predicted to be in the SAN phase which has a better affinity with MWCNT.

However, Majeste et al. [24] and Pötschke et al. [25] stated in their recent studies that the effect of thermodynamic interaction in the systems can be hampered by a very high polymer viscosity, especially in immiscible blends where the two components have significantly different viscosities. In their works, pristine MWCNT fillers were found to be favorable with the phase with lower viscosity where they can diffuse more rapidly. Thus, it is essential to take into account the influence of viscosity. In SAN/PPE blends, referring to our previous measurements of the used materials under the same processing conditions [26], the SAN component ($\eta_0 = 900$ Pas) is much less viscous than the PPE component ($\eta_0 = 45600$ Pas) at 260 °C. Therefore, even only considering the effect of viscosity, MWCNT would be still presumed to disperse selectively in the SAN phase, but neither in the PPE phase nor at the interface of the blends.

6.2.1.2 Theoretical prediction of microstructure of SAN/PPE/P(MMA-*co*-S) ternary blend

After functionalization, MWCNT will be wrapped by an organic layer with a certain thickness. In this case, the components of the blends will directly contact with the grafted polymer layer rather than the neat surface of MWCNT. Many examples revealed that the thermodynamic equilibrium between the blends and the grafted group on nanoparticles can provide a driving force to confine the localization of CNT in a specific phase or at the interface [26-29]. Thus, in order to understand the localization of functionalized MWCNT, it is necessary to study the localization of P(MMA-*co*-S) random copolymer in SAN/PPE 40/60 blend.

Generally, the microstructure of ternary blends can be predicted by means of the concept of the spreading coefficient. Such spreading coefficient is possible to be evaluated by the Harkin's equation [30] that was rewritten by Hobbes et al. [31]. Based on this theory, SAN/PPE/P(MMA-*co*-S) blends typically display as four kinds of morphologies, which can be elucidated by the minimization of the interfacial free energy. These types of morphologies and their corresponding thermodynamic state are listed in Table 6.5, where A, B and C denote P(MMA-*co*-S), PPE and SAN, respectively.

Table 6.5 Possible morphologies of SAN/PPE/P(MMA-*co*-S) ternary blends predicted by spreading coefficient

Type	Spreading coefficient ^(a)	Morphology ^(b)	Interaction
1	$\lambda_{BAC} = \gamma_{BC} - (\gamma_{AB} + \gamma_{AC}) < 0$ $\lambda_{ABC} = \gamma_{AC} - (\gamma_{AB} + \gamma_{BC}) < 0$ $\lambda_{ACB} = \gamma_{AB} - (\gamma_{AC} + \gamma_{BC}) > 0$	PPE SAN A	Complete wetting in the SAN phase
2	$\lambda_{BAC} = \gamma_{BC} - (\gamma_{AB} + \gamma_{AC}) < 0$ $\lambda_{ABC} = \gamma_{AC} - (\gamma_{AB} + \gamma_{BC}) > 0$ $\lambda_{ACB} = \gamma_{AB} - (\gamma_{AC} + \gamma_{BC}) < 0$	PPE SAN A	Complete wetting in the PPE phase
3	$\lambda_{BAC} = \gamma_{BC} - (\gamma_{AB} + \gamma_{AC}) > 0$ $\lambda_{ABC} = \gamma_{AC} - (\gamma_{AB} + \gamma_{BC}) < 0$ $\lambda_{ACB} = \gamma_{AB} - (\gamma_{AC} + \gamma_{BC}) < 0$	PPE SAN A	Complete wetting at the interface
4	$\lambda_{BAC} = \gamma_{BC} - (\gamma_{AB} + \gamma_{AC}) < 0$ $\lambda_{ABC} = \gamma_{AC} - (\gamma_{AB} + \gamma_{BC}) < 0$ $\lambda_{ACB} = \gamma_{AB} - (\gamma_{AC} + \gamma_{BC}) < 0$	PPE SAN A	Partial wetting morphology showing a three-phase line of contact

(a) Spreading coefficients are calculated according to the modified Harkin's equation, where λ_{ijk} is the spreading coefficient; γ_{ij} is the interfacial tension between phase i and j .

(b) The schematic diagram graphs are reproduced from Ref. [32].

Since the interfacial tension γ_{ij} is proportional to the square root of the Flory-Huggins interaction parameter, the calculation of spreading coefficient are approximated by Equation 6.4 when one assumes that all components of blends have the same effective length per repeating unit:

$$\lambda_{ijk} = \sqrt{\chi_{ik}} - (\sqrt{\chi_{ij}} + \sqrt{\chi_{jk}}) \quad \text{Eq. 6.4}$$

where λ_{ijk} is the spreading coefficient among the three components, χ_{ik} , χ_{ij} and χ_{jk} are the Flory-Huggins interaction parameters between the different components. For our system, the χ values needed for estimation of the spreading coefficient are listed in Table 6.6. The interaction parameters between the components of the blends and the P(MMA-*co*-S) copolymers ($\chi_{PPE/P(MMA-co-S)}$ and $\chi_{SAN/P(MMA-co-S)}$) are assessed by Equation 6.5 [33, 34]:

$$\chi_{A/P(MMA-co-S)} = f_S \chi_{A/PS} + (1 - f_S) \chi_{A/PMMA} - f_S (1 - f_S) \chi_{PMMA/PS} \quad \text{Eq. 6.5}$$

where $\chi_{A/P(MMA-co-S)}$, $\chi_{A/PS}$ and $\chi_{A/PMMA}$ are the interaction parameter of SAN or PPE with P(MMA-*co*-S), the PS segments and the PMMA segments, respectively; f_S is the mole fraction of PS in P(MMA-*co*-S) random copolymer.

Table 6.6 Miscibility and χ values for SAN/PPE/P(MMA-*co*-S) ternary blends pairs

Polymer pair	Miscibility	χ_{ij}	Ref.
PPE/SAN	immiscible	0.034	[9]
PPE/PS	miscible	-0.1	[9]
PPE/PMMA	immiscible	0.5	[9]
SAN/PS	immiscible	0.098 ^(a)	[35]
SAN/PMMA	miscible	-0.008	[9]
PS/PMMA	immiscible	0.0044	[9]
PPE/P(MMA- <i>co</i> -S)	immiscible	0.1629 ^(b)	-
SAN/P(MMA- <i>co</i> -S)	immiscible	0.05028 ^(b)	-

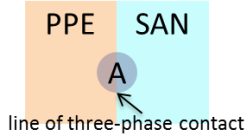
(a) The interaction parameter of SAN/PS pair is calculated according to the equation: $\chi_{SAN/PS} = f_{AN}^2 \chi_{S-AN}$

(b) The interaction parameter between SAN or PPE and P(MMA-*co*-S) are calculated by equation (6) using the data listed in the table.

Using χ values in Table 6.6, the spreading coefficients are estimated and shown in Table 6.7. Based on these results, it can be concluded that the grafted P(MMA-*co*-S) copolymer on the surface of MWCNT is not miscible with neither SAN nor PPE. Moreover, the spreading coefficients in all cases are negative. Thus, for *co*-continuous SAN/PPE blends, the grafted P(MMA-*co*-S) random copolymer with a minor fraction tend to form separated droplets at the interface forming a partial wetting morphology. However, it is notable that the microstructure of ternary blends also depends on the structure of major phases. When the SAN/PPE blend has a droplet structure with SAN as matrix and PPE as dispersed spheres, the minor components of PPE and P(MMA-*co*-S) will form relatively separated spheres in the SAN

phase which contact each other by a three-phase line. On the contrary, when PPE is the matrix, SAN and P(MMA-*co*-S) will separately disperse in the PPE phase. In order to minimize the surface tension in the system, the tendency of forming aforementioned microstructure should have significant influence and determine the final localization of functionalized MWCNT in SAN/PPE blends.

Table 6.7 calculated spreading coefficient and possible microstructure of SAN/PPE/P(MMA-*co*-S) ternary blends

Spreading coefficient	Morphology of SAN/PPE/P(MMA- <i>co</i> -S)
$\lambda_{BAC} = \gamma_{BC} - (\gamma_{AB} + \gamma_{AC}) = -0.4637 < 0$	
$\lambda_{ABC} = \gamma_{AC} - (\gamma_{AB} + \gamma_{BC}) = -0.3417 < 0$	 Type 4 : Partial wetting morphology showing a three-phase line of contact
$\lambda_{ACB} = \gamma_{AB} - (\gamma_{AC} + \gamma_{BC}) = -0.0051 < 0$	

6.2.1.3 Influence of molecular weight of grafted copolymers on the location of MWCNT fillers in immiscible SAN/PPE 40/60 blend

In Chapter 5, we demonstrated that the molecular weight of grafted polymer showed a pronounced effect on the transfer of MWCNT in SAN/PPE blends [26]. In this chapter, although no pre-mixing procedure was applied, the locations of MWCNT fillers were expected to vary with molecular weight of grafted copolymers.

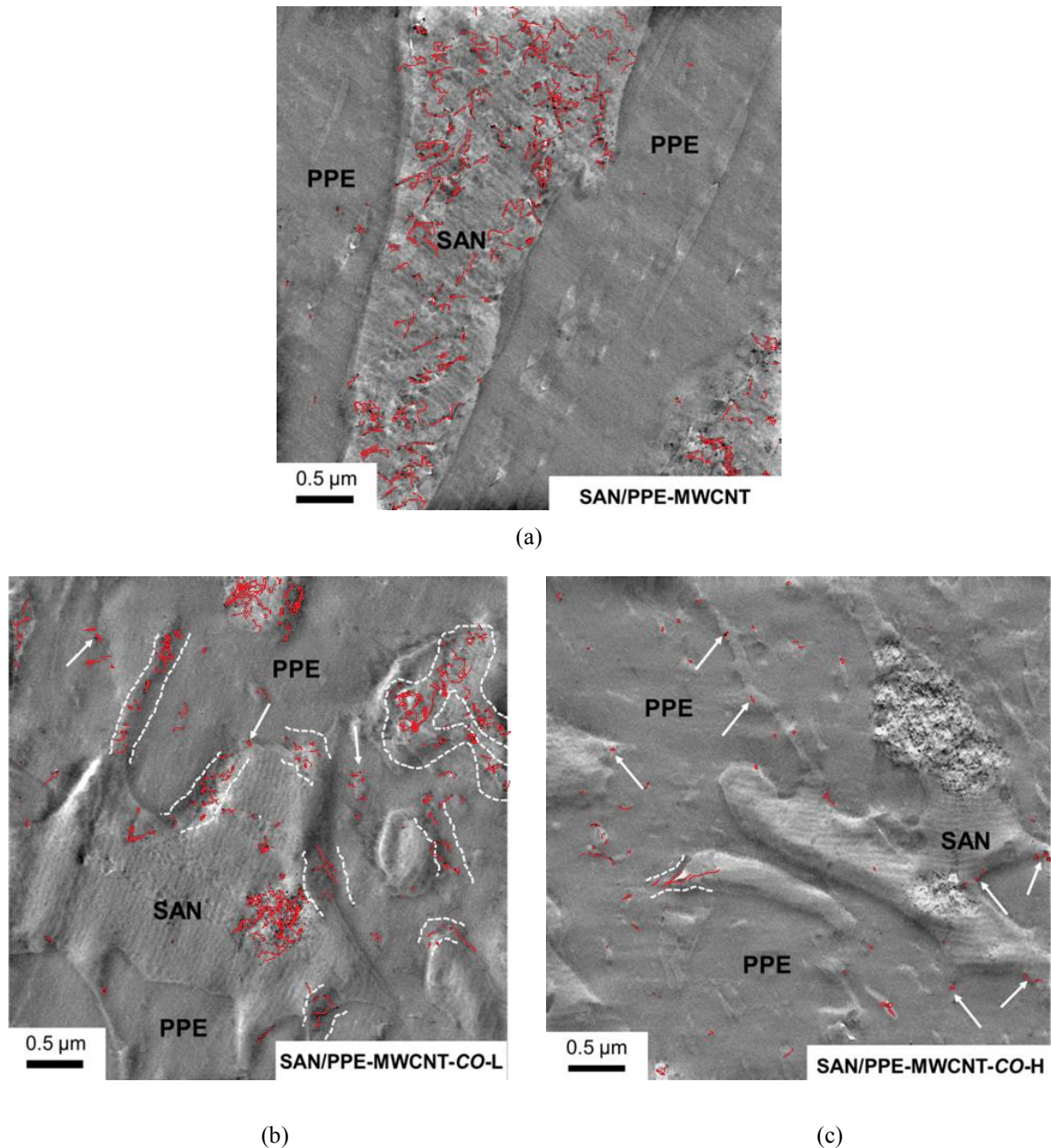


Fig. 6.1 TEM micrographs of SAN/PPE 40/60 blends filled with various MWCNT fillers: SAN/PPE-MWCNT (a), SAN/PPE-MWCNT-CO-L (b) and SAN/PPE-MWCNT-CO-H (c). The MWCNT locating at the interface are highlighted by the pairs of dashed lines and the arrows.

Transmission electron micrographs of SAN/PPE 40/60 blends filled with different MWCNT fillers are shown in Fig. 6.1. The PPE phase appears as grey and the SAN phase shows as brighter regions. As can be seen in Fig. 6.1(a), most of pristine MWCNT are initially located in the bright SAN phase. Only very few tubes can be found in the PPE phase. This micrograph confirms the prediction evaluated from the wetting coefficient and viscosity ratio

of SAN and PPE (see Section 6.2.1.1). Similar phenomenon was also observed in case of the composites with functionalized MWCNT with PS (see Chapter 5), where the MWCNT were premixed with SAN before blending with PPE [26].

In contrast to pristine MWCNT, the location of functionalized MWCNT with grafted polymers is mainly influenced by the thermodynamic relationship between the blend components and the grafted polymer. In Fig. 6.1(b), the main fraction of the functionalized MWCNT is found to arrange at the interface of the blends (highlighted by white dashed lines and arrows). The phenomenon is more pronounced at the boundary between the continuous PPE phase and the small SAN droplets. This localization can be explained by the microstructure of SAN/PPE/P(MMA-*co*-S) ternary blends where P(MMA-*co*-S) locates at the interface of SAN/PPE with partial wetting morphology. Moreover, the discontinuous network of MWCNT at the interface is more or less also caused by this partial wetting effect. Additionally, the low MWCNT loading could be another reason for such discontinuous dispersion of MWCNT at the interface. On the other hand, when the molecular weight of grafted polymer increases, more evident agglomerates form nearby in the SAN phase but also near the boundary (see Fig. 6.1(c)). In this case, less MWCNT are dispersed at the interface showing as individual nanotubes (highlight by white arrows). As it is known that large block copolymers with a high concentration in the system can lead to formation of micelles [1, 9], micellization of grafted P(MMA-*co*-S) might be one effect inducing functionalized MWCNT to aggregate. More important, the overall morphology of SAN/PPE is found to vary with the change of molecular weight of P(MMA-*co*-S), which might be a main reason leading to the different dispersion of MWCNT in system. This will be discussed in detail in the next section.

6.2.1.4 The influence of molecular weight of grafted copolymers on the morphologies of SAN/PPE blend

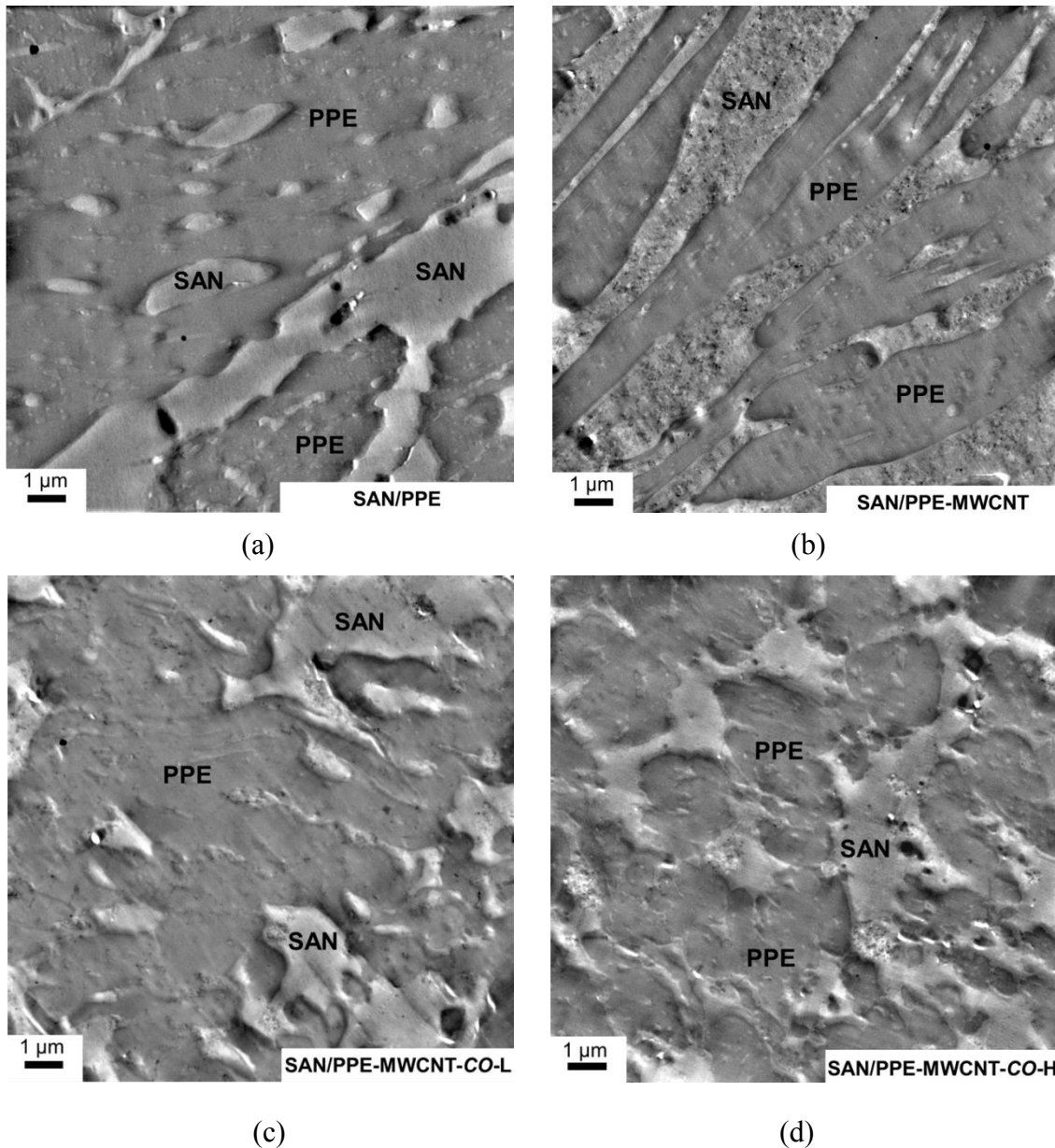


Fig. 6.2 Morphologies of SAN/PPE 40/60 blends and its composites with various MWCNT fillers: (a) SAN/PPE-MWCNT; (b) SAN/PPE-MWCNT-CO-L; (c) SAN/PPE-MWCNT-CO-H

As discussed above, the localization of MWCNT fillers is significantly influenced by the molecular weight of grafted P(MMA-*co*-S) copolymers on their surface. Due to this variation of location, the morphology of SAN/PPE 40/60 blend also changes. In Fig. 6.2, the micrographs of SAN/PPE 40/60 blend morphology and its composites with various MWCNT

fillers are shown.

In the TEM micrograph of the neat SAN/PPE blend (see Fig. 6.2(a)), PPE forms the continuous phase. The main fraction of SAN is also continuous and many small inclusions of SAN are dispersed in PPE. After filling with pristine MWCNT, both the SAN and the PPE phase present a high level of continuity and the size of SAN droplets in PPE significantly decreases (see Fig. 6.2(b)). These different morphologies are attributed from the change of the viscosity ratio between the two blend components. The selective location of fillers in SAN enhances the viscosity of the SAN phase and consequently bridges the viscous gap between SAN and PPE, leading to a *co*-continuous structure of the blend.¹ With the transfer of functionalized MWCNT from the SAN phase to the interface, the microstructure of SAN/PPE blends, especially the continuity of the PPE phase, is changed. In the case of SAN/PPE-MWCNT-CO-L, the breakup of the continuous PPE phase is observed in Fig. 6.2(c). However, both SAN and PPE phase still keep continuity to some extent. Therefore, many MWCNT are concentrated at the interface because of the localization of P(MMA-*co*-S) in *co*-continuous SAN/PPE blends. When molecular weight of grafted P(MMA-*co*-S) copolymers increases, the continuity of the PPE phase is considerably disrupted and turned into droplets dispersing in the continuous SAN phase (see Fig. 6.2(d)). This apparent variation of morphology might be originated from the softening effect of grafted copolymer and the change of the viscosity ratio between the two components in the melt. As we discussed in Section 6.2.1.2, P(MMA-*co*-S) copolymer in droplets structure of SAN/PPE blends cannot neither form a complete wetting layer encapsulating the PPE phase nor locate at the interface with a three-phase contact. Alternatively, they prefer to disperse in SAN as spheres. Therefore, agglomerates of functionalized MWCNT with large size are located in the SAN phase and nearby the boundary of blends.

On the basis of abovementioned theoretical prediction and TEM micrographs, it can be concluded that localization of MWCNT significantly depends on the grafted polymer on their surface. Moreover, with the change of molecular weight of the grafted polymers, both the localization of nanotubes and microstructure of SAN/PPE blend are varied.

6.2.2 Rheological properties of SAN/PPE 40/60 blend filled with MWCNT fillers

In order to further elucidate the influence of MWCNT on the microstructure of SAN/PPE blends, the rheological properties of SAN/PPE blends filled with various MWCNT are analyzed by comparing them with the neat blend. The frequency dependence of the storage modulus, the loss modulus and the complex viscosity of the neat SAN/PPE 40/60 blend and its composites are presented in double logarithmic scales in Fig. 6.3.

Since the storage modulus at low frequencies is very sensitive to the microstructure of the materials, a remarkable difference between the neat SAN/PPE blend and the composites is clearly demonstrated in Fig. 6.3(a), even if the effective loading of MWCNT in each sample is only 1 wt%. The slope of G' for the neat SAN/PPE blend is lower than 2 with a value of approx. 0.5, indicating the phase-separated structure of the blend [36]. After adding pristine MWCNT, the slope of SAN/PPE-MWCNT is further decreased with a higher storage modulus at low frequencies. The TEM micrograph in Fig. 6.1(a) shows that most pristine MWCNT are selectively located in the SAN phase. Thus, the increase of G' by addition of pristine MWCNT should be a response of the reinforcement of the SAN phase caused by the elasticity of the MWCNT and elastic MWCNT-MWCNT interactions [37, 38], which is generally observed for polymer composites filled with CNT [39-42].

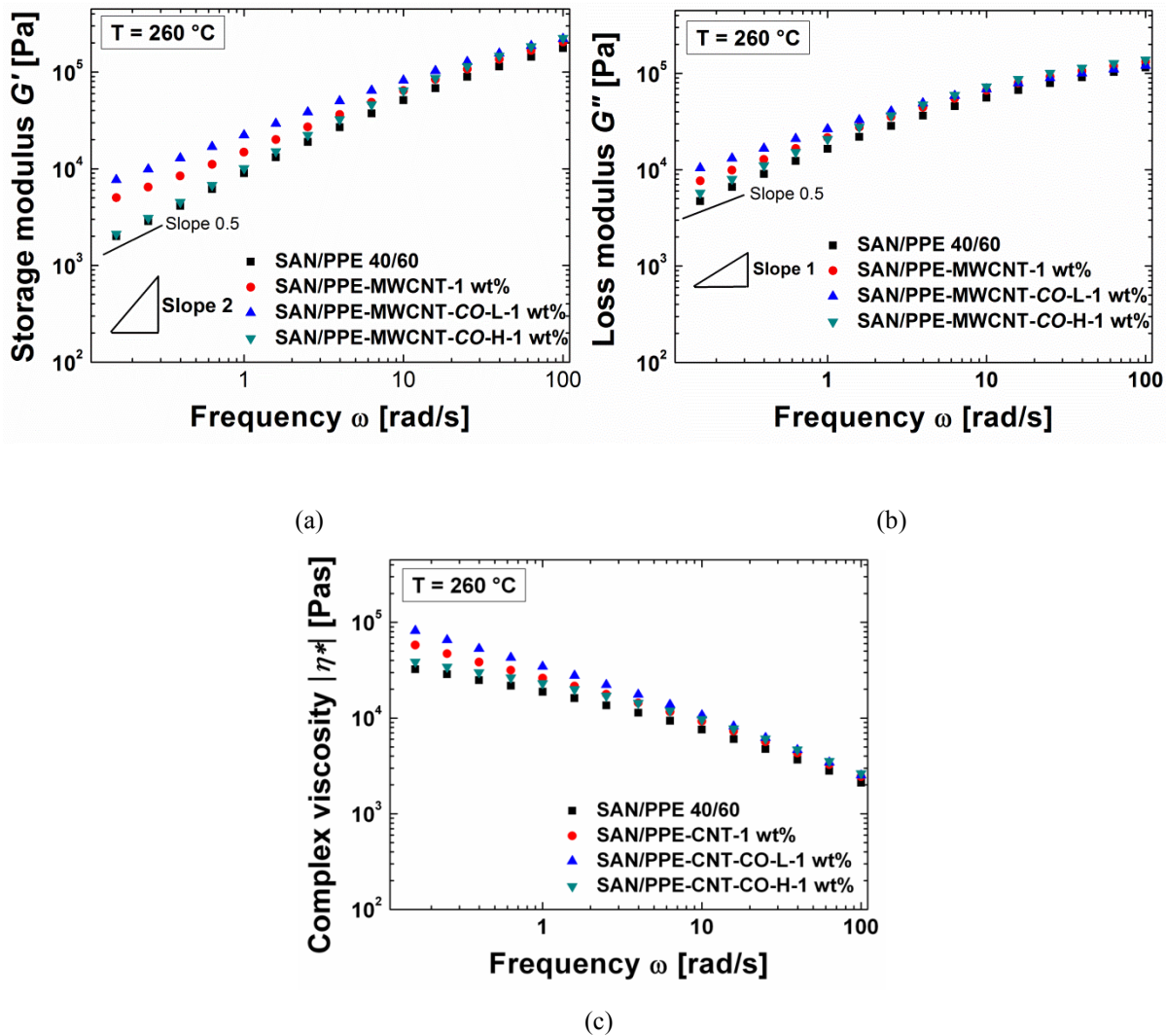


Fig. 6.3 Storage modulus G' (a), loss modulus G'' (b) and complex viscosity $|\eta^*|$ (c) of SAN/PPE 40/60 and its composites with MWCNT fillers as a function of angular frequency ω at $260\text{ }^{\circ}\text{C}$.

Interestingly, compared to other samples, the composite of SAN/PPE-MWCNT-CO-L presents the highest storage modulus at low frequencies. A slight increase of the loss modulus and the complex viscosity are also observed in Figs. 6.3(b) and (c). The increase of dynamic moduli and viscosity could be a result of formation of nanotube network due to the localization of MWCNT. In contrast to the random dispersion of pristine MWCNT with a long and visible distance between each other in the SAN phase, functionalized MWCNT locating along the interface are more or less concentrated together with good contact with each other. Thus, in these regions, the CNT-CNT interactions are enhanced [43]. This could be one of the contributions to the increase of elasticity of the composites. Nevertheless, such influence is overcome by the softening effect of grafted copolymers when the molecular weight of P(MMA-*co*-S) copolymers increases to a high level. As shown in Fig. 6.4, the

SAN/PPE-CNT-*CO*-H sample performs similar behavior to the neat SAN/PPE blends with relatively low dynamic moduli and complex viscosity. Furthermore, the pronounced agglomerates in SAN/PPE-CNT-*CO*-H could also be other fact resulting in the reduction of rheological values.

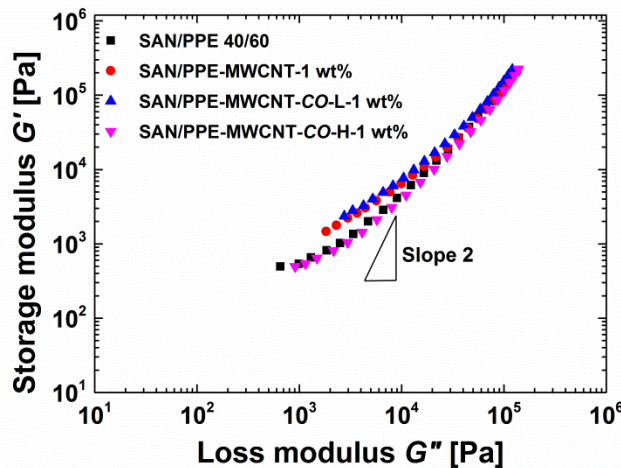


Fig. 6.4 Modified Cole-Cole plot of SAN/PPE 40/60 blend and its composites with MWCNT

The structural changes resulting from the localization of MWCNT are further elucidated by modified Cole-Cole plots (see Fig. 6.4). The Cole-Cole plots depict a slope of 2 for homopolymers without interfacial tension [44-46]. Owing to its multi-phase structure, the slope in the terminal region of the neat SAN/PPE 40/60 blend is less than 2. After addition of pristine MWCNT, the plot distinctively deviates from the curve of neat blend with a lower slope, which demonstrates the formation of a CNT-CNT network in the SAN phase. On the other hand, SAN/PPE-MWCNT-CO-L performs a more narrow distribution with a lower slope than the composite with pristine MWCNT. This phenomenon implies an interfacial interaction between functionalized MWCNT with SAN/PPE blends [47]. However, when the molecular weight of grafted polymer increases, the curve of SAN/PPE-MWCNT-CO-H is similar to the one of the neat blend. It is mainly attributed to the pronounced agglomeration in case of SAN/PPE-MWCNT-CO-H. Furthermore, the increased distance between individual nanotubes due to the wrapped polymer layer on the surface of MWCNT also weakens the interfacial interaction between MWCNT.

Combining these results, one can conclude that the molecular weight of grafted copolymer on the surface of MWCNT cannot only control the localization of MWCNT in SAN/PPE blends, but also has

an important influence on the morphological and rheological properties of the composites.

6.2.3 Dielectric properties of SAN/PPE 40/60 blend filled with MWCNT fillers

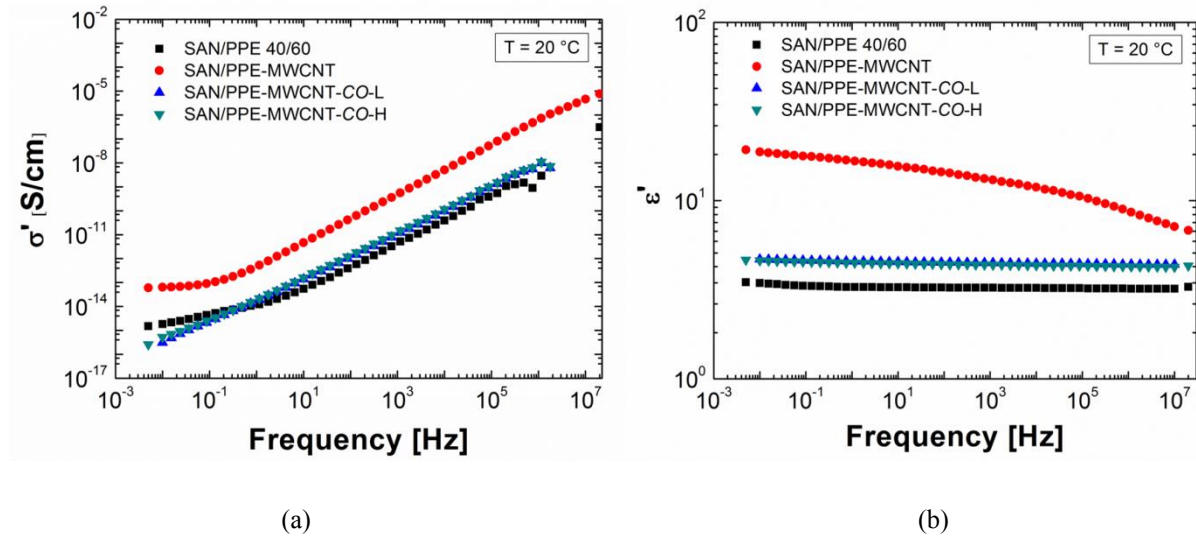


Fig. 6.5 AC conductivity δ' (a) and real part of complex permittivity ϵ' (b) of SAN/PPE 40/60 and its composites with MWCNT fillers as a function of frequency at 20 °C.

The electrical conductivity of SAN/PPE blend is detected by dielectric spectroscopy. SAN/PPE nanocomposite with pristine MWCNT show a significantly higher conductivity value (e.g. 10⁻¹³ S/cm at 0.001 Hz) than the neat blend (e.g. 10⁻¹⁵ S/cm at 0.005 Hz), since MWCNT cumulate in the SAN phase and forming a net-like structure with a good geometric and electrical contact with each other. The enhancement is larger than for pure SAN and a SAN/MWCNT composite under the same loading [11]. This is a typical evidence reflecting the decrease of the percolation threshold due to the double percolation. However, in this work, MWCNT loading of the composites does not reach the percolation threshold, which is characterized by a missing direct conductivity (DC) plateau at low frequencies [39, 48]. On the contrary, in Fig. 6.5(a), the real part of the conductivity of SAN/PPE-MWCNT is still frequency dependent at low frequencies, which means the MWCNT loading in the system is below the percolation threshold.

In cases of composites with functionalized MWCNT, the results perform a similar behavior to the neat SAN/PPE blend (e.g. 10^{-15} S/cm at 0.001 Hz), which is much smaller than the one with pristine MWCNT. It is widely known that, a three-dimensional network of MWCNT with good interactions formed by CNT is necessary to enhance the electrical conductivity [49, 50]. The MWCNT-MWCNT interactions are influenced by the state of dispersion of nanotubes. When pristine MWCNT are concentrated in the SAN phase, the concentration of MWCNT is sufficiently high to form an electrical network. Moreover, since the SAN phase present good continuity to some extend (see Fig. 6.2(b)), the conductive effect of MWCNT is strengthened. Consequently, pronounced enhancement of electrical conductivity is observed in this case. On the other hand, the functionalized MWCNT are scattered both in the interfacial region and in the PPE phase. Thus, the concentration of MWCNT in the filled region is too low to form CNT-CNT network. Furthermore, the fraction of PPE is predominant, so that, it is less possible to reach the percolation threshold when MWCNT were scattered in the entire blend in contrast to the situation when most of MWCNT only concentrate in the SAN phase. Thus, the dielectric data in Fig. 6.5 indicate a phenomenon that MWCNT mainly increase the electrical conductivity if they are located in the SAN phase, but not at the interface or in the PPE phase when it was functionalized with copolymers. Last but not least, compared to pristine MWCNT, more defects on the surface of functionalized MWCNT might be another important reason leading to a reduction of electrical conductivity, as the defects on functionalized MWCNT could deflect the electrons from their path leading to scattering of electrons [51]. In addition, it is notable that although there is no pronounced enhancement of electrical conductivity in the composites with functionalized MWCNT, an increase of dynamic moduli of SAN/PPE-MWCNT-CO-L was observed (see Fig. 6.3). Such phenomenon difference has also been observed in other composites [49], which should be mainly attributed to the different requirements of nanotubes network for electrical conductivity and rheological properties [39, 50]. For reaching the electrical percolation, nanotubes do not need to touch or geometrical overlap each other but it is necessary to have a

sufficiently small distance to allow hopping/tunneling processes (less than 5 nm). Nevertheless, the rheological properties of the composites are mainly determined by combination of the entangled polymer network, the nanotubes-polymer network, the MWCNT-MWCNT interactions as well as the elasticity of the nanotubes. In this case, the distance between two nanotubes is required to be smaller than the radius of gyration of a polymer chain (generally about dozens of nanometers) in order to ensure that two nanotubes can link together by a polymer chain and also can hinder the polymer chain mobility in the molten state. Thus, the required distance between two nanotubes for rheological percolation threshold is longer than the value for electrical percolation threshold. In other word, the critical loading of rheological percolation threshold should be lower the critical loading for electrical conductivity [50]. This could be the reason why the enhancement from the neat SAN/PPE blend to the SAN/PPE-MWCNT-CO-L composite is only visible in rheological moduli but not in the electrical conductivity.

In agreement with the Kramers-Kronig relation and the proportional relationship between AC conductivity and imaginary part of complex permittivity, the same information can be gathered from the permittivity plots (Fig. 6.5(b)) as from the conductivity plots (Fig. 6.5(a)). In the case of neat blends, the values remain frequency independent as an insulating material. A pronounced decrease of ϵ' with frequency is observed in the plots of SAN/PPE-MWCNT, implying an increased conductivity. However, the descent of the plot is strictly linear, illustrating that the loading of MWNCT is lower than the critical value of percolation threshold. In case of the composites with functionalized MWCNT, the permittivity of each sample is similar to the neat blend.

6.3 Conclusions

In this chapter, functionalized MWCNT with P(MMA-*co*-S) copolymers were used for modification of SAN/PPE immiscible blends. The influence of molecular weight of grafted

copolymer on the localization of MWCNT was studied.

From TEM micrographs, it showed that the grafted copolymer had a significant influence on the localization of MWCNT in SAN/PPE blend. The pristine MWCNT were found to selectively concentrate in the SAN phase, which was in agreement with theoretical prediction. After functionalizing with P(MMA-*co*-S) copolymers, MWCNT were preferentially located at the interface of the blends or agglomerated nearby the boundary, depending on the molecular weight of the grafted copolymers. With low molecular weight, a large fraction of functionalized MWCNT was confined at the interface. However, when the molecular weight of P(MMA-*co*-S) copolymers increased, pronounced agglomeration was observed in the SAN phase nearby the boundary. This phenomenon could be explained by the microstructure change of SAN/PPE blends and the micellization of high molecular weight of grafted copolymer.

The influence of functionalized MWCNT on the microstructure of the composites was also detected by rheological and dielectric measurements. The presence of pristine MWCNT remarkably increased the dynamic moduli and the complex viscosity of SAN/PPE blends. These values further rose when MWCNT were functionalized with low molecular weight P(MMA-*co*-S) copolymers. In this case, CNT-CNT interaction was improved owing to the well contacting MWCNT at the interface. However, with the increment of molecular weight, the composites showed a similar behavior to the neat blends with low dynamic moduli, which could be attributed to the softening effect of the grafted copolymers and the absence of CNT-CNT network. In the dielectric measurements, although the addition of pristine MWCNT pronouncedly enhance the conductivity of the composites even at low loading (1 wt%), little improvement was achieved in the cases of functionalized MWCNT. No complete conductive network formed by nanotubes and the location in the PPE phase is probably the main reason for the low conductivity..

In conclusion, grafting P(MMA-*co*-S) copolymers with appropriate molecular weight on the surface of MWCNT can be a feasible approach to confine MWCNT at the interface of SAN/PPE 40/60 blend due to the specific thermodynamic relationship between the grafted copolymers and the components in blend. The molecular weight of grafted polymer presents significant influence on the localization of MWCNT in the blends. . In this work, the influence of composition of copolymers on the localization is not discussed. According to the conception of spreading coefficient, P(MMA-*co*-S) copolymer with specific composition is possible to be miscible with both SAN and PPE forming a complete wetting at the interface of SAN/PPE blends. In other word, more uniform localization of MWCNT at the interface is probably realized by using functionalized MWCNT with such kind of random copolymer. This would be interesting and promising for investigation in future.

References

1. Lee MS, Lodge TP, and Macosko CW. *Journal of Polymer Science Part B: Polymer Physics* 1997;35(17):2835-2842.
2. Dai C-A, Dair BJ, Dai KH, Ober CK, Kramer EJ, Hui C-Y, and Jelinski LW. *Physical Review Letters* 1994;73(18):2472-2475.
3. Cho K, Tae Oan A, Hyun Soo R, and Kyung Hoon S. *Polymer* 1996;37(21):4849-4852.
4. Brown HR, Char K, Deline VR, and Green PF. *Macromolecules* 1993;26(16):4155-4163.
5. Kulasekere R, Kaiser H, Ankner JF, Russell TP, Brown HR, Hawker CJ, and Mayes AM. *Macromolecules* 1996;29(16):5493-5496.
6. Roe R-J and Rigby D. Phase relations and miscibility in polymer blends containing copolymers. *Polymer Physics*, vol. 82: Springer Berlin Heidelberg, 1987. pp. 103-139.
7. Lyatskaya Y, Gersappe D, Gross NA, and Balazs AC. *The Journal of Physical Chemistry* 1996;100(5):1449-1458.
8. Ruckdäschel H, Sandler JKW, Altstädt V, Schmalz H, Abetz V, and Müller AHE. *Polymer* 2007;48(9):2700-2719.
9. Ruckdäschel H, Sandler JKW, Altstädt V, Rettig C, Schmalz H, Abetz V, and Müller AHE. *Polymer* 2006;47(8):2772-2790.
10. Kirschnick T, Gottschalk A, Ott H, Abetz V, Puskas J, and Altstädt V. *Polymer* 2004;45(16):5653-5660.
11. Göldel A, Kasaliwal G, and Pötschke P. *Macromolecular Rapid Communications* 2009;30(6):423-429.
12. Wu M and Shaw L. *Journal of Applied Polymer Science* 2006;99(2):477-488.
13. Pötschke P, Pegel S, Claes M, and Bonduel D. *Macromolecular Rapid Communications* 2008;29(3):244-251.
14. Sun Y, Guo Z-X, and Yu J. *Macromolecular Materials and Engineering* 2010;295(3):263-268.
15. Sumita M, Sakata K, Asai S, Miyasaka K, and Nakagawa H. *Polymer Bulletin* 1991;25(2):265-271.
16. Wu S. *Journal of Macromolecular Science, Part C* 1974;10(1):1-73.
17. Everaert V, Groeninckx G, Pionteck J, Favis BD, Aerts L, Moldenaers P, and Mewis J. *Polymer* 2000;41(3):1011-1025.
18. Nuriel S, Liu L, Barber AH, and Wagner HD. *Chemical Physics Letters* 2005;404(4-6):263-266.

Chapter 6

19. Barber AH, Cohen SR, and Wagner HD. *Nano Letters* 2004;4(8):1439-1443.
20. http://www.accudynetest.com/polytable_01.html.
21. Baudouin AC, Devaux J, and Bailly C. *Polymer* 2010;51(6):1341-1354.
22. Zhang L, Wan C, and Zhang Y. *Polymer Engineering & Science* 2009;49(10):1909-1917.
23. Krasovitski B and Marmur A. *The Journal of Adhesion* 2005;81(7-8):869-880.
24. Fenouillot F, Cassagnau P, and Majesté JC. *Polymer* 2009;50(6):1333-1350.
25. Göldel A, Kasaliwal GR, Pötschke P, and Heinrich G. *Polymer* 2012;53(2):411-421.
26. Du B, Handge UA, Majeed S, and Abetz V. *Polymer* 2012;53(24):5491-5501.
27. Tao F, Nysten B, Baudouin AC, Thomassin JM, Vuluga D, Detrembleur C, and Bailly C. *Polymer* 2011;52(21):4798-4805.
28. Chen J, Shi YY, Yang JH, Zhang N, Huang T, and Wang Y. *Polymer* 2013;54(1):464-471.
29. Liu L, Wang Y, Li Y, Wu J, Zhou Z, and Jiang C. *Polymer* 2009;50(14):3072-3078.
30. Harkins WD. *The physical properties of surface films*. New York: Reinhold Publishing Corporation, 1952.
31. Hobbs SY, Dekkers MEJ, and Watkins VH. *Polymer* 1988;29(9):1598-1602.
32. Virgilio N, Sarazin P, and Favis BD. *Biomaterials* 2010;31(22):5719-5728.
33. Paul DR and Barlow JW. *Polymer* 1984;25(4):487-494.
34. Kammer HW. *Acta Polymerica* 1986;37(1):1-6.
35. Higashida N, Kressler J, and Inoue T. *Polymer* 1995;36(14):2761-2764.
36. Handge UA, Zeiler R, Dijkstra D, Meyer H, and Altstädt V. *Rheologica Acta* 2011;50(5-6):503-518.
37. Zeiler R, Handge UA, Dijkstra DJ, Meyer H, and Altstädt V. *Polymer* 2011;52(2):430-442.
38. Pötschke P, Abdel-Goad M, Alig I, Dudkin S, and Lellinger D. *Polymer* 2004;45(26):8863-8870.
39. Sung YT, Han MS, Song KH, Jung JW, Lee HS, Kum CK, Joo J, and Kim WN. *Polymer* 2006;47(12):4434-4439.
40. Lee SH, Cho E, Jeon SH, and Youn JR. *Carbon* 2007;45(14):2810-2822.
41. Kim JA, Seong DG, Kang TJ, and Youn JR. *Carbon* 2006;44(10):1898-1905.
42. Wu D, Zhang Y, Zhang M, and Yu W. *Biomacromolecules* 2009;10(2):417-424.
43. Han CD and Kim J. *Journal of Polymer Science Part B: Polymer Physics* 1987;25(8):1741-1764.
44. Pötschke P, Fornes TD, and Paul DR. *Polymer* 2002;43(11):3247-3255.
45. Ko SW, Gupta RK, Bhattacharya SN, and Choi HJ. *Macromolecular Materials and Engineering* 2010;295(4):320-328.
46. Kim JY, Han SI, and Hong S. *Polymer* 2008;49(15):3335-3345.
47. Pötschke P, Dudkin SM, and Alig I. *Polymer* 2003;44(17):5023-5030.
48. Cohen E, Zonder L, Ophir A, Kenig S, McCarthy S, Barry C, and Mead J. *Macromolecules* 2013;46(5):1851-1859.
49. Hu G, Zhao C, Zhang S, Yang M, and Wang Z. *Polymer* 2006;47(1):480-488.
50. Khare R and Bose S. *Journal of Minerals & Materials Characterization & Engineering* 2005;4(1):31-46.

Chapter 7

Summary and Outlook

7. 1 Summary and Outlook

The main objective of this work was to confine multi-walled carbon nanotubes (MWCNT) at the interface of binary blends by functionalizing MWCNT with desired polymers and study the effects of localization of MWCNT on the properties of the composites. In order to achieve this purpose, commercial MWCNT with amino groups were grafted with polystyrene (PS), poly(methyl methacrylate) (PMMA) and random copolymers of styrene and methyl methacrylate (P(MMA-*co*-S)). Since PS is miscible with poly(2,6-dimethyl-1,4-phenylene ether) (PPE) and PMMA has good miscibility with poly(styrene-*co*-acrylonitrile) copolymers (SAN) with specific acrylonitrile content, the grafted polymers on the surface of MWCNT are expected to provide a driving force to confine MWCNT at the interface of immiscible SAN/PPE phases.

The first part of this dissertation studied the functionalization of MWCNT by “*grafting-from*” and “*grafting-to*” methods. In both approach, the polymerization of selected polymers was realized by atom transfer radical polymerization (ATRP). In order to obtain sufficient functionalized MWCNT in one batch for preparing composites, the reactions of functionalization via “*grafting-from*” were significantly up-scaled. FT-IR spectra clearly indicated that the selected polymer chains were successfully grafted on MWCNT step by step

from anchoring initiator to synthesize polymer via ATRP. From thermal gravimetric analysis (TGA) results, the content of grafted PS was found to proportionally increase with the molecular weight of polymer, which implied good controllability of ATRP reaction in the presence of MWCNT. Similar results and phenomena were also observed in the case of functionalized MWCNT with PMMA under optimum reaction conditions. The formation of grafted P(MMA-*co*-S) random copolymers was determined by nuclear magnetic resonance spectroscopy ($^1\text{H-NMR}$), where signals of the main chains and the pendant groups were broad in all spectra and pronouncedly different from the ones of homopolymers. The controllability of the reaction was characterized by the fact that both the content and the molecular weight of grafted polymer increased linearly with the conversion of total amount of monomers. In present work, functionalizing MWCNT via “*grafting-to*” was also attempted by means of a Diels-Alder reaction between furfuryl-capped polymer and MWCNT. However, although both of PMMA and PS chains were successfully grafted on individual nanotubes, a much lower content of grafted polymer was achieved by “*grafting-to*” compared to the one in case of “*grafting-from*” because of the limited reactivity of MWCNT.

Then, the nanocomposites of SAN/PPE 40/60 blends filled with MWCNT were prepared by solution casting and melt processing. The localization of MWCNT in composites was characterized by transmission electron micrographs (TEM). The functionalized MWCNT with PS was found to migrate from the pre-mixed SAN phase to the PPE phase which had a better miscibility with grafted PS. The degree of migration was considerably influenced by the molecular weight of grafted PS. Nevertheless, as the dispersion of MWCNT in the pre-mixed phase was random, it was difficult to uniformly locate MWCNT at the interface through migration. Hence, introducing copolymer which contained both MMA and styrene units was considered as an alternative method. Through functionalizing with P(MMA-*co*-S) copolymers, many nanotubes were preferentially located at the interface of the blends. In

contrast, pristine MWCNT were observed to concentrate selectively in the SAN phase, which was in agreement with theoretical prediction according to the calculated wetting efficiency. However, when molecular weight of grafted copolymers increased, pronounced agglomeration was observed nearby the boundary which should be contributed to a micellization of the high molecular weight P(MMA-*co*-S) copolymers covering MWCNT and the formation of SAN/PPE/P(MMA-*co*-S) ternary blend with a specific composition of copolymer. For the rheological properties, the dynamic moduli and the complex viscosity of SAN/PPE blends were enhanced after filling pristine MWCNT. The values further increased when MWCNT were functionalized with low molecular weight P(MMA-*co*-S) copolymers, as MWCNT locating at the interface formed a CNT-CNT network with good contacting with each other even if the boundary of blend was not entirely occupied by MWCNT. However, when molecular weight increase, the composites showed a similar behavior to the neat blends with low dynamic moduli, which resulted from the softening effect of the grafted copolymers and the agglomerations of MWCNT. Besides, since a well conductive network of MWCNT was not formed and negative effect of grafted polymer, little improvement of electrical conductivity was achieved in the composites with functionalized MWCNT.

In summary, grafting selected polymer chains on the surface of MWCNT presented a possible approach to tune the localization of MWCNT in binary phase separated blends. The molecular weight of grafted polymer shows a significant influence on the localization of MWCNT and the properties of composites. When the grafted polymers had specific relationship (either miscible or immiscible) with both components in the blends, MWCNT might be more easily to be located at the interface, such as functionalized MWCNT with random copolymers. The functionalizing approach used in this thesis is not only valid in binary blends but also helpful to control the localization of MWCNT in block copolymers. Moreover, although the influence of composition of grafted copolymer on the localization of MWCNT was not discussed in this

work, it is possible to achieve more uniform localization of MWCNT at the interface by grafting random copolymer on MWCNT with specific composition which leads to good miscibility with both SAN and PPE. . It could be very interesting and promising for future investigation. The work studied in this dissertation also shows a potential of further investigation on the localization of other kinds of nanofillers, such as silica nanoparticles, metallic nanoparticles, and cellulose nanofibers, etc.

7.2 Zusammenfassung und Ausblick

Das Hauptziel dieser Arbeit stellt die gezielte Lokalisierung von mehrwandigen Kohlenstoffnanoröhrchen (MWCNT) durch eine Funktionalisierung mit verschiedenen Polymeren an der Grenzfläche binärer Polymerblends dar. Zudem erfolgt eine Untersuchung des Effekts der gezielten Lokalisation der MWCNT auf die Eigenschaften der Komposite. Um dieses Ziel zu erreichen wurden Polystyrol (PS), Polymethylmethacrylat (PMMA) und Copolymeren bestehend aus Styrol und Methylmethacrylat (P(MMA-*co*-S)) auf aminofunktionalisierte MWCNT aufgepropft. PS ist mischbar mit Polyphenylenether (PPE) und PMMA verfügt über eine gute Mischbarkeit mit Styrol-Acrylnitril (SAN) bei einem Acrylnitrilgehalt von 19 bis 35 wt%. Aufgrund dessen wird angenommen, dass die aufgepropften Polymere zu einer Anlagerung der MWCNT in der Grenzschicht zwischen der unmischbaren SAN/PPE Phase führen.

Der erste Teil dieser Arbeit konzentriert sich auf die Funktionalisierung der MWCNT mit der „grafting-from“ und der „grafting-to“ Methode. Die Funktionalisierung der MWCNT mit den ausgewählten Polymeren wurde für beide Methoden mit der radikalischen Atomtransfer-Polymerisierung (ATRP) realisiert. Um genug funktionalisierte MWCNT herzustellen, wurde die „grafting-from“ Reaktion in größerem Maßstab durchgeführt. Eine erfolgreiche

Funktionalisierung der MWCNT mit PS, vom Anbringen des Initiators bis zur Synthese des PS durch ATRP, konnte mithilfe von FT-IR Messungen belegt werden. Der Gehalt an aufgepropften PS erhöhte sich proportional mit dem Molekulargewicht des Polymers, was eine gute Kontrollbarkeit der ATRP-Reaktion impliziert. Bei der Funktionalisierung der MWCNT mit PMMA wurden ähnliche Ergebnisse erhalten. Die synthetisierten P(MMA-*co*-S) Copolymeren wurden mithilfe von Kernspinresonanzspektroskopie ($^1\text{H-NMR}$) untersucht. Die detektierten Signale der Haupt- und Nebenketten waren breit und unterschieden sich deutlich von den Signalen der Homopolymeren. Für den Polymergehalt und das Molekulargewicht des gepropften Polymers konnte ein linearer Zusammenhang in Bezug auf die Umwandlung der Gesamtmenge nachgewiesen werden. Dies lässt auf eine gute Kontrollierbarkeit der Reaktion schließen. Der Ansatz der „grafting-to“ Methode wurde mittels Diels-Alder Reaktion zwischen einem mit Furfurylgruppen bedeckten Polymer und MWCNT versucht. Im Gegensatz zu der „grafting-from“ Methode wurde hier aufgrund der limitierten Reaktivität zwischen den Furfurylgruppen und den MWCNT nur eine geringe Menge an gepropftem Polymer erhalten.

Durch Lösung und anschließender Schmelzverarbeitung wurden Nanokomposite aus MWCNT und einem SAN/PPE 40/60 Blend hergestellt. Die Lokalisierung der MWCNT wurde mithilfe von Transmissionselektronenmikroskopie (TEM) untersucht. Für die mit PS funktionalisierten MWCNT konnte beobachtet werden, dass sie aus der vorgemischten SAN-Phase in die PPE-Phase migrierten. Hierbei spielte das Molekulargewicht des gepropften PS eine entscheidende Rolle in Bezug auf den Migrationsgrad. Da in der vorgemischten SAN-Phase eine zufällige Verteilung der MWCNT vorlag, stellte die gleichmäßige Verteilung der MWCNT an der Grenzfläche durch Migration eine weitere Herausforderung dar. Um dies zu erreichen, wurde alternativ ein Copolymer aus MMA- und Styrol-Einheiten auf die MWCNT gepropft. Durch die Funktionalisierung mit P(MMA-*co*-S) konnte die Großzahl der MWCNT

an der Grenzfläche des Polymerblends lokalisiert werden. Im Gegensatz dazu sammelten sich die reinen MWCNT in der SAN-Phase an. Dieser Effekt stimmt mit den theoretischen Vorüberlegungen entsprechend des berechneten Benetzungsgrades überein. Jedoch führte eine Erhöhung des Molekulargewichts an gepropftem Copolymer zu einer Mizellenbildung und so zu einer ausgeprägten Agglomeratbildung der MWCNT an der Grenzfläche. Rheologische Untersuchungen der SAN/PPE-Blends mit reinen MWCNT zeigten verbesserte Eigenschaften in Bezug auf die dynamischen Moduli und die komplexe Viskosität. Eine weitere Erhöhung der Werte konnte durch die Funktionalisierung der MWCNT mit einem niedermolekularem P(MMA-*co*-S) Copolymer erreicht werden, da die MWCNT an der Grenzfläche partiell CNT-CNT-Netzwerke ausbildeten. Dagegen wiesen Copolymer mit einem hohen Molekulargewicht niedrige dynamische Moduli und somit ein ähnliches Verhalten wie das reine SAN/PPE-Blend auf. Dies ist auf den dämpfenden Effekt des gepropften Copolymers sowie der Agglomeration der MWCNT zurückzuführen. Da sich kein gut ausgeprägtes MWCNT-Netzwerk über das gesamte Polymerblend ausbildete, wurde in den Kompositen mit funktionalisierten MWCNT nur eine geringe Verbesserung der elektrischen Leitfähigkeit erreicht.

Zusammenfassend stellt das Propfen von ausgewählten Polymerketten auf MWCNT einen möglichen Ansatz dar um eine gezielte Lokalisation von MWCNT in binären Polymerblends zu erreichen. Das Molekulargewicht des gepropften Polymers zeigt einen signifikanten Einfluss auf die Lokalisation der MWCNT und die Eigenschaften der Composite. Wenn die thermodynamischen Verhältnisse der gepropften Polymere mit denen der Blendpolymere übereinstimmen, migrieren MWCNT leichter an die Grenzfläche. Dies zeigte die Funktionalisierung der MWCNT mit statistisch verteilten Copolymeren. Der in dieser Arbeit vorgestellte Funktionalisierungsansatz für eine kontrollierte Lokalisation von MWCNT kann für binäre Polymerblends, aber auch für Blockcopolymere angewendet werden. Obwohl der

Einfluss der Zusammensetzung des gepropften Copolymers auf die Lokalisierung der MWCNT nicht Gegenstand dieser Arbeit ist lässt sich prognostizieren, dass durch einen gezielten Aufbau der gepropften Polymerketten auf den MWCNT eine gute Mischbarkeit dieser sowohl mit San als auch mit PPE erreicht werden kann. Eine gleichmäßige Verteilung der MWCNT an der Grenzfläche zwischen beiden Matrixpolymeren könnte so realisiert werden, sodass dies einen interessanten und vielversprechenden Ansatz für weitere Forschungen darstellt. Darüber hinaus zeigt diese Arbeit ein Potential an der weiteren Untersuchung der Lokalisation von weiteren Arten an Nanofüllstoffen auf, wie z.B. Silica-Nanopartikel, metallische Nanopartikel, Zellulose-Nanofasern etc.

Acknowledgement

Working as Ph. D student and completing this dissertation are really a precious and excellent experience for my career and my life, but, it is also a challenging task for me. Without the support and help from many friendly people during these years, I would not have been able to finish my work.

First of all, I would like to express my deeply appreciation to Prof. Dr. Volker Abetz, for providing me this opportunity to come to Germany and work on carbon nanotubes. I greatly thank him for his continuous support, creative inspiration, nice discussions and constant trust on my work during the whole period of my study. Especially, when I had no positive outcome and the work progressed very slowly at the beginning period, he always delivery his kind encouragement to me and offer me convenient working conditions to solve issues. Without his encouragement and help, I cannot have a chance to complete this dissertation. I also wish to thank my supervisor Dr. Ulrich A. Handge for his supervision, good discussion and patient help on my daily work. He pays a lot of effort and gives me numerous suggestions on my publications. The same gratitude is also to my previous supervisor, Dr. Boschetti-de-Fierro, for her friendly help and kind guidance at the initial stage of my research work, helping me to adapt into a new environment.

I feel immense pleasure to say thanks to my colleagues in Polymer Research Institute, Helmholtz-Zentrum Geesthacht. Particularly, I am grateful to my office and laboratory mate, Wiebke Junior, who always gives me her warm hands whenever I need help. She

also help me a lot not only to modify but to correct, I have to say, the German version of summary part in this thesis. I am also thankful to Dr. Shahid Majeed and Dr. Julio Albuerne for the knowledge and trips I learn from them and to Md. Mushfequr Rahman for his kind help and good discussion in lab. Special thanks to Clarissa Abetz, Catrin Witte, Ivonne Ternes, Heinrich Böttcher, Dr. Sofia Rangou, Dr. Prokopios Georgopanos, Dr. Mona Wambach, Silvio Neumann, Berthold Wendland, Maren Brinkmann, Khan Muntazim, Bahadir Gacal, Ilona Zillich, Dr. Andreas Haase, Dr. Golda-Louis Chakkalakal, Dr. Christian Zenkel for their support and help on my work.

I also have to express my great thank to my Chinese colleagues and friends in Geesthacht, especially to Dr. Xi Lu and Dr. Lan Xia. I will treasure the life with them in Germany.

Finally, limited words but heartfelt appreciation is given to my parents and my boyfriend for their constant understanding, support and love.

Appendix

Safety instruction of the used chemical substances

Substance	GHS symbol	Hazard Statements	Precautionary statements
2,2-dimethoxypropane	GHS02, GHS07	H225-H319	P210-P305 + P351 + P338
anisole	GHS02, GHS07	H226-H315- H319	P305 + P351 + P338
Carbon Nanotubes	GHS08	H351+H373	P202+P260
copper (I) bromide	GHS07	H315-H319- H335	P261-P305 + P351 + P338
copper (I) chloride	GHS07, GHS09	H302-H410	P273-P501
copper (II) chloride	GHS07, GHS09	H302-H315- H319-H335- H410	P261-P273- P305 + P351 + P338-P501
diethyl ether	GHS02, GHS07	H224-H302- H336	P210-P261
2,2-Dimethoxypropane	GHS02, GHS07	HS02, GHS07	P210-P305 + P351 + P338
Ethyl α -bromoisobutyrate	GHS02, GHS05, GHS07	H226-H302- H318	P280-P305 + P351 + P338
furfuryl alcohol	GHS06, GHS08	H302-H312- H319-H331- H335-H351- H373	P261-P280- P305 + P351 + P338-P311
methanol	GHS02, GHS06, GHS08	H225-H301 + H311 + H331-H370	P210-P260- P280-P301 + P310-P311
Methyl methacrylate	GHS02, GHS07	H225-H315- H317-H335	P210-P261-P280

Substance	GHS symbol	Hazard Statements	Precautionary statements
N,N,N',N'',N''-Pentamethyldiethylenetriamine	GHS05, GHS06	H302-H311- H314	P280-P305 + P351 + P338- P310
Poly(2,6-dimethyl-1,4-phenylene ether)	-	-	-
poly(styrene- <i>co</i> -acrylonitrile)	GHS07	H302	-
<i>tetrahydrofuran</i>	GHS02, GHS07, GHS08	H225-H319- H335-H351	P210-P261-P281- P305 + P351 + P338
tetrahydrofurane	GHS02, GHS07, GHS08	H225-H319- H335-H351	P210-P261-P281- P305 + P351 + P338

List of Publications

1. **Bing Du**, Ulrich A. Handge, Shahid Majeed, Volker Abetz*. Localization of functionalized MWCNT in SAN/PPE blends and their influence on rheological properties. *Polymer*. Vol 53, Issue 24: 5437-5600
2. **Bing Du**, Ulrich A. Handge, Mona Wambach, Clarissa Abetz, Sofia Rangou, Volker Abetz*. Functionalization of MWCNT with P(MMA-*co*-S) copolymers via ATRP: Influence on localization of MWCNT in SAN/PPE 40/60 blends and on rheological and dielectric properties of the composites. *Polymer*. Vol 54, Issue 22: 6165-6176
3. Shahid Majeed, Daniel Fierro, Kristian Buhr, Jan Wind, **Bing Du**, Adriana Boschetti-de-Fierro, Volker Abetz*. Multi-walled carbon nanotubes (MWCNTs) mixed polyacrylonitrile (PAN) ultrafiltration membranes. *Journal of Membrane Science*. Vol 101-109: 403-404